Universidad de Alicante
Departamento de Matemática Aplicada

Técnicas de geodesia espacial aplicadas al estudio de las variaciones estéricas y eustáticas del nivel del mar

Space geodesy techniques applied to study the steric and eustatic sea level variations

Memoria para la obtención del grado de doctor

David García García

Dirigida por / *Supervised by*:

Dra. Isabel Vigo Aguiar
Dr. Benjamin Fong Chao

Contents

Agradecimientos

En primer lugar, me gustaría expresar mi más sincero agradecimiento a mis directores, la Dra. Isabel Vigo Aguiar y el Dr. Benjamin F. Chao, sin los cuales este trabajo de investigación no hubiera sido posible. Quiero agradecerles la confianza que desde el primer momento depositaron en mí, así como el margen de libertad que me dieron para desarrollar mis propias ideas. Gracias a ellos he disfrutado de un fascinante primer contacto con el mundo de la investigación y he aprendido tantas cosas que no podría enumerarlas. Gracias a los dos, de verdad. Y gracias, Isabel, por apiadarte de mí aquella mañana de mayo del 2002.

Al Dr. Benjamin F. Chao quiero además agradecerle la calurosísima acogida en su grupo de geodesia espacial en el *Goddard Space Flight Center* de *NASA* (Greenbelt, MD, EEUU) durante el verano de 2004. Los tres meses que pasé allí fueron maravillosos y supusieron un punto de inflexión en mi formación científica. Durante esta estancia se finalizó el primer capítulo de esta memoria y se desarrolló el segundo. Ben, gracias por encontrar siempre un hueco para atenderme pese a tus enormes obligaciones y por enseñarme que dormir era un lujo al que estaba mal acostumbrado.

Este trabajo, al igual que la mayoría de los que no son rentables económicamente, ha necesitado un 'mecenas', y en este caso ha sido el Dr. José Manuel Ferrándiz Leal. Quiero agradecerle que me financiase (con su proyecto de investigación del Ministerio de Ciencia y Tecnología, PNE-015/2001-C) la casi total elaboración de este trabajo, así como la inolvidable estancia de investigación en *NASA*. Además quiero agradecerle, conjuntamente a la Dra. Isabel Vigo, sus sabias e innumerables enseñanzas sobre la vida universitaria.

También quiero agradecer a la Dra. Anny Cazenave su infinita amabilidad

al acogerme en su grupo de geodesia espacial en el *Laboratoire d'Etudes en Géophysique et Océanographie Spatiales* (Toulouse, Francia) durante el verano de 2005, así como la financiación que recibí de su parte. Además de con Anny, tuve la suerte de trabajar con el Dr. Guillaume Ramillien y la Dra. Alix Lombard, quienes me enseñaron tanto que no sé cómo agradecérselo. El resultado de estos tres meses de colaboración ha quedado reflejado en el tercer capítulo. Gracias.

Por supuesto, no puedo dejar de agradecer a Jorge del Río Vera y a su director, el Dr. Jesus García Lafuente, ambos de la *Universidad de Málaga*, su magnífica colaboración en la elaboración del segundo capítulo, así como la de María del Carmen Martínez Belda, doctoranda del Dr. José Manuel Ferrándiz, en el cuarto capítulo.

Este trabajo no hubiera sido posible sin la publicación desinteresada, por parte de las correspondientes agencias, de todos los datos geodésicos utilizados. A todas ellas, gracias.

Gracias a mis compañeros, Alberto, Juan y Xaro, por estar ahí y hacerme las jornadas más amenas.

Y como no, gracias a mis padres, por haberme permitido elegir mi camino y por haberme ayudado a que lo siguiera. Y gracias a mis hermanos y hermanas, por su apoyo incondicional y por creer en mí.

Alicante, 29 de mayo de 2006
David García García

Resumen

0.1 Introducción

Dos terceras partes de nuestro planeta están cubiertas por agua, por lo que la tierra se puede considerar un planeta de océanos. Éstos, junto con la atmósfera, almacenan y distribuyen la mayor parte de la la energía que recibe del sol, y por tanto, dirigen en gran medida la climatología del planeta. De la energía recibida del sol, aproximadamente el 30% es reflejada o dispersada al espacio exterior, y el resto es almacenado principalmente en el océano en forma de calor. Levitus et al. (2000a, 2005) demostró que en la segunda mitad del siglo XX, aproximadamente el 80% de la energía absorbida por el planeta fue almacenada en los océanos, principalmente en los 700 primeros metros. En promedio anual, los trópicos reciben mayor cantidad de energía, y este exceso de calor es redistribuido hacia los polos mediante corrientes atmosféricas y oceánicas (vease, por ejemplo, Gill, 1982). Cualquier alteración en la energía recibida del sol o en la manera en que ésta es redistribuida, podría implicar cambios climáticos a escala global.

Para que la tierra sea un sistema en equilibrio, debe de emitir tanta energía como recibe del sol. Como media anual y global, la tierra recibe una radiación del sol de 342 W/m^2 [Kiehl and Trenberth, 1997], por lo que siguiendo la ley de Stefan, la superficie de la tierra debería tener una temperatura de -19°C. Sin embargo, la temperatura media de la tierra es de unos 14°C. Esta diferencia se explica gracias a los gases de efecto invernadero, los cuales absorben parte de la radiación infrarroja emitida por la superficie de la tierra, la cual es emitida en todas direcciones, y en particular de vuelta a la tierra (figura 1). De esta forma, se consigue aumentar la temperatura de la superficie, siendo las capas superiores de

la atmósfera con temperatura media de -19°C las que emiten la radiación equivalente a la absorbida desde el sol.

De acuerdo con el Tercer Informe de Evaluación del Intergovernmental Panel on Climate Change [IPCC, 2001], la temperatura media global de la tierra ha aumentado entre 0.4 y 0.8°C desde finales del siglo XIX, siendo la década de los 90 la que ha registrado las mayores temperaturas del último milenio en el hemisferio norte, y siendo 1998 el año más caluroso. A lo largo de los siglos y de los milenios, la temperatura media de la tierra ha variado de forma natural. Sin embargo, existen pruebas que demuestran que este último aumento está relacionado, al menos parcialmente, con la emisión de gases de efecto invernadero procedentes de la actividad industrial, por lo que tendría un origen antropológico. Uno de los gases invernaderos más importantes es el CO_2, cuya concentración en la atmósfera ha aumentado un 30% desde la era pre industrial, debido fundamentalmente a la combustión de combustibles de origen fósil y a la deforestación. Si la concentración actual de CO_2 se duplicase, se piensa que la temperatura de la superficie aumentaría entre 1.5 y 4.5°C. Para apreciar la magnitud de este cambio, baste pensar que la temperatura media global sólo ha aumentado 5 o 6°C desde la última era glacial.

Algunas de las consecuencias del aumento de temperatura durante el siglo XX que han sido observadas son: aumento global del nivel del mar; disminución de unas dos semanas de la duración de las capas de hielo en ríos y lagos de latitudes medias; disminución de la extensión y el espesor del hielo marino en el Ártico; retiro generalizado de los glaciales no polares; disminución de la extensión de las capas de nieve; fusión, calentamiento y degradación del permafrost en las zonas polares, subpolares y regiones montañosas; mayor frecuencia, persistencia e intensidad de los efectos asociados con El Niño durante los últimos 20-30 años, con respecto a los últimos 100 años; aumento de 1 a 4 días por decenio de la época de crecimiento durante los últimos 40 años en el hemisferio norte, especialmente en latitudes altas; desplazamiento de plantas, insectos, pájaros y peces hacia los polos o hacia altitudes más altas; adelanto de la floración, la llegada de las primeras aves migratorias y la época de cría; aumento de la frecuencia en la decoloración de arrecifes de coral, especialmente durante los fenómenos asociados con El Niño.

Determinar la evolución del cambio climático y sus consecuencias es una tarea complicadísima, dónde la única solución es el uso de Modelos de Circulación

Global (Global Circulation Models, GCM), tanto atmosféricos como oceánicos. Los resultados de las simulaciones de varios GCM en varios posibles escenarios (dependiendo de las estimaciones de emisión de CO_2 en el próximo siglo), se pueden encontrar en el IPCC (2001). En todos los escenarios de emisiones proyectados por el IPCC se prevé que tanto las concentraciones de CO_2 como la temperatura media de la superficie del planeta y el nivel del mar aumenten durante el siglo XXI. De hecho, se espera que la temperatura media global de la superficie del planeta aumente entre 1.4 y 5.8°C en el periodo 1990-2100. Esta cantidad es de 2 a 10 veces superior al calentamiento observado en el siglo XX. Además, se espera un aumento global del nivel del mar entre 9 y 88 cm, con importantes variaciones regionales y que los glaciares y las capas de hielo continúen su deshielo.

Puesto que la mayor parte del calor absorbido por la tierra se acumula en los océanos, y a ellos va a parar el agua proveniente del hielo y la nieve que se derriten en el continente, la observación y estudio de los océanos constituyen un elemento clave para comprender del proceso de cambio climático. El primer paso es la medición de las variaciones del nivel del mar (Sea Level Variations, SLV). Desde el siglo XIX, las únicas mediciones existentes eran las realizadas a partir de mareógrafos situados en la costa de continentes e islas alrededor del planeta. A partir de datos de decenas de estos mareógrafos se ha establecido que el nivel del mar ha aumentado 1.8 mm/año durante el siglo XX, lo que supone una razón de cambio 10 veces superior a la de los últimos milenios [Douglas, 1997, 2001; Peltier, 2001]. Otras estimaciones con los mismos datos varían entre 1 y 2 mm/año [IPCC, 2001]. Pese a su indudable utilidad, los mareógrafos presentan dos importantes limitaciones. La primera es que sólo proporcionan las SLV en la costa, pero no es posible tener mediciones en mar abierto. La segunda es que sus mediciones pueden incluir SLV ficticias, debidas a movimientos de tierra verticales que pueda sufrir el punto costero sobre el que se sitúa el mareógrafo. Por ejemplo, supongamos un mar en calma en el que no hay variaciones de nivel, entonces, si el punto de referencia del mareógrafo se hunde (eleva), el mareógrafo registrará un aumento (disminución) del nivel del mar.

Estas limitaciones se han superado con las medidas desde altímetros a bordo de satélites que proporcionan el nivel del mar absoluto con respecto a un marco de referencia terrestre. Esta idea se basa en la combinación de:

1. La altura del satélite sobre el nivel del mar, medida a partir del tiempo usado por un pulso de radar en ir y volver del satélite a la superficie.

2. La altitud del satélite, obtenida del posicionamiento preciso de éste con respecto a un elipsoide de referencia.

La diferencia entre altura y altitud nos da la altura del nivel del mar respecto al elipsoide de referencia para el lugar y el tiempo dado (figura 2). La idea de la altimetría satelitaria se desarrollo a principios de los años 60. Y confirmó su éxito como el mayor avance del siglo para el estudio de la topografía dinámica del océano con el primer satélite altimétrico que consiguió una precisión de 2-3 cm, el franco-americano TOPEX/Poseidon (T/P) lanzado en 1992. Debido a la configuración de su órbita, T/P puede medir las SLV del océano global entre las latitudes 66°S y 66°N (figura 3). Con una órbita a 1336 km de altitud, T/P pasa por el mismo punto cada 9.92 días y la separación entre dos pasos ascendentes o descendentes en el ecuador es de 315 km. La precisión sin precedentes obtenida por T/P ha encontrado innumerables aplicaciones [Fu and Cazenave 2001], como el estudio de la circulación oceánica y sus variaciones (por ejemplo, en 1996-1997 El Niño fue completamente observado por primera vez), corrientes, mareas, ondas de superficie, geoide, batimetría y SLV. La presente memoria se centra en esta última aplicación, el estudio de las SLV, y también se incluye un estudio que tiene como objetivo la determinación de los movimientos de tierra verticales a lo largo de la costa, combinando datos de nivel del mar relativo proporcionados por mareógrafos y datos de nivel del mar absolutos proporcionados por los altímetros a bordo de distintos satélites. El mapa de velocidades obtenido esta en concordancia con las velocidades verticales estimadas a partir de datos de GPS (Global Positioning System) y con la estructura tectónica de la región objeto de estudio, lo que valida la metodología y muestra como la altimetría también puede ser de utilidad para estudios tectónicos.

El crecimiento global del nivel del mar ha sido determinado en 2.8 $\pm$ 0.4 mm/año a partir de más de una década de datos de T/P [Cazenave and Nerem, 2004]. Sin embargo, a esta estimación se debe añadir un crecimiento de 0.3 mm/año para considerar la deformación sufrida por la cuenca oceánica debida al ajuste isostático glacial (Glacial Isostatic Adjustment, GIA) [Douglas and Peltier, 2002], dando por tanto lugar a un crecimiento de 3.1 mm/año. Esta estimación es

1.3 mm/año superior a la que Douglas (2001) y Peltier (2001) realizaron a partir de datos mareográficos registrados durante el siglo XX, lo que hace pensar en una posible aceleración del crecimiento en la década de los 90. Con el crecimiento actual, el nivel medio del mar aumentará unos 30 cm en el siglo XXI, aunque las previsiones del IPCC (2001) auguran un crecimiento entre 9 y 88 cm, con un valor central mayor. A priori, estas variaciones de nivel no deberían ser sorprendentes, ya que por ejemplo, el nivel del mar ha subido más de 100 m desde la última era glacial hace aproximadamente 18000 años [Kearney, 2001]. Sin embargo, se piensa que el crecimiento actual ha sido acelerado por el aumento de gases de efecto invernadero emitidos por la actividad humana (ver por ejemplo IPCC, 2001, o Levitus et al., 2001), los cuales han aumentado la temperatura del planeta. En particular, Levitus et al., (2000a) demostraron que la temperatura de los primeros 300 m del océano ha aumentado 0.31°C desde la década de los 60, aunque de forma no homogénea, ni espacial ni temporalmente [Lombard et al., 2005; Antonov et al., 2002].

Cuando la temperatura aumenta en el planeta, el nivel del mar aumenta por dos mecanismos diferentes. Por un lado, si la temperatura (T) de una columna de agua aumenta (disminuirá), ésta se expandirá (contraerá), produciendo las llamadas variaciones termo-estéricas del nivel del mar. Aunque menos importantes, las variaciones de salinidad (S) también producen variaciones del nivel del mar, las llamadas variaciones halo-estéricas. Si la salinidad aumenta (disminuye), la columna de agua se contraerá (expandirá). La relación entre las variaciones de temperatura y salinidad y las variaciones (termo- y halo-) estéricas del nivel del mar, viene descrita en la ecuación de estado del agua de mar [Gill, 1982]. En este caso, las variaciones de nivel del mar se producirían mediante un cambio de volumen del agua implicada, sin sufrir modificaciones de masa. Denotaremos a este tipo de variaciones por SLV_{steric} (acrónimo en inglés). Por otro lado, cuando la temperatura aumenta, el hielo y la nieve de los continentes tiende a derretirse, aumentando de ese modo la cantidad de agua de los océanos. Obviamente, el nivel del mar subirá al aumentar su masa de agua. Este tipo de variación corresponde al término eustático y lo denotaremos por SLV_{mass}. Además del incremento de masa de agua debida al deshielo, SLV_{mass} también incluye cualquier tipo de intercambio de agua de los océanos con la atmósfera y los continentes, dentro del llamado ciclo del agua (figura 4).

En la actualidad, uno de los problemas prioritarios para la comunidad científica es determinar qué porcentaje del incremento observado del nivel del mar (que denotaremos por SLV_{total}), es debido a SLV_{steric} y cuál a SLV_{mass}. Obviamente, la suma de estos dos últimos términos nos debe devolver SLV_{total}, de donde se deduce la siguiente ecuación (1), que es de gran importancia pese a su simplicidad:

$$SLV_{total} = SLV_{steric} + SLV_{mass}.$$

Durante el siglo XX, sólo dos términos de esta ecuación podían ser calculados: SLV_{total} a partir de datos mareográficos y SLV_{steric} a partir de la combinación de la ecuación del estado del agua de mar y los perfiles de T y S obtenidos por campañas in situ. Sin embargo, ambos tipos de datos tienen problemas de muestreo, principalmente en el hemisferio sur. A principios de la década de los 90, la altimetría supuso un gran avance para la estimación de SLV_{total}. Y poco después, con la publicación de la primera malla global de perfiles de T por Levitus et al. (2000b), la cual fue seguida por otras [Levitus et al., 2005; Ishii et al., 2005; Willis et al., 2004], se han podido calcular las estimaciones de SLV_{steric} globalmente. Pero de momento, no se disponía de observaciones suficientes que permitiesen una estimación directa del término SLV_{mass}, y la única vía era la determinación indirecta a través de la ecuación anterior como la sustracción a SLV_{total} de SLV_{steric}. Otros métodos indirectos se basan en estudiar las variaciones de las aguas continentales, a partir de la observación del derretimiento del hielo y nieve continental (e.g., Meier and Dyurgerov, 2002; Rignot et al., 2005), además de a partir de modelos hidrológicos [Milly et al., 2003; Ngo-Duc et al., 2005a].

La resolución de la ecuación (1) tiene dos posibles enfoques dependiendo de la escala temporal, a saber interanual o anual (ciclo estacional). En el primer caso, diferentes opiniones estuvieron confrontadas al principio del siglo XXI. Cabanes et al. (2001) afirmaba que el crecimiento del nivel del mar estaba totalmente explicado por expansión térmica en la segunda mitad del último siglo. Sin embargo, Miller and Douglas (2004) atribuyeron estas conclusiones a un error en la interpolación de los datos hidrográficos usados. Estudios más recientes (como por ejemplo Lombard et al., 2005; Antonov et al., 2005) arrojaron luz sobre este problema, encontrando diferencias entre SLV_{total} y SLV_{steric}. Las mediciones de

nivel del mar realizadas por mareógrafos durante el último siglo revelan un crecimiento del nivel del mar de 1.8 mm/año [Douglas, 1997, 2001; Peltier, 2001], y el análisis de los mismos datos para los últimos 55 años revela un crecimiento de 1.7 mm/año [Holgate and Woodworth, 2004]. Sin embargo, el SLV_{steric} estimado a partir de perfiles de T desde la superficie hasta los 3000 m de profundidad, en la segunda mitad del siglo XX muestra un crecimiento de 0.4 mm/año. Por tanto, hay un crecimiento de 1.3 mm/año que debería ser producido por SLV_{mass}, según la ecuación (1). Por otro lado, si miramos el periodo 1993-2003, se observa un escenario similar. Para ese periodo, un crecimiento de 3.1 mm/año y de 1.6 mm/año es estimado para SLV_{total} y SLV_{steric}, respectivamente a partir de altimetría y perfiles de T. La diferencia entre ellos, 1.5 mm/año, de nuevo por (1) debe estar producida por SLV_{mass}. Otro importante argumento a favor de un término eustático no nulo lo proporciona el análisis de perfiles de S, los cuales muestran que el agua de los océanos se está haciendo más dulce [Antonov et al., 2002]. Lo que implica que SLV_{mass} juega un papel importante en la subida del nivel del mar. Además, la variación debida al término eustático parece mantenerse constante (1.3-1.5 mm/año) durante los últimos 50 años, cosa que no sucede con el término estérico. Con todo ello, se podría afirmar que la aceleración en la subida del nivel del mar observada en los 90 estaría producida por una aceleración en el término estérico. En la tabla 1 se presenta un resumen de estos resultados.

En el segundo caso, cuando se quiere estudiar el ciclo anual, la controversia es menor. Varios estudios [Chen et al., 1998; Minster et al., 1999; Cazenave et al., 2000; Milly et al., 2003] han deducido SLV_{mass} a partir de la ecuación (1), usando datos altimétricos de T/P y datos climatológicos de la T de los océanos, y han demostrado que dicho término está bien explicado por variaciones estacionales del contenido de vapor de agua en la atmósfera y del agua almacenada en los continentes (estimados a partir de modelos). SLV_{total} tiene una amplitud anual de $\backsim$9 mm con un máximo entre finales de septiembre y principios de octubre y SLV_{steric} tiene una amplitud anual de $\backsim$5 mm con un máximo a mediados de marzo. Claramente, estas dos señales no están en fase. Por tanto, deduciendo el término eustático como $SLV_{mass} = SLV_{total} - SLV_{steric}$, encontramos que muestra una señal anual de amplitud $\backsim$9 mm con un máximo a mediados de septiembre.

Intrínsecamente, SLV_{mass} se debe a variaciones de la distribución de la masa

de agua del planeta y por tanto, producirá variaciones en su campo gravitatorio. Por su parte, SLV_{steric} se debe variaciones de volumen de la misma masa, que no dan lugar a variaciones gravitacionales apreciables. En los últimos años, las distintas agencias espaciales han centrado su atención en la determinación de las variaciones temporales de la gravedad (Time Variable Gravity, TVG) diseñando para este fin distintas misiones (CHAMP, GOCE, GRACE) que se han puesto en marcha con la llegada del siglo XXI. Las medidas de TVG pueden ser utilizadas para estimar de un modo directo la componente eustática del SLV, esto es SLV_{mass}. Los mejores resultados se están obteniendo de la misión GRACE (Gravity Recovery And Climate Experiment), lanzada en marzo de 2002 por la NASA y la agencia espacial alemana (DLR), consiste en dos satélites en órbita casi circular a 500 km de altitud y con una inclinación de 89.5°. Ambos satélites siguen la misma órbita, separados por unos 220 Km en media, y pueden medir con gran precisión las variaciones en la distancia que les separa. De esas variaciones se pueden deducir las TVG [Jekely, 1999].

A una escala anual, podemos asumir que las variaciones de la gravedad se producen por redistribuciones de masa, fundamentalmente agua, en la superficie de la tierra. En ese caso, es posible estimar las anomalías de masa de superficie [Wahr et al., 1998; Chao, 2005], la cual puede ser equivalentemente expresada como una película de agua de un grosor (no uniforme) determinado. La misión GRACE se ha convertido rápidamente en una herramienta fundamental para estimar las variaciones de masa de agua en la superficie. Chambers et al. (2004) fueron los primeros en estimar SLV_{mass} a nivel global a partir de datos TVG de GRACE, obteniendo una gran concordancia con la estimación indirecta $SLV_{total} - SLV_{steric}$. En ambos casos, SLV_{mass} presentaba un ciclo anual de amplitud $\backsim$8.5 mm y con máximo entre principios y mediados de octubre. Estos resultados concuerdan muy bien con estudios previos [Chen et al., 1998; Minster et al., 1999; Cazenave et al., 2000], validando la capacidad de GRACE para calcular SLV_{mass}.

Además, la misión GRACE ha encontrado otras muchas aplicaciones. Por ejemplo, Wahr et al. (2004) estimó la variación de masa de la cuenca del río Mississippi, del Amazonas y de Bahía de Bengal (sur de Asia), mostrando una buena concordancia con modelos hidrográficos. En Groenlandia, Velicogna et al. (2005) han estimado un ciclo anual con una amplitud de 8 cm (grosor equivalente

de agua) y un máximo en abril/mayo. GRACE también ha sido utilizado para estimar aguas continentales [Schmidt et al., 2005; Ramillien et al., 2005], evapotranspiración [Rodell et al., 2004] y la cantidad de agua desembocada por los ríos a los océanos [Chao and Au, 2006]. Como último ejemplo, Andersen and Hinderer (2005) detectaron con GRACE las inundaciones ocurridas en centro Europa en verano de 2002 y las sequías en el Canadá occidental en 2003.

El estudio de las variaciones globales del nivel del mar como ya hemos comentado resulta de gran importancia, pero éstas no se producen de forma homogénea en todo el planeta, por lo que resulta necesaria la realización de estudios locales y/o regionales. En particular, nosotros vamos a realizar un estudio del mar Mediterráneo, que muestra una gran sensibilidad a los efectos producidos por el sistema atmosférico. La rápida respuesta de la cuenca mediterránea, comparándola con las escalas de tiempo de los océanos hace de la señal de la variación interanual del nivel del mar en el mediterráneo, una señal de gran importancia que, en varias regiones, puede prevalecer sobre el ciclo anual. Destaca particularmente su carácter marcadamente distinto al de las variaciones globales. Por ejemplo, el nivel del mar Mediterráneo estuvo bajando desde la década de los 60 hasta principio de los 90 [Tsimplis and Baker, 2000], lo cual no ocurrió a nivel global. Además, en los 90 el nivel del mar Mediterráneo presentó una variación de un orden de magnitud superior al del crecimiento global [Cazenave et al., 2001]. Por tanto, debido al especial carácter del mar Mediterráneo, este debe ser estudiado separadamente. El Mar Negro también se ha incluido en los estudios cuando la disponibilidad de los datos así lo han permitido. En el capítulo 1 de esta memoria se lleva a cabo un estudio completo de las variaciones interanuales del mar Mediterráneo y del Mar Negro.

Por otra parte, la naturaleza semi-cerrada del mar Mediterráneo, cuyo único intercambio de agua con el mar abierto es a través del estrecho de Gibraltar, hace que resulte un 'laboratorio' natural de calibración y validación de los datos de GRACE. Otros posibles intercambios de agua se darían en la desembocadura de los ríos y a través del mar de Mármara con el Mar Negro, pero estos intercambios son pequeños en comparación con el anterior. Por otra parte, estarían los intercambios de agua con la atmósfera mediante evaporación y precipitación. Todos estos intercambios pueden, en principio, ser estimados mediante modelos y

mediciones, por lo que la variación de masa de agua del Mediterráneo podría ser calculada, y posteriormente comparada con las estimaciones realizadas con GRACE, mostrando el nivel de precisión de estas últimas. En el capítulo 2 se ha trabajado en este sentido, realizando un estudio del ciclo anual de las variaciones de masa de agua del mar Mediterráneo.

En el capítulo 3, siguiendo la metodología desarrollada en el capítulo 2, se ha extendido el estudio del ciclo anual de SLV_{mass} al océano global a partir de datos de GRACE. Además, se ha utilizado la ecuación (1) para calcular SLV_{steric} a partir de altimetría y datos TVG de GRACE, i.e., $SLV_{total} - SLV_{mass}$.

Por último, en el capítulo 4 se incluye una aplicación distinta de los datos de altimetría, realizando un estudio de los movimientos verticales de la corteza terrestre a lo largo de la costa norte del Mediterráneo y del Mar Negro. Para ello se ha realizado una comparación de las mediciones de las variaciones nivel del mar de altimetría, las cuales son absolutas, con las realizadas por mareógrafos, que son relativas a la costa.

0.2 Capítulo 1

En este capítulo se estudian las variaciones interanuales del nivel del mar del Mediterráneo y del Mar Negro. A partir de datos de mareógrafos, Tsimplis y Baker (2000) encontraron un cambio de tendencia en el mar Mediterráneo alrededor de 1960, pasando de una subida de nivel de +1.2/1.5 mm/año a un descenso de 1.3 mm/año. Este descenso continuó en el Mediterráneo hasta principio de los 90. Al otro lado del estrecho de Gibraltar, en el océano Atlántico, se pasó de un crecimiento de +1.8 mm/año a otro de +1.1 mm/año. En el Mar Negro, sin embargo, un crecimiento de +2.2 mm/año fue observado antes y después de 1960. Este cambio de tendencia parece estar relacionado con un cambio, también de tendencia, del índice del North Atlantic Oscillation (NAO) [Tsimplis and Josey, 2001], que mide la diferencia de presión entre las islas Azores e Islandia.

Cazenave et al. (2001, 2002) estudiaron los datos altimétricos de T/P para el periodo 1993-1999 en el Mediterráneo, encontrando un crecimiento generalizado del nivel del mar, excepto en el mar Jónico donde un descenso fue observado. Además, encontraron que este patrón estaba fuertemente relacionado con

las variaciones de temperatura de la superficie del mar (Sea Surface Temperature, SST).

0.2.1 Datos utilizados

Este estudio se basa en el análisis de la solución combinada de varios satélites altimétricos (T/P, Jason-1, ERS-1/2 y ENVISAT) durante el periodo 01/1993 - 11/2003. Las correcciones aplicadas a estos datos altimétricos incluyen las correcciones de los efectos de la troposfera y la ionosfera en la señal del altímetro, estado de la superficie del mar, mareas (oceánicas, de tierra sólida y del polo) y el efecto del barómetro inverso (la aplicación de esta última corrección no varía los resultados obtenidos, tal y como puede observarse en la figura 1.3, donde se comparan los resultados obtenidos con datos T/P sin aplicar dicha corrección). También se incluye en el estudio el análisis de las observaciones de la temperatura en la superficie del mar (Sea Surface Temperature, SST), solución combinada a partir de observaciones desde satélite y medidas in situ, para el mismo periodo. Además de los datos de observaciones de nivel del mar tomados por mareógrafos. En este caso el periodo de tiempo viene marcado por la disponibilidad según la estación mareográfica.

0.2.2 Resultados

Tanto para los datos de altimetría como los de SST se ha optado por trabajar con una resolución de mallas mensuales de $1^{o} \times 1^{o}$. Puesto que estamos interesados en las variaciones interanuales, en este capitulo se ha eliminado la señal anual en ambos conjuntos de datos (esta señal será estudiada en el capítulo 2). Una de las herramientas matemáticas fundamentales para el análisis de los datos es la descomposición en funciones empíricas ortogonales (Empirical Orthogonal Functions, EOF). Los distintos modos resultantes mediante esta técnica, debidamente interpretados nos proporcionan los patrones de variación de los datos con sus pesos. En el caso de las variaciones de nivel del mar del Mediterráneo el primer modo explica un 55.1% de la variación de los datos y presenta un patrón positivo en todo el Mediterráneo, lo que implica un movimiento en fase de todo el mar acorde con la serie temporal asociada, la cual no presenta ninguna variación in-

teranual destacable (figura 1.8a). Fukumori et al. (2003) sugieren que este modo está relacionado con transporte de masa, forzado por vientos, a través del estrecho de Gibraltar.

Por otra parte, el segundo modo, que explica un 15.9% de la variación de los datos, presenta un patrón positivo en la cuenca de Levante, el mar Egeo y el mar Mediterráneo, y un patrón negativo en el mar Jónico y en la cuenca Occidental (figura 1.8b). A su vez, la serie temporal asociada presenta una tendencia positiva hasta 06/1999 y negativa a partir de esa fecha. Su análisis junto con el modo correspondiente implica un crecimiento generalizado en todo el mar Mediterráneo, excepto en el Jónico y la cuenca Occidental, con un cambio de tendencia a partir de junio del 1999. Al realizar una descomposición en EOFs en el Mar Negro, observamos que aquí el primer EOF es dominante, explicando el 90.4% de la variación, y muestra un patrón positivo homogéneo en todo la región, y nuevamente la serie temporal asociada presenta un cambio de tendencia en 06/1999, lo que implica un cambio de subida de nivel del mar a descenso en torno a mediados de 1999. Estos hechos se confirman al estudiar los mapas de tendencias para los periodos 01/1993 - 06/1999 y 07/1999 - 11/2003 (figuras 1.5a y 1.5b), y al estudiar las variaciones medias de las distintas regiones (figura 1.1a-h), así como los índices de crecimiento en cada uno de los periodos para cada una de las regiones (tabla 1.1).

Realizando un estudio similar para los datos de SST (figuras 1.5c, 1.5d, 1.7a-h, 1.9a y 1.9b), no se observa el cambio presente en los datos de altimetría. Al igual que en Cazenave et al. (2001, 2002), se tiene una correlación muy elevada entre los índices de crecimiento de nivel del mar y SST en el Mediterráneo para el periodo 01/1993 - 06/1999 (figuras 1.5a y 1.5c). Sin embargo, esta correlación desaparece para el periodo 07/1999 - 11/2003 (figuras 1.5b y 1.5d). Indicando que las variaciones de nivel del mar del Mediterráneo estaban principalmente dirigidas por variaciones estéricas (usando SST como un indicador) hasta 1999, pero que a partir de ese momento se produjo un cambio en el sistema. En el caso del Mar Negro, y la correlación con SST se mantiene antes y después de 1999, por lo que aquí no parece que tal cambio se haya producido. En este caso, el cambio de tendencia podría estar motivado por cambios de temperatura en la zona.

0.2.3 Discusión y conclusiones

Un cambio de tendencia ha sido observado, a partir de datos de altimetría desde satélite y validado con las observaciones tomadas en los mareógrafos, en diferentes regiones del mar Mediterráneo a mediados de 1999. Las variaciones interanuales de nivel del mar Mediterráneo han estado dirigidas por variaciones de SST en el periodo 01/1993 - 06/1999, y sin embargo, esa relación parece desaparecer en el periodo 07/1999 - 11/2003. Una de las claves del problema sería saber si ese cambio se ha debido a alguna fluctuación de periodo superior a una década, o si se debe a un cambio en la circulación termohalina del Mediterráneo. Un estudio de la bibliografía existente nos hace inclinarnos por la segunda opción.

En la cuenca este del Mediterráneo, una única fuente de aguas profundas ha sido registrada al sur del mar Adriático durante el siglo XX. Sin embargo, entre 1987 y 1995 una nueva fuente apareció en el mar Egeo [Roether et al., 1996]. Este hecho fue llamado el Eastern Mediterranean Transient (EMT). Años después, tal y como predijeron Klein et al. (2000), el Adriático recuperó su rol de principal fuente de aguas profundas entre 1997-1999 [Manca et al, 2003]. Manca et al. (2003) también confirmaron el restablecimiento del tránsito de aguas intermedias de la cuenca de Levante al mar Jónico a través del pasaje de Creta, restaurando así la célula de circulación termohalina en 1999. El cambio de tendencia registrado en este estudio es más importante en las regiones implicadas en el EMT. Por tanto, una hipótesis razonable es que el cambio de tendencia en el Mediterráneo de 1999 está relacionado con el fin del EMT.

En el caso del Mar Negro, parece que las variaciones de nivel están dirigidas por variaciones estéricas, aunque Tsimplis et al. (2004) no encontraron una tal relación en las últimos 40 años. Como conclusión podemos decir que las causas y los efectos de las variaciones de nivel en el Mediterráneo y en el Mar Negro no son sencillas de determinar, y que además son muy dependientes del periodo estudiado. Confirmando por tando , que el Mediterráneo y el Mar Negro están regidos por dos sistemas dinámicos distintos y separados.

0.3 Capítulo 2

En este capítulo se estudia la señal anual de las variaciones de nivel del mar Mediterráneo (SLV_{total}), así como las componentes estérica (SLV_{steric}) y eustática (SLV_{mass}) que la motivan, teniendo en cuenta la relación dada por la ecuación (1):

$$SLV_{total} = SLV_{steric} + SLV_{mass}.$$

El objetivo de este estudio es doble. Por un lado se pretende estudiar la señal de SLV_{mass} en el Mediterráneo. Estudios anteriores [García-Lafuente et al., 2002; Bouzinac et al., 2003; Larnicol et al., 1995] han estimado este término indirectamente y han apuntado la posibilidad de que tuviese un ciclo anual. Sin embargo, estas estimaciones nunca han sido del todo concluyentes por el ruido en la señal. Aquí se pretende estudiar esta señal directamente, estudiando los inseparables cambios de gravedad que la acompañan mediante datos de GRACE. Además, se realizará una estimación indirecta, $SLV_{total} - SLV_{steric}$, para calibrar y validar el resultado obtenido. Por otro lado, se calculará el flujo vertical de masa del Mediterráneo, i.e., evaporación menos precipitación, a partir de un GCM, para estimar después los flujos de masa horizontales, descontando los verticales de los totales (calculados con GRACE).

0.3.1 Datos utilizados

Aquí se han utilizado los mismos datos altimétricos que en capítulo anterior para la estimación de la componente SLV_{total}, pero en esta ocasión el periodo es 01/1993 - 07/2004. La estimación del término SLV_{steric}, se basa en perfiles cada 10días de T y S del modelo oceánico de circulación global ECCO (Estimating the Circulation and Climate of the Ocean) para el periodo 01/1997 - 06/2004. Estos datos pueden ser convertidos en anomalías de densidad, siguiendo la ecuación de estado del agua de mar [Gill, 1982], que tras ser integradas verticalmente (ecuación 2.1) nos dan una estimación de SLV_{steric}.

Para calcular el término SLV_{mass} se han usado 22 meses de datos (consistentes en coeficientes de Stoke) de la misión GRACE para el periodo 04/2002 - 07/2004. Después de aplicar la ecuación 2.2 a dichos datos, se obtiene SLV_{mass}.

Durante el proceso de estos datos, se ha realizado un minucioso estudio de la correcciones aplicadas para comprobar su consistencia con los datos altimétricos.

También se han usado datos de precipitación menos evaporación derivados del GCM atmosférico de NCEP (National Center for Environmental Prediction) para el periodo 01/2002 - 07/2004 [Chao and Au, 2006].

0.3.2 Resultados

Los datos de GRACE pierden bastante calidad más allá de los coeficientes de grado 15, por lo que sólo tienen una resolución espacial de unos 1500 km. Por tanto, para estudiar el mar Mediterráneo, nos centraremos en el estudio de la media espacial de SLV_{mass}. Para realizar esta media y disminuir la contaminación de las variaciones gravitacionales producidas en la costa, así como el ruido presente en los coeficientes de mayor grado, se ha realizado un filtro gaussiano con un radio de 1500 km, tal y como se describe en Swenson and Wahr (2002).

En la figura 2.2 se pueden observar las medias en el Mediterráneo de SLV_{total} y SLV_{steric}, las cuales muestran una gran concordancia. Sin embargo, la primera presenta una señal anual de amplitud 83 ± 13 mm y phase $281^o\pm10^o$, y la segunda tiene una amplitud y una fase anual de 94 ± 5 mm y $258^o\pm3^o$, respectivamente. Esto quiere decir que las señales no concuerdan perfectamente, siendo SLV_{total} de menor amplitud y alcanzando el máximo cerca de un mes después que SLV_{steric}. Por tanto, al calcular el residuo $SLV_{total} - SLV_{steric}$, que representa una estimación indirecta de SLV_{mass}, obtenemos una señal anual de amplitud 38 ± 16 mm y fase $16^o\pm27^o$. Este residuo concuerda muy bien con la estimación directa de SLV_{mass} realizada a partir de datos de GRACE, la cual presenta una señal anual de amplitud 55 ± 15 mm y fase $52^o\pm15^o$. La concordancia es muy buena teniendo en cuenta los errores en las estimaciones y las fuentes de error que cada tipo de datos lleva asociadas.

La diferencia entre las estimaciones de masa de dos meses seguidos representa el flujo de variación de masa. Realizando estas diferencias entre las estimaciones realizadas con datos de GRACE, se obtiene el flujo de variación de masa del Mediterráneo. Por otro lado, a partir de los datos de precipitación menos evaporación, se puede calcular el flujo de masa vertical, el cual es negativo a lo largo de casi todo el año. La sustracción de este último respecto del primero, pro-

duce una estimación del flujo de masa horizontal, el cual tiene una señal anual de amplitud 17±16 mm/mes y fase 263°±76°. Debido a la naturaleza semicerrada del Mediterráneo, este flujo horizontal está principalmente representado por el flujo a través del estrecho de Gibraltar, el cual debe existir para compensar el flujo negativo de precipitación menos evaporación, suponiendo claro está, que la masa del Mediterráneo sea constante de un año a otro. Comparando esta estimación del flujo horizontal con registros históricos del flujo del estrecho de Gibraltar realizados a partir de boyas, como los realizados por García-Lafuente et al. (2002) (quienes encuentran una señal anual de amplitud 78±44 mm/mes y fase 234°±33°), encontramos una buena concordancia en fase.

0.3.3 Discusión y conclusiones

Por primera vez se ha estimado de forma directa el término SLV_{mass} en el mar Mediterráneo y se ha demostrado que presenta una clara señal anual con máximo en Febrero. Además, se ha remarcado la relación de los términos estéricos y eustáticos que dan como resultado las variaciones de nivel observadas. Se ha establecido que la variación anual del nivel del mar Mediterráneo está principalmente dirigida por variaciones estéricas y parcialmente compensada por variaciones de masa. Y tal y como se observa en la figura 2.2, el nivel del mar sube (baja) cuando se pierde (gana) masa de agua, por lo que el nivel es máximo (mínimo) cuando hay menor (mayor) cantidad de agua. Los resultados obtenidos se han validado también mediante la estimación indirecta de SLV_{mass}.

Por otra parte, se ha desarrollado un nuevo método que permite realizar estimaciones de los flujos horizontales de agua del Mediterráneo, mediante la combinación de datos de GRACE y GCM atmosféricos. La estimación realizada del flujo horizontal concuerda muy bien en fase con estimaciones de registros históricos de flujo en el estrecho de Gibraltar [García-Lafuente et al., 2002].

0.4 Capítulo 3

En este capítulo, se ha estudiado el ciclo anual de la componente eustática, SLV_{mass}, del océano global, que representa el ciclo anual del agua, a partir de datos de

GRACE. La importancia de estudiar este término se discute ampliamente en la introducción de esta memoria (0.1). Este estudio introduce varias mejoras respecto a otros existentes [Chambers et al., 2004]: i) datos mensuales (en lugar de años medios) de altimetría y de T para la estimación de SLV_{total} y SLV_{steric}; ii) mayor precisión de la serie temporal del armónico esférico de grado 2 y orden 0 de GRACE (calculada a partir de mediciones de Satellite Laser Ranging (SLR) [Cox and Chao, 2002]); iii) la presión atmosférica media sobre los océanos ha sido tenida en cuenta. Además, el término SLV_{steric} ha sido calculado a partir de SLV_{total} (estimado con altimetría) y SLV_{mass} (estimado con GRACE), obteniendo de esta forma una estimación global e independiente de las realizadas a partir de datos de T y S.

0.4.1 Datos utilizados

Para calcular el término SLV_{total} se han utilizado datos altimétricos de T/P para el periodo 04/2002 - 12/2003. Todas las correcciones habituales han sido aplicadas, incluida la del barómetro inverso. Para esta última, se ha adoptado la corrección según se propone en Minster et al. (1999). Estos datos vienen dados en mallas de $1^{o} \times 1^{o}$ cada 10 días, las cuales han sido promediadas sobre los océanos entre 60°S y 60°N, y convertidas en medias mensuales. Para realizar la media espacial se ha tenido en cuenta el área real que representa cada punto de la malla, ya que por ejemplo, un punto de la malla en el ecuador representa mucha más área que un punto de latitud 60°N (ver la ecuación 3.2).

Se ha obtenido una estimación de SLV_{mass} a partir de los mismos datos de GRACE que en el capítulo anterior, pero para el periodo 04/2002 - 12/2003. Se ha calculado la señal media para la misma región que en altimetría, i.e., los océanos entre 60°S y 60°N, y para ello se ha aplicado un filtro gaussiano de 1000 km de radio [Swenson and Wahr, 2002]. Para que la comparación de estos datos con los altimétricos, corregidos para el efecto del barómetro inverso, sea coherente, se han añadido a GRACE las correcciones oceánica y atmosférica (que habían sido aplicadas en el procesado de los datos de altimetría por las agencias que los distribuyen), y se le ha restado la presión atmosférica media sobre la superficie total de los océanos.

Para el término SLV_{steric} se han usado los datos de temperatura globales de

Ishii et al. (2006). Estos datos consisten de mallas mensuales de $1^o \times 1^o$ hasta una profundidad de 700 m, y van de 1945 a 2003, aunque aquí nos restringiremos al periodo que coincide con los datos de GRACE, i.e., 04/2002 - 12/2003. Una vez estimado el término SLV_{steric} de forma análoga a la estimación realizada en el capítulo anterior, se calcula la media espacial para el océano entre 60°S y 60°N, teniendo en cuenta el área que representa cada punto de la malla (ver la ecuación 3.2).

0.4.2 Resultados

Las figuras 3.2a, 3.2b y 3.2c representan las medias espaciales de SLV_{total} (calculado con T/P), SLV_{mass} (calculado con GRACE) y la diferencia entre estas dos series temporales, $SLV_{total} - SLV_{mass}$. Todas esas curvas están promediadas entre las latitudes 60°S y 60°N. SLV_{total} presenta una clara señal anual de amplitud 6.1 ± 1.2 mm y fase $309^o \pm 11.3^o$, representando un máximo a principios de noviembre. SLV_{mass} también presenta una señal anual de amplitud 10.9 ± 1.1 mm y fase $276.5^o \pm 7.8^o$, representando un máximo a principios de octubre. La diferencia de las dos curvas, $SLV_{total} - SLV_{mass}$, también presenta una clara señal anual de amplitud 6.4 ± 2.1 mm y fase $72.7^o \pm 22.3^o$ (máximo a mediados de marzo). Esta diferencia es una estimación indirecta de SLV_{steric}, la cual coincide bastante bien con estimaciones basadas en datos climatológicos de T, como por ejemplo Chen et al. (1998), Minster et al. (1999) and Cazenave et al. (2000).

La señal calculada de SLV_{mass} no representa el ciclo anual del agua (i.e., el intercambio de agua de los océanos con la atmósfera y los continentes), porque puede incluir intercambios de masa con latitudes superiores a 60°. Por tanto, para realizar una estimación de la señal producida por el ciclo del agua, también calculamos la variación media de SLV_{mass} a partir de datos de GRACE sobre todo el océano. En este caso, encontramos una señal anual de amplitud 10.0 ± 2.3 mm y fase $282.1^o \pm 16.3^o$ (máximo a mediados de octubre). Teniendo en cuenta la superficie total de los océanos, esta señal representa un intercambio de $6.86 \cdot 10^{12}$ m^3 de agua de máximo a mínimo a lo largo del año.

Para validar el resultado obtenido en la estimación del término estérico a partir de datos de T/P y de GRACE, hemos calculado SLV_{steric} a partir de los datos de T de Ishii et al. (2006). Esta estimación puede observarse en la figura 3.3, donde

se muestra una señal anual de amplitud 5.3±1.0 mm y fase 101.4°±11.3° (con máximo a principios de abril). Esta señal coincide bastante bien con la estimada indirectamente teniendo en cuenta los errores asociados.

0.4.3 Discusión y conclusiones

En este estudio se ha realizado una estimación del intercambio de agua de los océanos con los continentes y la atmósfera, la cual incluye ciertas mejoras respecto a trabajos previos [Chambers et al., 2004]. Esta estimación proporciona una valiosa información para su asimilación en los modelos hidrológicos.

Por otra parte, se ha estimado la componente estérica de las variaciones de nivel a partir de datos altimétricos y de variaciones de la gravedad, la cual concuerda bastante bien con la estimación realizada a partir de perfiles mensuales de temperatura. Esta nueva metodología para estimar SLV_{steric} puede ser de gran ayuda para superar los problemas existentes de muestreo en regiones poco frecuentadas.

Es importante destacar que hay un periodo de 5 o 6 meses entre el máximo alcanzado por SLV_{mass} y por SLV_{steric}. Este comportamiento ha sido también observado en estudios previos [Chen et al., 1998; Minster et al., 1999; Cazenave et al., 2000], así como en estudios locales como el realizado en el capítulo 2. Este desfase significa que la cantidad de agua es mínima cuando el calor contenido en los océanos es máximo.

0.5 Capítulo 4

En este capítulo se incluye una aplicación de la altimetría distinta a la del estudio de las variaciones de nivel del mar. En particular, lo que se pretende es deducir variaciones verticales de la costa del Mediterráneo y del Mar Negro. Para ello, vamos a comparar las mediciones altimétricas con las realizadas por mareógrafos. Como ya se ha comentado en la introducción, las mediciones altimétricas se realizan respecto de un elipsoide de referencia, mientras que las de los mareógrafos son respecto al punto en la costa sobre el que se sitúa el mareógrafo Por tanto, las mediciones de estos últimos pueden estar contaminadas por movimientos ver-

ticales de la costa. De ahí, que la diferencia entre las mediciones altimétricas y las mareográficas incluya información sobre los movimientos de tierra verticales en la costa [Nerem and Mitchum, 2002; Cazenave et al., 1999]. Los resultados obtenidos han sido comparados con mediciones de estaciones GPS cercanas, mostrando en general una buena concordancia en el sentido del movimiento (únicamente se realiza una comparación de signo en la tendencia debido a que la disponibilidad de observaciones de GPS y mareógrafos en la mayoria de los casos no se superponen en el tiempo).

0.5.1 Datos utilizados

Los datos altimétricos utilizados son los mismos que los utilizados en los capítulos 1 y 2, pero para el periodo 01/1993 - 12/2001. Por otra parte, se han usado datos de 42 mareógrafos en el Mediterráneo y 7 en el Mar Negro, cuya distribución espacial y temporal puede verse en las figuras 4.1 y 4.2, respectivamente. Para las mediciones GPS, usamos las series de la componente vertical de 22 estaciones (ver figura 4.1).

0.5.2 Resultados

Para cada mareógrafo se ha seleccionado el punto de medición altimétrica más próximo a la posición del mareógrafo, obteniendo así para cada posición dos series temporales. Entonces, se ha calculado la serie de diferencias, altimetría menos mareógrafo, la cual en principio contiene información sobre los movimiento verticales de costa. Una vez corregida la señal estacional para cada una de estas series de diferencias, se calcula la variación lineal de la serie. De esta forma se obtiene un mapa de índices de crecimiento (ver figura 4.4 y tablas 4.1 y 4.2). Excepto para unos cuantos mareógrafos para los que no se identifica un claro movimiento y para algunos que se sabe que tienen fuertes influencias locales, la mayoría de subidas y bajadas se presentan en agrupaciones, lo que podría indicar un origen tectónico.

El mismo análisis se ha realizado para las variaciones verticales, obteniendo el correspondiente mapa de variaciones (ver figura 4.4 y la tabla 4.3). En general, una buena concordancia en el sentido del movimiento es observada con las estima-

ciones de altimetría menos mareógrafos. Estos últimos también se han comparado con las campañas realizadas en el proyecto SELF (Sea Level Fluctuations) durante el periodo 1993-1998 [Becker et al., 2002], mostrando concordancia en general.

0.5.3 Discusión y conclusiones

Los movimientos verticales calculados en este estudio son de varios mm/año, por lo que se excluye que sean debidos únicamente al GIA, estudios al respecto [Peltier, 2001] ha estimado estos últimos en torno a $\pm$0.1-0.2 mm/año para los mareógrafos estudiados. Nos centramos por tanto en el origen tectónico de los mismos. En el Mediterráneo se produce la colisión de las placas Euroasiática, Africana y Arábiga (figura 4.5), produciendo un complicado sistema de microplacas que está lejos de ser resuelto [R. Sabadini, H. Drewes, personal communication, 2003]. Pero en general, los resultados obtenidos en este estudio encajan bien dentro de los movimientos estimados de las placas [McKenzie, 1972; Jimenez-Munt and Sabadini, 2002, Jimenez-Munt et al., 2002, Rahl et al., 2004]. En especial, el descenso generalizado encontrado a lo largo de la costa oriental del Adriático y la costa occidental de Grecia, parece estar producido por la subducción de la litosfera del Adriático bajo la placa Euroasiática a lo largo de la falla de Dinarides.

Introduction

Two thirds of the Earth surface are covered by ocean water, that makes the Earth an ocean planet. The ocean, together with the atmosphere, store and distribute most of the energy received from the sun, and then, they highly drive the climatology of the planet. Around 30% of the impinged energy on the earth is reflected or scattered, and the rest is stored in the atmosphere and more so in the oceans. In the 2nd half of 20th century, $\backsim$80% of the total heat absorbed by the Earth system was stored in the world ocean, mainly in the upper 700 m layer [Levitus et al., 2000a, 2005]. The global ocean circulation together with the atmosphere constitute the mechanism by which solar energy received in the tropics is re-distributed to the entire planet [e.g., Gill, 1982]. Variations in the energy budget received from the sun or in the way it is re-distributed may imply a climatic change in a global scale.

For a stable climate, a balance is required between incoming solar radiation and the outgoing radiation emitted by the climate system. The earth receives from the sun an average throughout the year of 342 W/m^2 [Kiehl and Trenberth, 1997], and then, following the Stefan's law, earth's surface should have a temperature of -19°C. However, the mean temperature of the earth's surface is of 14°C. This difference is explained by the so-called greenhouse gases, which absorb infrared radiation, emitted by the earth's surface, and emit it in all directions including downward to the earth's surface (figure 1). As a result, the earth's surface is warmed and the infrared radiation is effectively radiated back into space from an altitude with an average temperature of -19°C.

Accordingly to the contribution of the Working Group I to the Third Assessment Report of the Intergovernmental Panel on Climate Change [IPCC, 2001], the mean global temperature of the atmosphere at the surface increased from 0.4°C

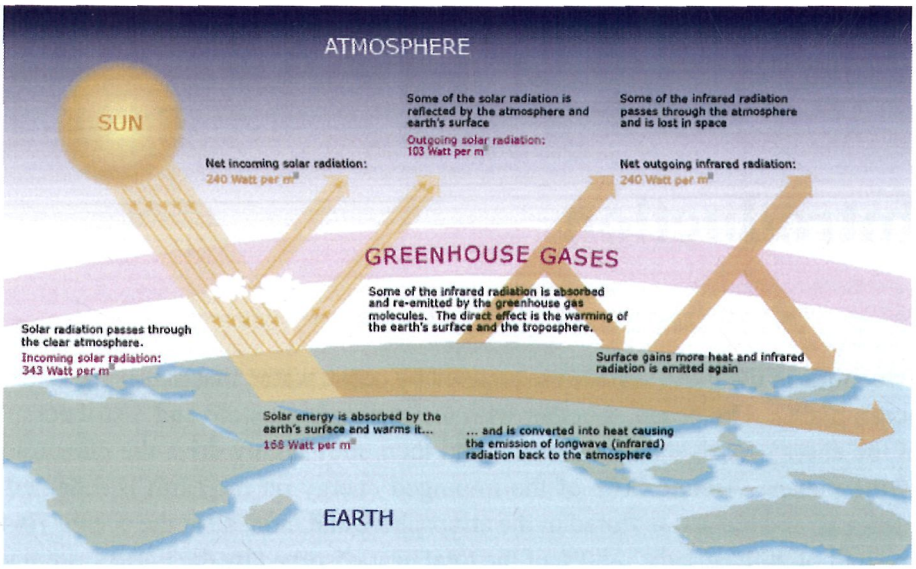

Figure 1: Greenhouse effect (source <http://www.greenhouse.crc.org.au>).

to 0.8°C since de late 19th century. Besides, the 1990s are likely to have been the warmest decade of the millennium in the northern hemisphere, and 1998 is likely to have been the warmest year. The mean temperature of the planet have been naturally varying along the centuries and the millennia. However, it has been shown that the recent increase of temperature is related to the emission of greenhouse gases from the industry. The amount of CO_2, for example, has increased by more than 30% since pre-industrial times, mainly due to the combustion of fossil fuels and deforestation. It is believed that a doubling of CO_2 concentration would imply an increase between 1.5 and 4.5°C of the mean temperature. To appreciate the magnitude of this temperature increase, it should be compared with the global mean temperature difference of perhaps 5 or 6°C from the middle of the last Ice Age to the present interglacial.

Some of the consequences of this temperature increase that has been observed in the 20th century are: increase of global mean sea level; decreased by about

2 weeks in the mid- and high latitudes of the duration of ice cover of rivers and lakes; thinned of the Artic sea-ice extent and thickness; widespread retreat of non-polar glaciers; decrease in area of snow cover; thaw, warming and degradation of the permafrost in the polar, sub-polar and mountainous regions; more frequency, persistency and intensity of the associated El Niño events during the last 20 to 30 years compared to the previous 100 years; extension by about 1 to 4 per decade during the last 40 years of the growing season; shift poleward and up in elevation for plants, insects, birds and fish; earlier plant flowering, earlier bird arrival, earlier dates of breeding season and earlier emergence of insects in the northern hemisphere; increase of frequency of coral reef bleaching, especially during El Niño events.

To forecast the evolution of the climatic change and its climatic change is a very complicated issue, which only can be solved by atmospheric and oceanic Global Circulation Models (GCM). The results of several GCM in the different possible scenarios (depending on the estimated emissions of CO_2 in the next century), can be found in IPCC (2001). In general, all the projections of the climate change predict an increase during the 21st century of the CO_2 concentration, of the global mean temperature at the surface and of the global mean sea level. It is believed that the global mean temperature increase between 1.4 to 5.8°C in the period 1990-2100. This is about two to ten times larger than the central value of observed warming over the 20th century. Besides, global mean sea level is projected to rise by 9 to 88 cm between the years 1990 and 2100 with significant regional variations.

As the global ocean stores most of the heat absorbed by the earth and receives the water melted in the continents, its study is of paramount importance to understand the climatic change. The first step is to understand the sea level variations (SLV), which is a complex interdisciplinary scientific challenge. Since the 19th century, the only SLV records were provided by tide gauges (TG) located at many places along the world's continental as well as island coasts. Using the SLV recorded by tenths of tide gauges, the global mean sea level has been estimated to be rising around 1.8 mm/year during the twentieth century, that is 10 times faster than the average of the past several millennia [Douglas, 1997, 2001; Peltier, 2001]. Although TG continuously measure the SLV, it can only be done on the coast, which is a severe limitation. Moreover, SLV are measured with respect

to the benchmark of the TG, which is attached to the ground. It means that any vertical motion of the coastal ground will masquerade as SLV in the TG records. For example, if the benchmark of a TG drops (rises), for whatever the reasons, an apparent SL rise (drop) will arise in its records.

On the other hand, altimeter measures the 'absolute' SL relative to a terrestrial reference frame, hence avoids the above-mentioned problem. This idea is based on the combinations of:

1. The satellite height over the surface measured by means of laser or radar pulses sent from the satellite and bounced back from the target surface.

2. The precise satellite position with respect to a reference ellipsoid.

The subtraction of the former from latter gives the sea surface height (SSH) relative to the reference ellipsoid at the given location and time (figure 2). In this sense the altimetry measurement gives the absolute geocentric SSH in the terrestrial reference frame. The idea of radar altimeters on board artificial satellites was developed in early 1960s. The first successful radar altimetry experiment was done in the NASA (National Aeronautics and Space Administration) SkyLab in 1974, and the first altimetry satellite was launched on board the Geos-3 spacecraft in 1975. The first altimetry satellite for oceanography was Seasat (1982), followed by U.S. Navy's Geosat (1985-1989), the European Space Agency's (ESA) ERS-1 (1991-1996) and the US-French TOPEX/Poseidon (T/P; 08/1992 - 01/2006). The latter was the first one getting an unprecedented accuracy of 2-3 cm in SLV measurements. This success has motivated the present altimetry missions: ESA's ERS-2 (1995) and ENVISAT (2002), Geosat Follow-on (GFO) (1998) and Jason-1 (2002) which is the successor of T/P. The latter exactly repeats the T/P orbit and is now achieving comparable data, if not of even higher precision [Luthcke et al., 2003].

T/P was the first highly precise altimeter and 'revolutionized' oceanic monitoring. Due to its orbit inclination, T/P measures the global ocean between 66°S and 66°N (figure 3). With an orbit altitude of 1336 km, T/P exactly repeats its ground track every 9.92 days, and the distance between two ascending or descending passes at the equator is 315 km. A description of the numerous altimetry applications can be found in Fu and Cazenave (2001), in terms of of the steady

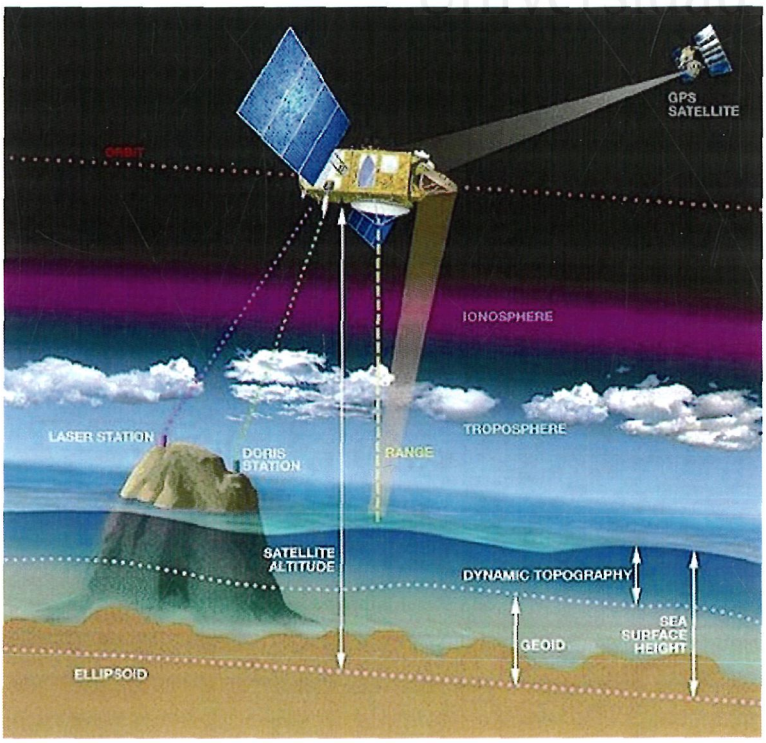

Figure 2: Altimetry principle (source <http://www.aviso.oceanobs.com>).

ocean circulation and its variations (for example, in 1997-1998 the ENSO SLV had been "completely" observed for the first time), currents and eddies, ocean tides, ocean surface waves, geoid and bathymetric determination, and sea level change. The latter is the aim of the present Ph. D. dissertation. As aforementioned, the *relative SL* as a result from TG measurements may be corrupted by vertical ground movements, unlike altimetry which provides the *absolute SL*. An appropiate combination of the two data sets will reveal those vertical ground motions [Nerem and Mitchum, 2002; Cazenave et al., 1999]. Such a study for the Mediterranean and the Black Sea is presented in chapter 4. The resultant map of

Figure 3: T/P ground track.

vertical motions agrees well with vertical velocities estimated from Global Positioning System (GPS) data and the tectonics structure in the region, which validates the methodology and illustrates how altimetry also provides information that can be useful to tectonic studies.

The global mean SL rise has been estimated, with more than a decade of T/P data, to be 2.8 $\pm$ 0.4 mm/year [Cazenave and Nerem, 2004]. However, a value of 0.3 mm/year must be added to this estimation to account for the ocean basin deformation due to the global isostatic adjustment (GIA) [Douglas and Peltier, 2002], yielding a SL rate of change of 3.1 mm/year. This new estimation is $\backsim$70% larger than that estimated for the 20th century by Douglas (2001) and Peltier (2001) from TG data. This implies an acceleration of the SL rise in the last decade, which presumably continues in the future. If this rate holds, the SL may rise between 10-15 cm in the next 50 years producing important socioeconomic and natural changes around the world [IPCC, 2001]. Keeping in mind that 30 % of world population lives within 100 Km distance fromthe coast, and that humans have depended on the ocean for food and economic growth for hundreds of years, this is a very seri-

ous problem with important socio-economics implications. A priori, this SL rise may not be amazing because it has risen, for example, more than 100 meters since the last glacial maximum around 18000 years ago [Kearney, 2001]. However, this SL rise is believed to be associated with anthropogenic global warming of the planet, in particular to the emission of gases to the atmosphere that produce the *greenhouse effect* (reported by Revelle et al., 1965; and supported by several studies as e.g. Levitus et al., 2001). The greenhouse gases retain part of the solar heat which should go to the outer space after being reflected by the Earth surface (see figure 1). It means that the Earth gets an 'extra' heat due to anthropogenic causes, much of which is stored in the oceans. Levitus et al., (2000a) showed that the heat content in the global ocean has been increasing since 1960s. In particular, the global mean temperature increase for the 0-300 meters ocean layer was 0.31°C. Moreover, the temperature increase is neither evenly distributed nor constant in time [Lombard et al., 2005; Antonov et al., 2002].

When Earth's temperature (T) increases a global mean SL rise follows via two separate mechanisms. On the one hand, if the T of a column of water increases (decreases), it will expand (contract), producing the so-called *thermo-steric* SLV. The salinity (S) variations are also significant because when its concentration increases (decreases), the SL will drop (rise), producing the so-called *halo-steric* SLV. The relation between T and S variations and the associated (thermo- and halo-) *steric height* variations is given by the *equation of state of sea water* [Gill, 1982]. The contribution of T variations are more important than S ones, because they produces $\backsim$80% of steric height variations [Steward, 2003]. In that case, the SL rise is affected by a change of volume, with no change of water mass . We will denote these variations by SLV_{steric}. On the other hand, T increase can produce ice melting of polar ice (as Antarctica or Greenland) and mountain glaciers. In that case, the melted water should go to the ocean rising its level via a mass increase. We will denote these variations by SLV_{mass} and it corresponds to the *eustatic* term. The increase of this factor may be partly compensated by the great number of dams constructed in the second half of 20th century, and partially favored by the urban development and wetland drainage where water can no longer be absorbed and stored by land. SLV_{mass} also accounts for other water mass variations such as evaporation or precipitation, and oceanic currents in a regional scale. However, when the global ocean is concerned, the addition of all oceanic

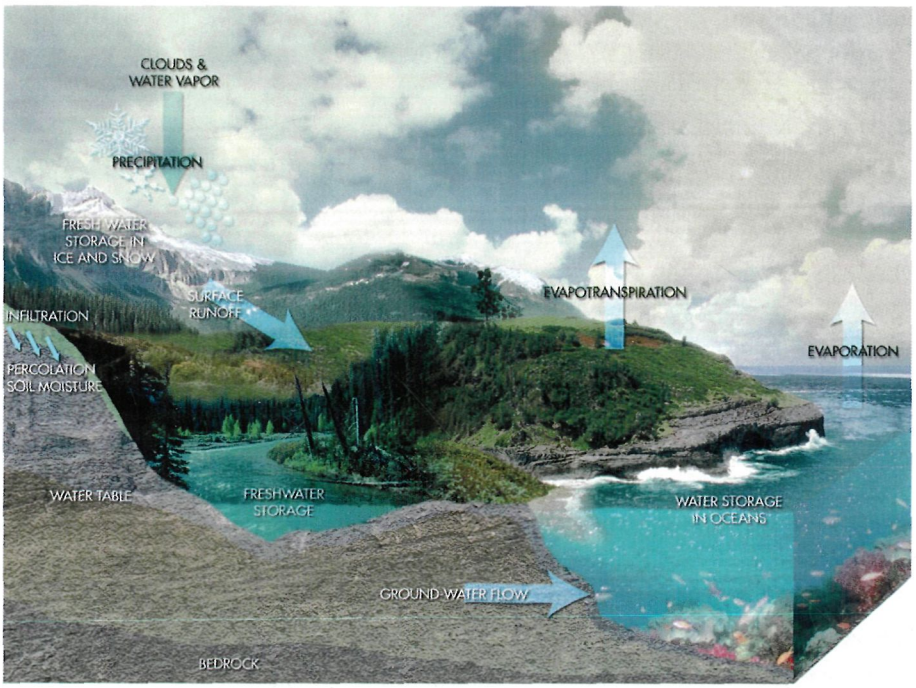

Figure 4: The water cycle represents the exchange of water between ocean, continents and atmosphere (source <http://www.csr.utexas.edu>).

currents vanishes, and then SLV_{mass} only accounts for the water mass exchanged between the global ocean and the continents/atmosphere, the so-called *water cycle* (figure 4).

At present, the scientific community is greatly interested in estimate how much of the observed global mean SL rise, which we will denote SLV_{total}, is produced by SLV_{steric} and how much by SLV_{mass}. Obviously, the addition of the two should return SLV_{total}, with the simple, but important, equation:

$$SLV_{total} = SLV_{steric} + SLV_{mass}. \quad (1)$$

For all 20th century, only 2 variables in this equation could be directly estimated in situ: SLV_{total} via TG data and SLV_{steric} via the combination of the equation of state of sea water and T and S profiles obtained by *in situ* campaigns. However, both kind of data do not cover the whole ocean, with sampling problems in the Southern hemisphere. Since the 1990s, altimetry overcame the problem of sampling to estimate SLV_{total}. With the compilation of the first global gridded ocean temperature data set by Levitus et al. (2000b), followed by several others [Levitus et al., 2005; Ishii et al., 2005; Willis et al., 2004], the SLV_{steric} component can be globally estimated. But still no direct measurement of SLV_{mass} were available, therefore the only way to estimate it was subtracting SLV_{steric} from SLV_{total}, according to equation 1. Other indirect methods to estimate SLV_{mass} are based on studying the variations of the continental waters from observations of total land ice -glaciers and ice sheet- melt (e.g., Meier and Dyurgerov, 2002; Rignot et al., 2005) as well as from model estimates of land water storage change [Milly et al., 2003; Ngo-Duc et al., 2005a]. This however is infeasible at present because such estimates are by no means good enough.

To solve equation 1, two different approaches are possible depending on the time scale of interest, namely inter-annual and annual (seasonal cycle). In the first case, different conclusions were reached at the beginning of 21st century. Cabanes et al. (2001) stated that global mean SL rise was fully explained by thermal expansion in the 2nd half of last century. While Miller and Douglas (2004) thought that this conclusion is a consequence of an error in the interpolation of the hydrographic data used. Recent studies (e.g. Lombard et al., 2005; Antonov et al., 2005) shed some light on this debate, revealing a difference between the global mean SL rise and the thermo-steric component (see below). The analysis of TG data for the last century reveals a SL rise of 1.8 mm/year [Douglas, 1997, 2001; Peltier, 2001], and the analysis of the same data of the past 55 years yields a SL rise of 1.7 mm/year [Holgate and Woodworth, 2004]. However, the SLV_{steric} estimated from T profiles from the surface to 3000 m, in the 2nd half of last century, shows a steric SL rise of 0.4 mm/year. Then, 1.3 mm/year left to be explained due to SLV_{mass}, according to equation 1. During 1993-2003, a similar scene is observed– a rise of 3.1 mm/year and 1.6 mm/year is estimated for SLV_{total} and SLV_{steric}, respectively, from altimetry and T profiles. The difference between them is 1.5 mm/year, which should be produced by SLV_{mass}. Another important

	Linear rate of change (mm/year)		
Period	SLV_{total}	SLV_{steric}	SLV_{mass}
1950-2000	1.7	0.4	1.3
1993-2003	3.1	1.6	1.5

Table 1: Linear rate of change (mm/year) of the different components of equation 1 over the global ocean for 2 periods: 1950-2000 and 1993-2003. SLV_{total} has been estimated from TG data in the first period and from altimetry data in the second one. SLV_{steric} has been estimated from T profiles and SLV_{mass} from equation 1: $SLV_{mass} = SLV_{total} - SLV_{steric}$.

argument in favor of the existence of the eustatic term comes from the analysis of S data, which shows that ocean water is freshening [Antonov et al., 2002]. Therefore, it seems that SLV_{mass} plays an important role in SL rise, contrary to Cabanes et al. (2001). Besides, the increase of the eustatic term seems to be constant (1.3-1.5 mm/year) during last 50 years, unlike the steric term. Then, the acceleration of SL rise in the 1990s is associated to an acceleration in the thermo-steric term. These results are summarized in table 1.

In the second case, less controversy appears when equation 1 is applied to the seasonal cycle. Several previous studies [Chen et al., 1998; Minster et al., 1999; Cazenave et al., 2000;Milly et al., 2003] have also inferred SLV_{mass} from equation 1, using T/P altimetry and climatological ocean temperature data, and they have shown that it is well explained by seasonal variations in atmospheric water vapor content and in land water storage (as estimated from outputs of global land surface models). SLV_{total} shows an annual amplitude of $\backsim$9 mm with a maximum between late September and early October and SLV_{steric} shows an annual amplitude of $\backsim$5 mm with a maximum in mid-March. Note that both signals are out of phase. Then, the inferred eustatic term, i.e. $SLV_{mass} = SLV_{total} - SLV_{steric}$, shows an annual signal with an amplitude of $\backsim$9 mm and a maximum phase in mid-September. This signal agrees quite well with the water mass change estimated from atmospheric and hydrologic continental models. In the comparison, a small residual with annual amplitude 2.9 mm and maximum in December 30, has been explained by Cazenave et al. (2000) as the Antarctica ice sheet mass

balance.

As aforementioned, the eustatic SLV is produced by water mass variations, this mass anomaly produces gravity variations. In recent years space missions have been designed in order to have the capability of measure the *Time-variable gravity (TVG)* field of the earth regularly in both time and space. They include

- CHAMP (Challenging Minisatellite Payload) mission -launched in 2000. The gravity variations are inferred from orbital perturbations measured with GPS and from a high-precision three-axes accelerometer which measures the surfaces forces accelerations as a correction term.
- GRACE (Gravity Recovery And Climate Experiment) mission -launched in 2002. This mission inherits the CHAMP techniques, but with much improved accuracy by utilizing the variations of the distance between two satellites following each other in tandem in the same orbit.(figure 5) [Tapley et al., 2004a, 2004b].
- GOCE (Gravity Field and Steady-State Ocean Circulation Explorer) mission - to be launched in 2006. A combination of highly accurate gradiometer to measure high resolution features and satellite to satellite tracking by GPS to obtain low resolution data, will measure the second-order derivative of the gravitational potential of the Earth in a low orbiting satellite by differential accelerometry.

In this dissertation, we use GRACE data to estimate the SLV_{mass}. The GRACE mission is a joint project between NASA and the Deutsches Zentrum für Luft - und Raumfahrt (DLR), the German space agency. The two identical satellites of this mission were launched on March 17, 2002. They follow a near-circular orbit at $\backsim$500 km altitude and 89.5° inclination, separated from each other by approximately 220 km along-track, and linked by a highly accurate inter-satellite, K-Band microwave ranging system. The distance variations between both satellites are converted to gravity variations [Jekeli, 1999].

The earth system is mass conserving. However, the *geopotential*, that is the gravitational potential of the Earth system, depends on its mass distribution. The

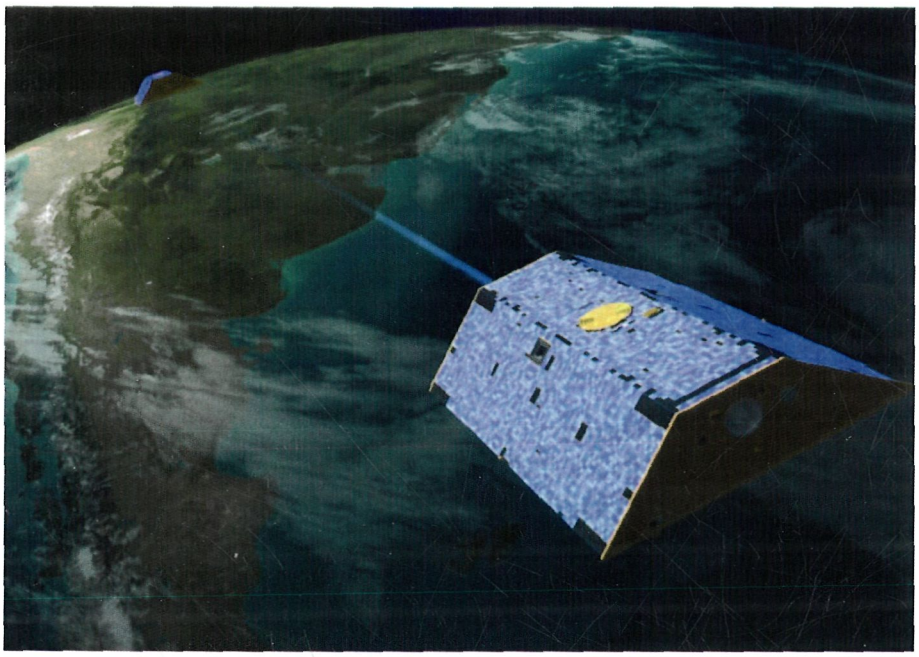

Figure 5: GRACE satellites (source <http://www.earth.nasa.gov>).

problem of estimating the former from the latter is known as the *direct problem* of potential theory, which has a unique solution following Newton's integral (A.6).

GRACE mission measures the geopotential changes, that is, the TVG of the earth. Is it possible to infer the mass redistribution that produces such TVG changes? This question is the so-called *inverse problem of potential theory*. However, this problem has infinite solutions. If it is assumed that the mass redistribution is produced in the surface of the earth, the situation radically changes and then a unique solution arises [Chao, 2005]. But, can we make such an assumption to estimate the Earth system's water cycle? After some geophysical correction have been applied to GRACE data (see appendix A.6 or Bettadpur, 2004a; for further details), only mass redistribution on the surface of the earth is observed at

a seasonal scale, because all other processes inside the earth at such frequencies are eliminated during the data processing. Other remaining processes, as for example the redistribution of mass in the mantle produced by the GIA, show small linear trends, but no seasonal cycles. For that reason, when looking at the seasonal scale, we will assume that the geopotential changes are produced by surface mass redistributions, which are mainly produced by water mass redistribution within the water cycle. Then, it will be possible to estimate the *surface mass anomaly* generating the observed TVG changes [Wahr et al., 1998; Chao, 2005]

GRACE mission has quickly become a fundamental tool to estimate mass changes on the surface of the earth, which, next to the atmospheric variations that are removed beforehand based on atmospheric models, are mainly produced by water mass redistribution within the water cycle. Chambers et al. (2004) was the first estimating the global SLV_{mass} from GRACE data, obtaining a very good agreement with non-steric altimetry data ($SLV_{total} - SLV_{steric}$). Both direct and indirect estimation of SLV_{mass}, show a seasonal exchange of water mass with the continents which has an amplitude of $\backsim$8.5 mm and a maximum in early- to mid-October. This result agrees well with previous studies [Chen et al., 1998; Minster et al., 1999; Cazenave et al., 2000], validating GRACE's capability to measure SLV_{mass}.

The GRACE mission has numerous applications. For instance, Wahr et al. (2004) estimated the mass variation of the Mississippi River basin, Amazon River basin and the Bay of Bengal (South Asia), showing a good agreement with hydrology models. In Greenland, Velicogna et al. (2005) have estimated a seasonal cycle with a peak-to-peak variation of 16 cm of water thick equivalent and a maximum in April/May. GRACE has also been used to estimate continental water storage [Schmidt et al., 2005; Ramillien et al., 2005], evapotranspiration [Rodell et al., 2004] and river run-off [Chao and Au, 2006]. As another example, flooding in Central Europe in summer 2002 and drought in Western Canada in 2003 have also been seen in the GRACE data [Andersen and Hinderer, 2005].

So far we have introduced the SLV from the global oceans, but oceans are not homogeneously subject to the same conditions such as heat or water fluxes. Thus when talking about changes in global SL, we are averaging the geographical distribution of the SLV. Obviously this geographical distribution is of high

interest and studies cannot be carried out without paying particular attention to the different ocean basins, or regions thereof. In particular, here we would like to focus our attention to the Mediterranean Sea which is vital to the livelihood of a large surrounding population. The need to understand and forecast the SLV and their ocean dynamics is increasing significantly. But local studies are necessary given the different conditions that drive the dynamics of this near-enclosed basin. For example, its SL was dropping from 1960s to early 1990s, unlike the global ocean [Tsimplis and Baker, 2000]. In the 1990s, the rate of change of the Mediterranean SL was about an order of magnitude larger than the one of the global ocean [Cazenave et al., 2001]. Due to its special behavior, the Mediterranean sea must be studied separately. Part of this dissertation will be dedicated to understanding the spatial and temporal variabilities of SL and the dynamics and balance of water mass transport in the Mediterranean Sea and the Black Sea when feasible.

In chapter 1, a decade of altimetry data are used to study the SL tendency of the Mediterranean and Black Sea. Several studies [Cazenave et al., 2001, 2002; Fenoglio-Marc, 2001, 2002] analyzed the SLV in the Mediterranean from altimetry data for the period 1993-1999, which was an order of magnitude larger than the global average. An SL rise in the whole Mediterranean, although less pronounced in the Western basin, was observed with the only exception of the Ionian Sea where the SL was dropping. This pattern was highly correlated with SST, showing that it probably was driven by steric height variations. In our study, the span of altimetry data is extended up to 2003 and a change of this pattern is observed in mid-1999. After that, little correlation between SLV and SST is observed. The reported change of tendency will be placed in the framework of thermohaline circulation changes in the eastern Mediterranean in 1999, in particular with the end of the Eastern Mediterranean Transient (EMT). On the other hand, a similar change of tendency is observed in the Black Sea in 1999. However, the reason of its origin seems to be related to interannual-to-decadal fluctuations.

The importance to study the Mediterranean Sea is further enhanced as it has an added value given its near-enclosed nature that makes it a natural laboratory to validate GRACE data. The Mediterranean is surrounded by land with the only connection to the open ocean through the narrow Gibraltar Strait (see figure 6). It means that the Mediterranean water mass budget may be monitored with enough

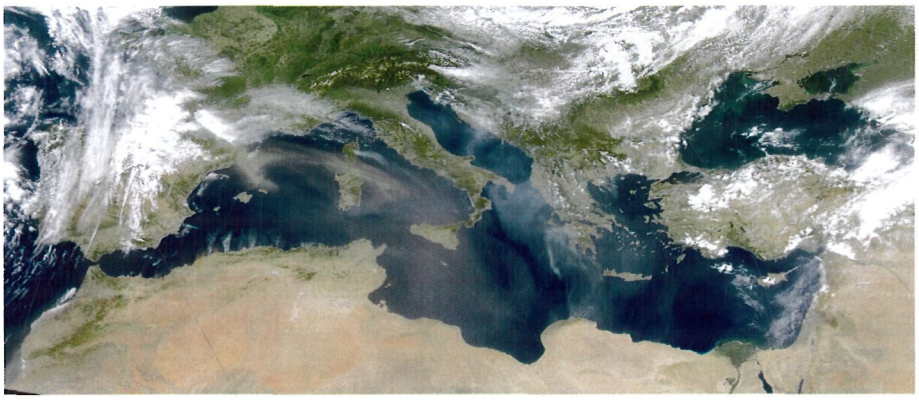

Figure 6: Mediterranean Sea (source <http://visibleearth.nasa.gov>).

data, namely: precipitation (P), evaporation (E), river run-off (R) and the flux of water through the Gibraltar Strait (denoted GF from Gibraltar Flux). Let the water influx into the Mediterranean be of positive sign,then,

$$\Delta M_{med} = P - E + R + GF, \tag{2}$$

where ΔM_{med} is the water mass variation of the Mediterranean. Therefore, the Mediterranean has the special characteristic that its water mass budget may be a priori tractable independently from GRACE mission.

In chapter 2, the eustatic term of the annual SLV, that is SLV_{mass}, in the Mediterranean Sea is directly and indirectly estimated for the period 04/2002–07/2004. The indirect estimate is the difference $SLV_{total} - SLV_{steric}$, where SLV_{total} is estimated from altimetry data and SLV_{steric} from T and S profiles, which are outputs of the ECCO (Estimating the circulation and climate of the ocean) ocean model[1]. The latter are used because of the unavailability of real T and S data for the very recent period of time. SLV_{mass} is estimated directly from GRACE data, and then compared with the indirect estimate of the same quantities. A very good agreement is observed between both methods, showing a clear annual

[1] <http://www.ecco-group.org>

signal in the Mediterranean water mass budget. As an application, the GF has been estimated combining P and E data derived from the proxy atmospheric humidity data as provided by the National Center for Environmental Prediction (NCEP) atmospheric global circulation model [Chao and Au, 2006], with GRACE data. Then, a good agreement is observed in phase with previous GF estimates from buoys [Garcia-Lafuente et al., 2002].

In chapter 3, once the GRACE's ability to estimate the SLV_{mass} term has been demonstrated in the Mediterranean Sea, we return to the global ocean problem. Chambers et al. (2004) showed the GRACE ability to estimate the global SLV_{mass} term, validating the GRACE estimate with the non-steric altimetry result. However, they did not use monthly data, but averaged years of altimetry and T and S fields. Thus, we propose to go a step further, doing the comparison with monthly data corresponding to the studied period. In that case, the importance of the mean sea level pressure (MSLP) over the whole ocean can be highlighted. This factor, when it is not accounted for, can produce a fictitious phase displacement of 30^{o} ($\backsim$1 month). As an application of these improvements, the SLV_{steric} term has been estimated as $SLV - SLV_{mass}$, showing a very good agreement with the estimation of SLV_{steric} from the existing T and S data. In the future, this methodology may overcome sampling problems in the collection of T and S data. As another application, the total ocean water mass budget implicated in the cycle water has been estimated.

In chapter 4, a comparison of SLV data from altimetry and 42 TG, from the Mediterranean and the Black Sea, is conducted. As aforementioned, the differences between these measurements contain information about the vertical land movement along the coast where the TG are located. As a result, a map of vertical motions along the Mediterranean and Black sea coasts can be obtained. This result is validated with GPS vertical velocities estimates and regional tectonic models. In general a good agreement is observed, showing that this technique can be very useful to obtain independent vertical motion estimates complementary to those from GPS, which can be used to constrain/validate tectonic models.

Chapter 1

Sea Level Trend in Mediterranean and Black Seas

1.1 Introduction

In this chapter we examine the sea level variations (SLV) in the Mediterranean and Black Seas, as a function of space and time. Here we define SLV as the non-tidal, non-seasonal signals relative to the 'static' mean geoid; our timescale of interest is longer than 1 month. The Mediterranean SLV has been enigmatic, and, as we will show, continues to be so. From historical records it was known that around 1960 the mean sea level (MSL) of Mediterranean underwent a change of average rate from a general rise of +1.2/1.5 mm/year to a drop at a rate of about -1.3 mm/year [Tsimplis and Baker, 2000]. The MSL drop continued in the Mediterranean till early 1990s. Less dramatic changes took place in the Atlantic where the rate changed from +1.8 mm/year to +1.1 mm/year around 1960, while that of the Black Sea stayed around +2.2 mm/year. The relation between the Mediterranean sea level and the North Atlantic Oscillation (NAO), in terms of the so-called NAO index, has been examined by, e.g., Tsimplis and Josey (2001) and Woolf et al. (2003). The NAO is a large scale variation in atmospheric pressure between the Azores and Iceland, and the NAO index consists on the pressure difference between the mentioned places. Using altimetry and tide gauge data

during the last decade, positive correlation around northwest Europe and negative correlation around southern Europe and northeastern North America were found. This Mediterranean-NAO correlation pattern was also appreciated for the whole 20th century [Hurrell, 1995]. NAO's influence on the Mediterranean sea level is largely uniform although stronger in the north Adriatic than in south Greece and northern Levantine Basin. Furthermore, a change of NAO index from negative to positive states during 1960-1990 was connected with the afore-mentioned change in the Mediterranean MSL rate in 1960 [Tsimplis and Josey, 2001].

Cazenave et al. (2001, 2002) studied T/P altimetry data from 1993 to 1999 for the Mediterranean, reporting a general rise in the Mediterranean SL except in the Ionian where a drop was observed. This new pattern in the Mediterranean SL is very well correlated with that of the sea surface temperature (SST) for that same time period. Tsimplis and Rixen (2002) indicated that the Ionian upper water was subject to strong heating in 1985-1990 and a subsequent cooling, and that the Levantine basin was cooled after 1990 with a minimum in 1994. Thus it appears that the pattern is a return of a previous situation [Tsimplis and Rixen, 2002]. This pattern has also been reported in other studies [Fenoglio-Marc, 2001, 2002].

With the background of the above knowledge, we will perform a comprehensive study of the Mediterranean and Black Seas' SLV for an eleven years period using multi-mission ocean radar altimetry data, primarily T/P's. Upon confirming the known pattern and correlation with SST for the earlier period of 1993-1998, we will report a reversal of this SLV pattern that occurred around mid-1999, after which the correlation with SST virtually disappeared in the Mediterranean. Corresponding, but significantly different, behavior is found for the Black Sea. We will examine these variabilities, and place them in the framework of thermohaline circulation changes in the eastern Mediterranean in 1999 and of interannual to decadal fluctuations in the Black Sea, which appear to be two separate and distinct dynamic systems.

1.2 Data Analysis and Results

The altimetry data used are monthly SLV maps, on a $1^o \times 1^o$ grid, solved from the ocean radar altimetry data from satellite missions of T/P, Jason-1, ERS-1/2 and

ENVISAT for an 11-year period of 01/1993 - 11/2003. Data are a combination of T/P+ERS, except for the period 01/1994 - 03/1995 (ERS-1 geodetic phase), up to August 2002, when Jason-1 replaced T/P. ERS-2 was also replaced by ENVISAT since 06/2003. SLV are given in units of cm, where a 7-year (01/1993 - 01/1999) T/P mean map representing the static geoid is removed from the altimeter data. There are about 310 grid points in the Mediterranean and about 61 grid points in the Black Sea. Several corrections have been applied to the data: orbit error reduction of ERS and ENVISAT via the precise orbit of T/P and Jason-1, geophysical (dry and wet troposphere, ionosphere and inverse barometer effect), sea state bias, and tides (ocean and load tides, solid earth tide and pole tide). For further details see Aviso (1996, 1998). Whether one should allow inverse barometer (IB) correction or not in this case is debatable as it was noted that IB is not prevalent for the Mediterranean Sea at relatively short periods [LeTraon and Gauzelin, 1997] nor for the Black Sea [Ducet et al., 1999; Tsimplis et al., 2004]; we here use IB corrected data as we are interested in long-period variations, and mean atmospheric pressure has small effect due to its small seasonal and interannual changes. In any case, we have also reproduced the study with T/P data for the period 10/1992 - 07/2002 without applying the IB correction (see below) and the differences in the linear rates of change are small (as in previous studies, e.g., Ducet et al., 1999) relative to the level of amplitudes that are of interest in the results we are presenting here. The only appreciable difference occurs in the Adriatic Sea, and it is due to the lower resolution of the T/P data versus the multimission data used in this study (multimission data has 9 extra points covering the northwest area where the negative linear trend is observed after 1999).

The data span 01/1993 - 11/2003 (11 years) will be referred to as the "whole period". The whole period will be divided into two parts to accommodate for the abrupt change in the SLV behavior that took place around mid-1999: Period I = 01/1993 - 06/1999 (6.5 years), and Period II = 07/1999 - 11/2003 (4.5 years). The first part 07/1999 - 06/2002 (3 years) of Period II, called Period IIa, is sometimes further singled out for more detailed study.

The sea surface temperature (SST) anomaly data set is provided by NOAA (National Oceanic and Atmospheric Administration). We use the National Center for Environmental Prediction (NCEP) Optimally Interpolated (OI) SST version 2 data set which is produced monthly on a $1^o \times 1^o$ grid for the same period of time as

for SLV above. The analysis uses SST from the Advanced Very High Resolution Radiometer (AVHRR) on board of NOAA satellites, and in situ SST collected from buoys and ships. AVHRR measures emitted and reflected radiation from Earth in two visible channels and three infrared channels. Before the analysis is computed, the satellite data is adjusted for biases using the method described in Reynolds (1988). The bias correction improves the large scale accuracy of the OI. A description of the OI analysis can be found in Reynolds et al. (2002).

Both SLV and SST data series are dominated by strong seasonal signals, primarily annual and semi-annual. We are only interested in the non-seasonal, especially the interannual, anomalies. Thus, as the first step in processing the data, we least-squares fit the time series point by grid point, for the given time span as the case may be, with annual and semiannual sinusoids. Then we remove the latter by simple subtraction from the data, forming a new, non-seasonal series of maps. The average annual amplitude of the SLV that we remove is about 7.5 cm for the Mediterranean Sea, and 2.5 cm for the Black Sea, and for the semi-annual is 1.1 cm for the former and 1.7 cm for the latter. The seasonal signals will be studied in chapter 2 together with the GRACE TVG data. Once the seasonal signal has been removed, we can assume a linear relation between the data, $\{y_i\}_{i=1}^n$, and the time, $\{t_i\}_{i=1}^n$, that is,

$$y_i = a \cdot t_i + b + \varepsilon. \tag{1.1}$$

If the errors in the data $\{y_i\}_{i=1}^n$, ε, are independent normal with mean zero and constant variance, then the parameters a and b can be approximated as

$$\hat{a} = \frac{\sum_{i=1}^n (t_i - \bar{t}) \cdot (y_i - \bar{y})}{\sum_{i=1}^n (t_i - \bar{t})^2}, \tag{1.2}$$

$$\hat{b} = \bar{y} - a \cdot \bar{x}, \tag{1.3}$$

where $\bar{t} = \frac{1}{n}\sum_{i=1}^n t_i$ and $\bar{y} = \frac{1}{n}\sum_{i=1}^n y_i$. Besides, the standard deviation of $\hat{a}$ can be estimated as

$$\sigma_{\hat{a}} = \sqrt{\frac{\sum_{i=1}^n (y_i - \hat{b} - \hat{a}t_i)^2}{(n-2)\sum_{i=1}^n (t_i - \bar{t})^2}}. \tag{1.4}$$

To validate the altimetry results, we will analyze the monthly tide gauge (TG) data available from the Permanent Service for Mean Sea Level (PSMSL) [Spencer

and Woodworth, 1993]. In PSMSL, there are 42 TGs in the Mediterranean and 7 in the Black Sea with data spanning the altimetry period (01/1993 - 11/2003). However, only few of those TG's have a time span suitable to study the change of linear trend in 1999.

1.2.1 Linear trends in mean sea level (MSL)

To obtain an overall idea of the long-term SLV in the Mediterranean and Black Seas, we first study the time series for the MSL. The previously reported rise in the Mediterranean MSL (as mentioned above) is confirmed for Period I, after which the MSL apparently starts dropping (figure 1.1a). In figure 1.1b the overall MSL curve for the Black Sea shows very dramatically this mid-1999 "kink" in the rate-of-change slope, or linear trend. The same MSL kink for the Mediterranean Sea clearly exists as well, although not as prominent; see figure 1.1a.

Regional break-down of Mediterranean, however, proves more revealing, and hence more insightful, about the behavior of the 1999 kink in the MSL rates of change. We divide the Mediterranean Sea into 6 regions as in figure 1.2 for which figure 1.1c-h examine the regional MSL variations in detail. This division is based upon the regional differences in the SL variability as discussed in detail in the EOF analysis (see section below). Similar divisions have been adopted for the Mediterranean in previous studies (e.g. Tsimplis and Rixen, 2002). Figure 1.3 shows the MSL time series for the different regions, estimated from multimission altimetry corrected for the IB response of the ocean and from T/P non-IB corrected data [Brian Beckley, personal communication, 2004]. It can be seen that there are no significant differences between them, except for the Adriatic Sea, as aforementioned.

The Levantine basin and the Aegean Sea (figures 1.1f and 1.1h) demonstrate a behavior similar to the Black Sea albeit of a smaller magnitude, while the Ionian Sea (figure 1.1d) demonstrates a surprising, completely opposite behavior. This slope drop in the Ionian Sea relative to the pre-1999 rise in the rest of the Mediterranean has been reported from altimetry data [Cazenave et al., 2001, 2002; Fenoglio-Marc, 2001, 2002] that this is a manifestation of a return to the situation of mid-1980s [Tsimplis and Rixen, 2002]. In figure 1.1 we also plot the data series with the seasonal signals, just for comparison purposes. Here we can safely

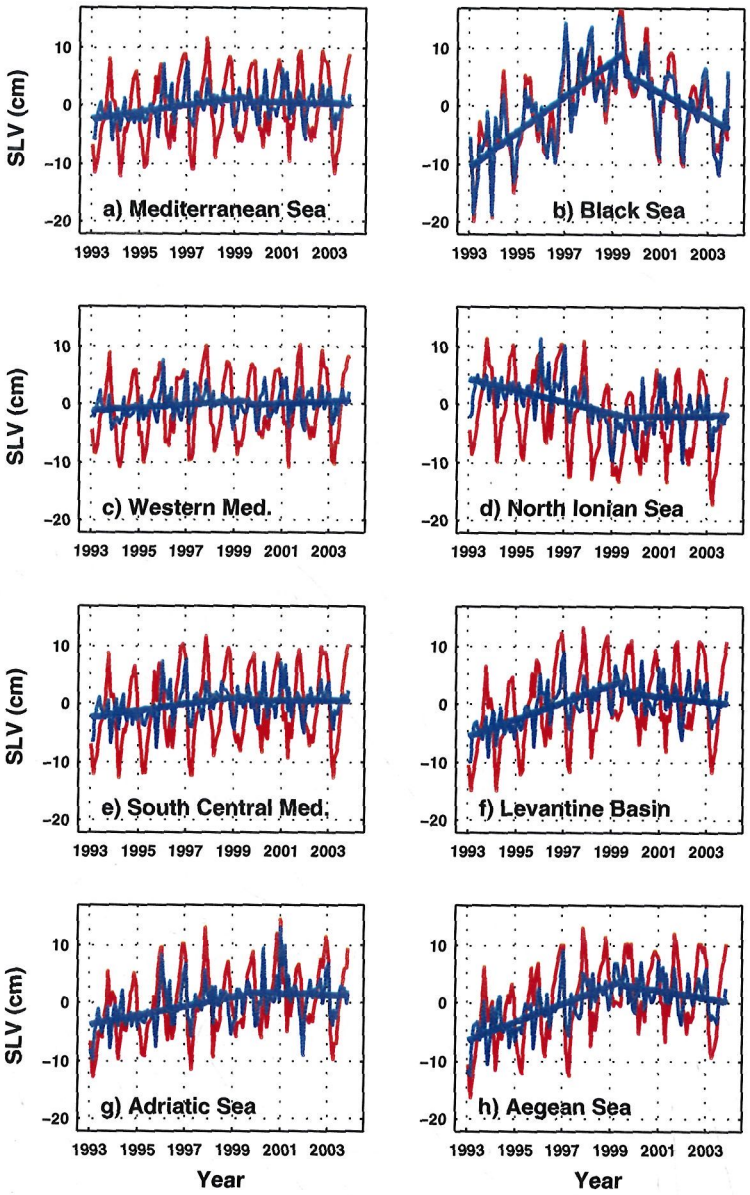

Figure 1.1: A kink in the linear rate-of-change in MSL between Periods I and II. Each time series corresponds to a different region. In all cases is shown the non-seasonal signal (blue curve) and with seasonal signal (red curve).

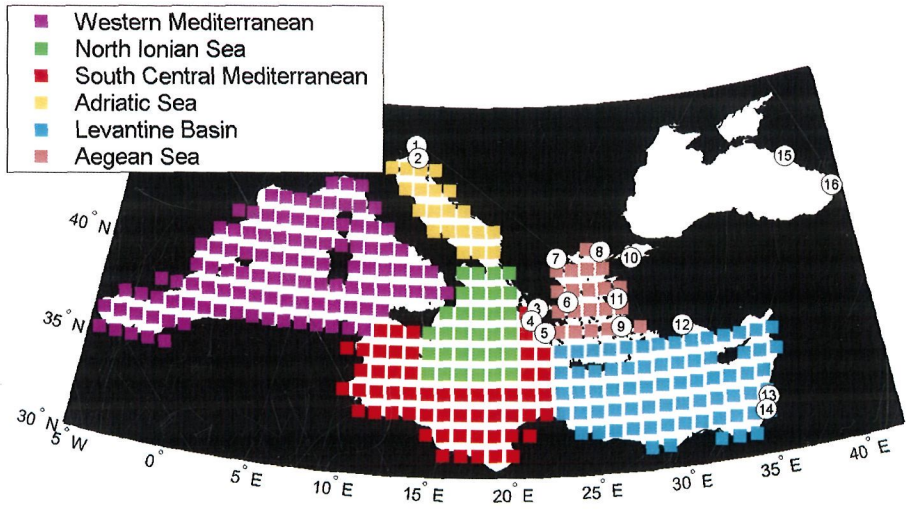

Figure 1.2: Regionalization in the Mediterranean Sea used in this study.

preclude the possibility that the 1999 kink is an artifact due to the switchover of the Side-A to Side-B altimeter on T/P that happened in early 1999, for the following reasons: First of all, the observed sea level changes are simply too large to be related to an instrument calibration error (B. Beckley, personal communication, 2005). Secondly, we note that in 1999 there are three different situations: a) a change from dropping to rising sea level was observed in the Ionian Sea; b) a change from rising to dropping was observed in the Levantine Basin, Adriatic, Aegean and Black seas; and c) no change of trend was observed in the Western Mediterranean. If the change of trend were related to the switchover of the altimeter, one would expect similar changes of trend for all cases.

The MSL rates of change of each region for Periods I, IIa, and II are given in table 1.1. Comparing the values for the latter 2 periods, it can be seen that the behavior is similar between Periods II and IIa in all the regions except in the North Ionian and Black Sea. Generally a decreasing of the rate of change is observed for Period II as compared with Period IIa, indicating that the trending was stronger

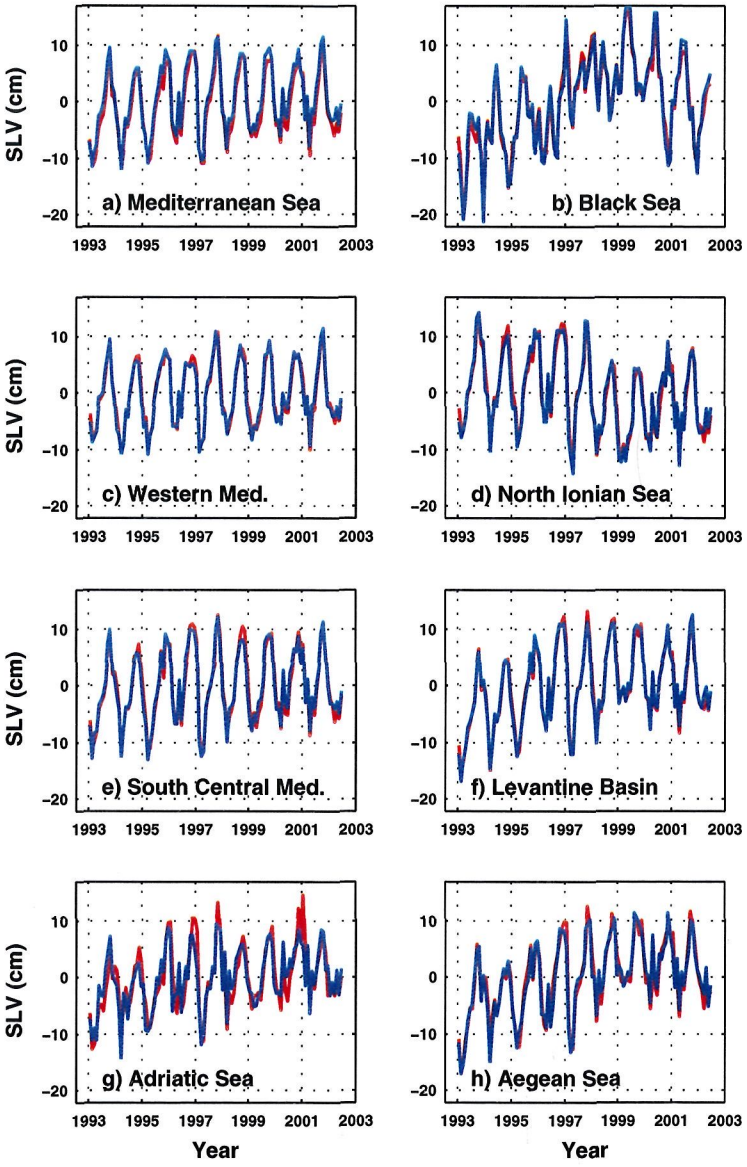

Figure 1.3: MSL variations for different regions. Red curve represents multimission altimetry corrected for the IB response of the ocean; blue curve represents T/P altimetry non corrected for the IB effect.

	Region	Linear rate of change (cm/year) of MSL 01/93 - 06/99 (Period I)	07/99 - 06/02 (Period IIa)	07/99 - 11/03 (Period II)
a)	Mediterranean Sea	+0.6 ± 0.1	0.0 ± 0.5	0.0 ± 0.3
b)	Black Sea	+3.0 ± 0.3	-3.0 ± 0.8	-2.2 ± 0.5
c)	W. Mediterranean	+0.3 ± 0.1	+0.3 ± 0.5	+0.2 ± 0.2
d)	North Ionian Sea	-1.0 ± 0.2	+0.8 ± 0.6	+0.1 ± 0.3
e)	S. cen. Mediterranean	+0.6 ± 0.2	-0.1 ± 0.5	0.0 ± 0.3
f)	Levantine basin	+1.5 ± 0.2	-0.4 ± 0.6	-0.5 ± 0.3
g)	Adriatic Sea	+0.8 ± 0.2	-0.2 ± 0.8	-0.1 ± 0.4
h)	Aegean Sea	+1.6 ± 0.2	-0.6 ± 0.5	-0.6 ± 0.3

Table 1.1: Linear rate of change for MSL, for different regions in the Mediterranean and Black Seas, during three different periods. The error corresponds to 1 standard deviation estimated from equation 1.4.

in the first 3 years after mid-1999. The slowing down in the rate of change when including the last 1.5 years of data does not appear to be related to the replacement of T/P by Jason-1, because in that case such a slow-down would have been perceptible in all the regions.

Next we examine the linear rate-of-change maps of SLV and SST for the Mediterranean and Black Seas. The contours in figure 1.4 and 1.5 depict the respective spatial pattern of the linear rate-of-change, obtained by a least-squares fit of a linear slope at each grid point that makes up the maps.

Figure 1.4 shows the rate-of-change of SLV and SST for the whole period. We can observe a moderate, general sea level rise in the Mediterranean and Black Seas at a rate of less than +0.5 mm/year, with the exception of the north Ionian Sea which dropped at a rate up to -1 mm/year. At the same time, SST exhibited a general rise in the whole Mediterranean and Black Seas with values up to 0.1 ^{o}C/year.

The spatial correlation between the rate-of-change maps of SLV and SST is obvious: 0.5 in the Mediterranean and as high as 0.99 (but see below) in the

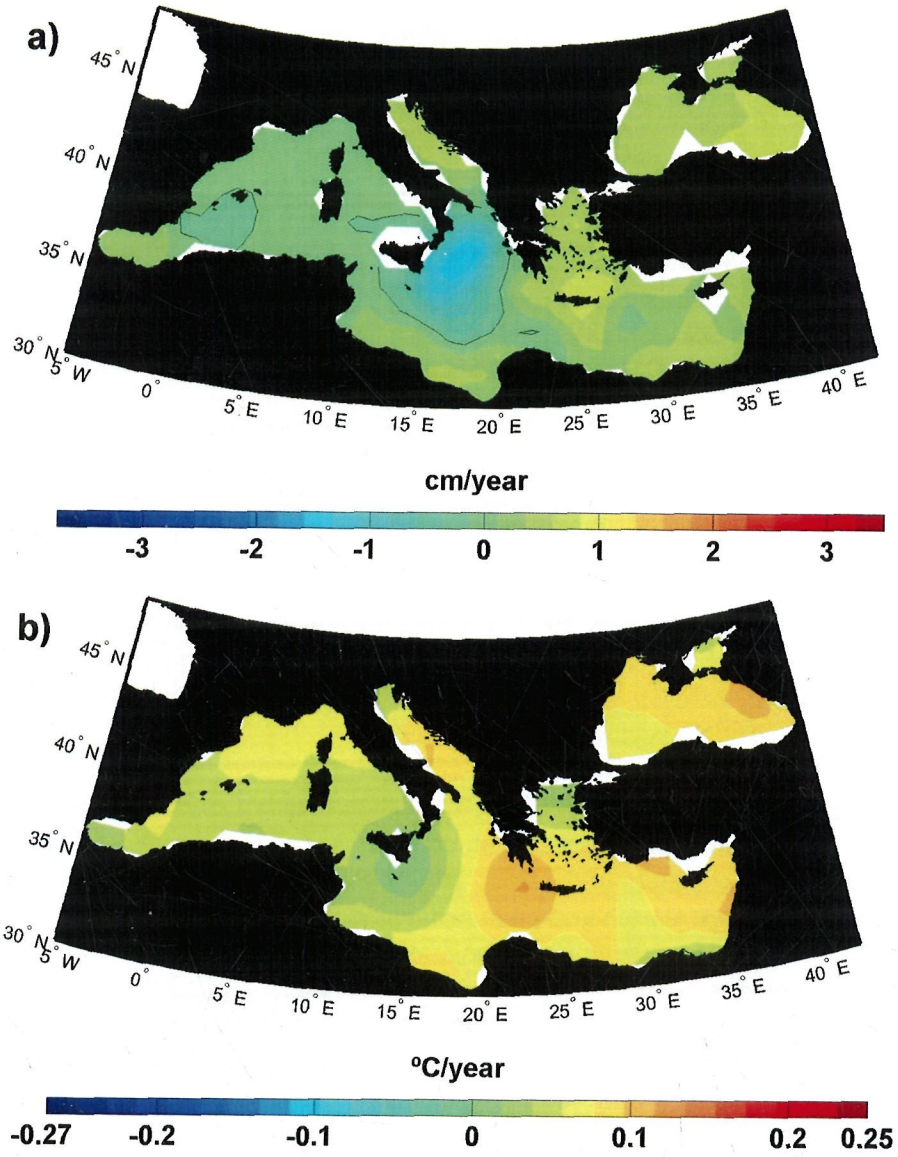

Figure 1.4: Linear rate-of-change map for the whole period, 01/1993 - 11/2003: (a) SLV (cm/year), (b) SST (°C/year)

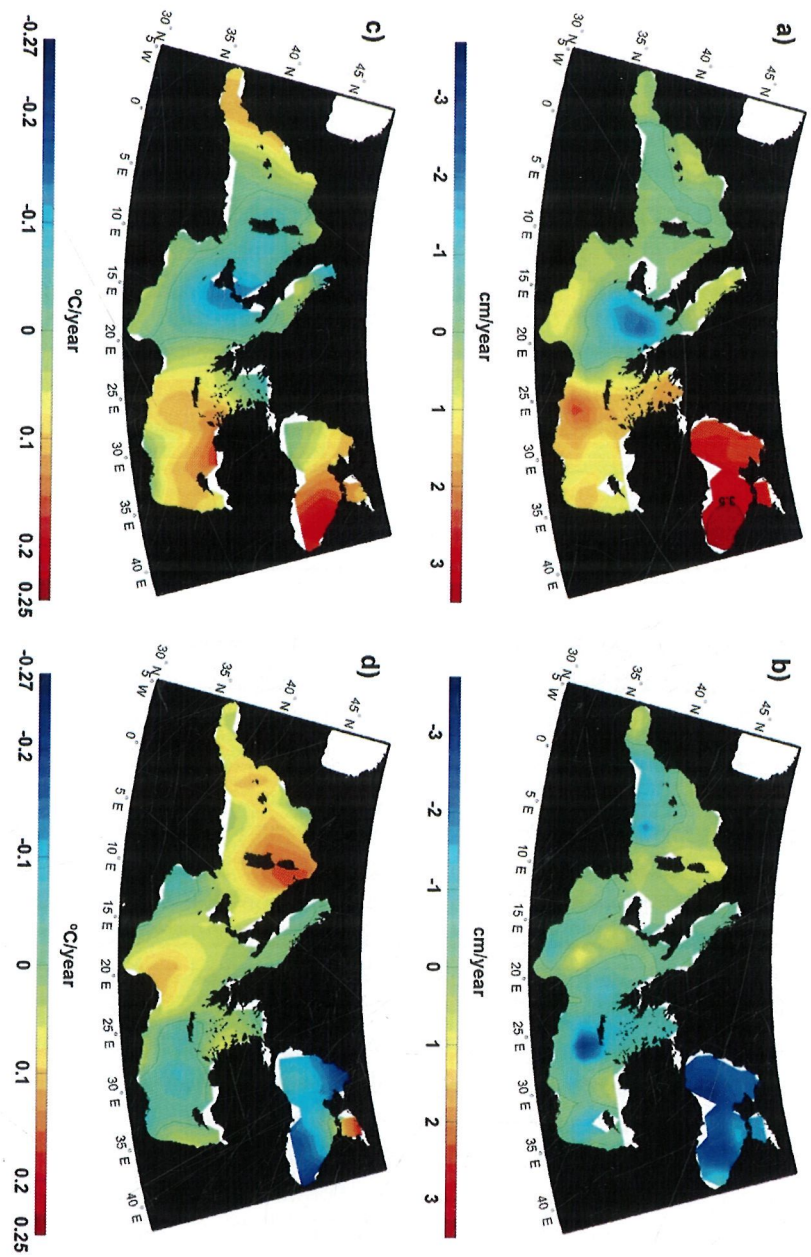

Figure 1.5: Linear rate-of-change map of: (a) SLV for Period I (cm/ year); (b) SLV for Period II (cm/year); (c) SST for the Period I (°C/year); (d) SST for Period II (°C/year). Period I: 01/1993 - 06/1999, Period II: 07/1999 - 11/2003.

	Correlation coefficients (SLV Vs SST)			
Time Period	01/93-11/03 (whole period)	01/93-06/99 (Period I)	07/99-06/02 (Period IIa)	07/99-11/03 (Period II)
Mediterranean Sea	0.51	0.72	0.15	0.17
Black Sea	0.99	0.93	-0.20	0.72

Table 1.2: Spatial correlation coefficient for linear rate-of-change of SLV vs SST.

Black Sea (table 1.2). As SST is an indicator of thermo-steric variations, this correlation implies that the interannual linear trend of SLV has been largely driven by thermo-steric changes in the Mediterranean and Black Seas. Tsimplis et al., (2004) demonstrated that the long-term sea level rise in the Black Sea from mid-1950s to late-1990s was related to changes in P-E (precipitation - evaporation) instead of steric changes. Our result pertains to post-1993 on a shorter timescale, and then it may be related to an interannual oscillation with no trend in the 40-year period studied by Tsimplis et al., (2004). This also manifests the strong dependence of the Mediterranean and Black Seas' behavior on the timescale under consideration.

Based on figure 1.1, it is of high interest to examine the linear rate-of-change maps separately for Periods I and II before and after 1999, as in figure 1.5. For Period I one sees a general SL rise in the Mediterranean Sea where the SST generally rose, and a SL drop in the Ionian Sea where the SST dropped, with the apparent exception of the western Mediterranean basin. The SST, and hence the steric effect, seems to be the major cause of the SL trend, given its high correlation on the pattern (figures 1.5a and 1.5c; table 1.2), as first reported by Cazenave et al. (2001). In contrast, as seen in figures 1.5b and 1.5d, during Period II after mid-1999 this SLV-SST correlation became greatly reduced (table 1.2) in the Mediterranean Sea, where an inversion of the pattern in SLV took place (figure 1.1). Similar phenomenon occurs in the Black Sea, although much less severe. Table 1.2 also reports the spatial SLV-SST correlations for Period IIa. In the Mediterranean Sea, a lower yet correlation between SLV and SST is observed, with virtually no correlations

except perhaps in the Levantine Basin and Adriatic Sea (figure 1.6).

We note that, since the value of the SLV or SST rate is hardly independent from point to point, the statistical degrees of freedom involved in evaluating the above spatial correlation coefficients are rather low relative to the number of the grid points in both cases of the Mediterranean and Black Seas. Therefore the high correlation values for the Black Sea are actually not out of the ordinary, while the low values in table 1.2 do mean weak or no correlation. Here, rather than trying to determine the effective degrees of freedom, the correlation coefficients in table 1.2 should be judged in a quasi-quantitative and comparative manner.

In summary, the results above indicate that some oceanographic change took place in mid-1999, when certain factor seemingly related to changes in thermohaline circulation became more relevant for SLV in the Mediterranean Sea to the detriment of the steric effect. Similarly, a significantly lower SLV-SST correlation appeared for the Black Sea during Period IIa, presumably related to a 4-5 year periodicity in SST (e.g., Cazenave et al., 2001) but absent in SLV. The 1999 kink in the rate of-change in the Black Sea could be part of the interannual to decadal variability reported by Tsimplis et al. (2004).

We should emphasize that the above results only apply to the linear trends and the corresponding rate-of-change maps for SLV. While the SLV series see a clear kink in 1999 as above, the corresponding SST series (figure 1.7) only exhibit general interannual fluctuations, with little indication of such a kink.

1.2.2 EOF/PC spatial-temporal variations

To determine the spatial-temporal variations of SLV and SST in more detail, we conduct an Empirical Orthogonal Function (EOF) analysis with their associated time series (or the Principal Components PC) (e.g., Preisendorfer, 1988), done separately for the Mediterranean and Black Seas. We shall normalize the EOF maps to unit variance, so that the PC time series has the unit of cm. Remember that the seasonal signals have already been removed, and the following describes the non-seasonal anomalies.

Let us examine the first two EOF/PC modes of SLV in the Mediterranean for the whole period of 01/1993 - 11/2003. The first EOF (figure 1.8a) explains 55% of the variance of the data and we see that every point has the same sign (here

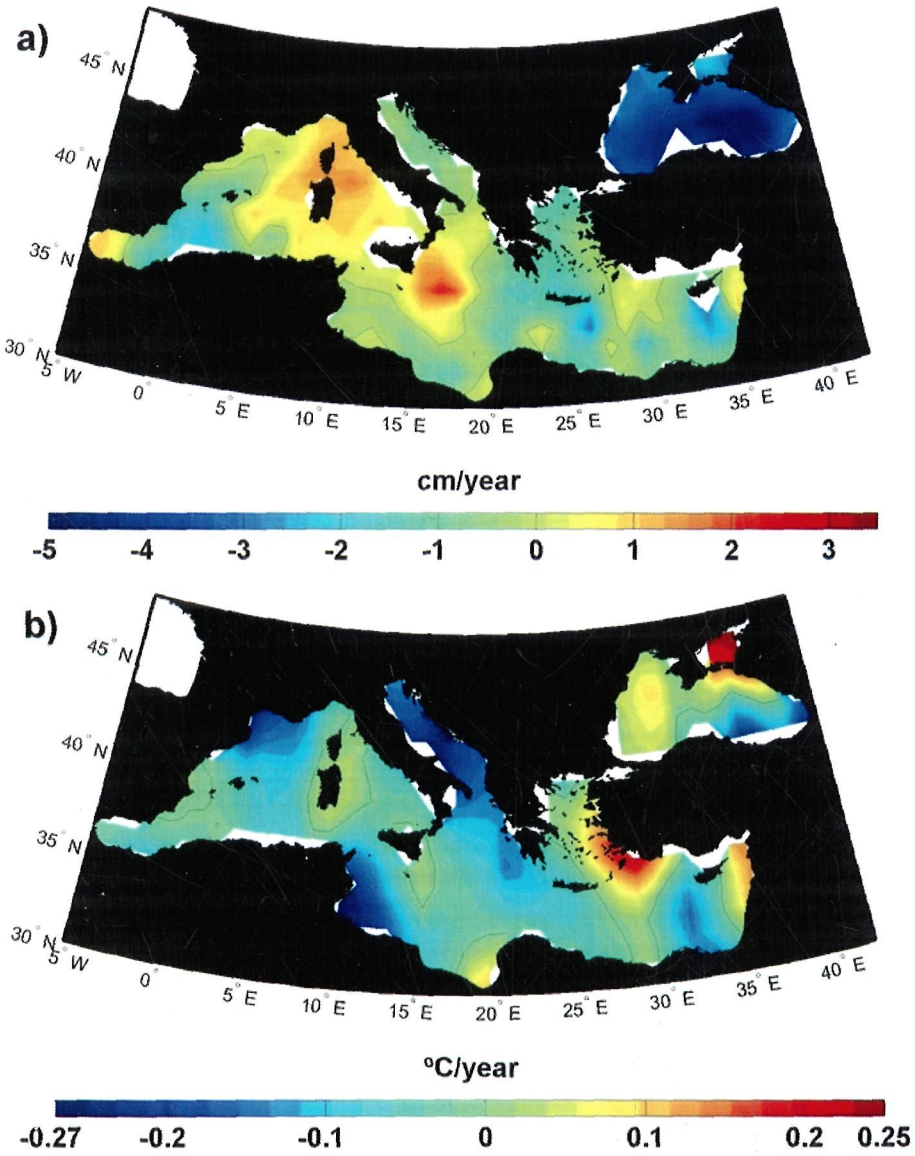

Figure 1.6: Linear rate-of-change map for the period IIa, 07/1999 - 06/2002: (a) SLV (cm/year), (b) SST (°C/year)

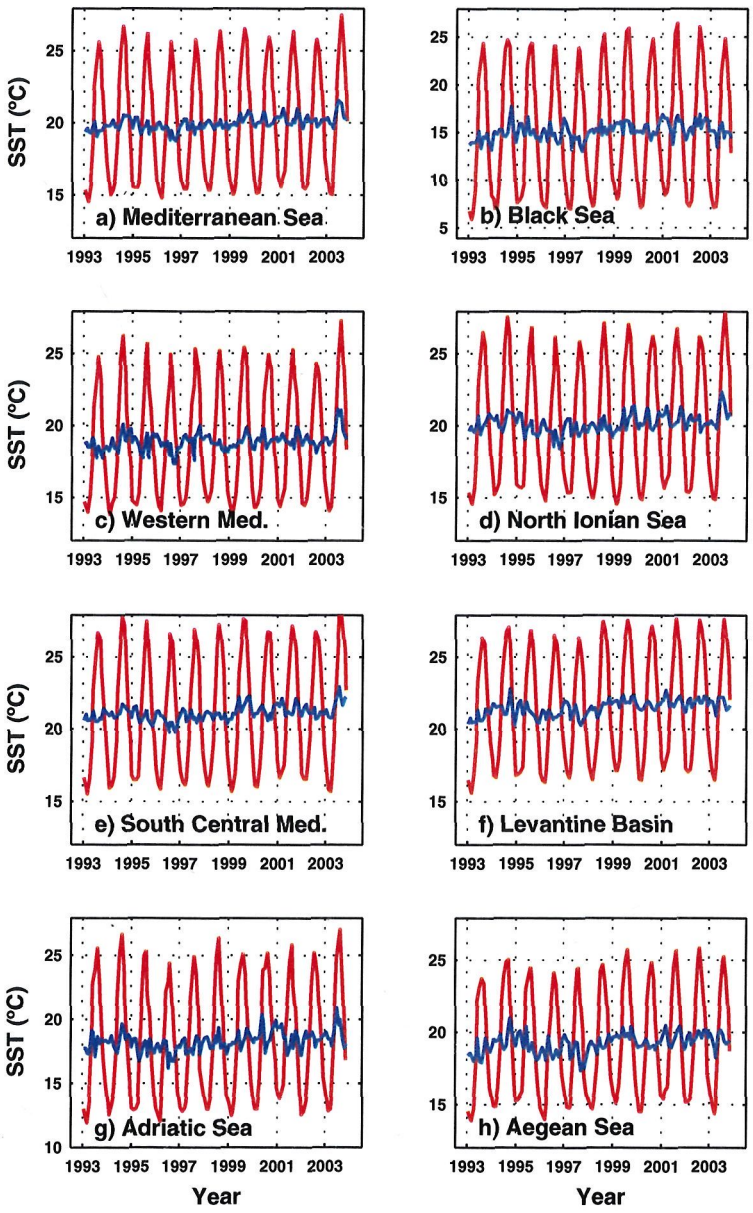

Figure 1.7: Mean SST averaged over the regions described in figure 1.2. Red and blue curves represent the seasonal and non-seasonal signal, respectively.

taken as positive), implying a "breathing" mode or an oscillation of the whole Mediterranean moving up or down in phase. The peak-to-peak amplitude of this mode is on the order of 2 cm. Conceivably this can be a manifestation of an in-phase heating or cooling of the whole Mediterranean, or simply an addition or loss of water mass that is distributed over the whole Mediterranean. Fukumori et al. (2003) suggest that this oscillation is associated with wind-driven mass transport across the Strait of Gibraltar. A wind driven transport in the Strait should have a baroclinic compensation while this "breathing" mode actually implies a barotropic net exchange between the Mediterranean and the North Atlantic. Even though the SL data has been corrected for an IB effect the oscillation implied by this mode could be mainly driven by the atmospheric pressure difference between the Mediterranean and the North Atlantic as the simple analytical model proposed by Candela et al. (1989) might suggest. The corresponding PC time series showing no significant trend, implies this mode has little to do with the 1999 kink in SLV.

On the other hand, the second EOF (figure 1.8b), which explains 16% of the variance, is nearly identical to the SL rate-of-change map in the Mediterranean for the whole period (figure 1.4). This mode corroborates our findings above with respect to the change of behavior associated with the 1999 kink and observed in figure 1.5a,b, as follows. The positive points in the EOF pattern undergo the same variations as the PC, and the negative ones undergo the variation of the inverse of the PC. In both cases, the relation to the PC is proportional to the magnitude of the value of the point in the EOF pattern. The PC shows a positive trend up to mid-1999 and a negative one afterward. As the third and subsequent EOF's explain less than 4.6%, which is not a significant percentage of variance, it can be inferred that the information related to the linear trends is summarized in the second EOF. Therefore, a positive region with high values will undergo a positive linear trend up to 1999 and a negative one afterward, and vice versa. We can observe negative high values in the Ionian sea and positive high values in the Levantine Basin and the Aegean Sea, meaning an SL drop in the former and a rise in the latter till 1999, and a reversal of the pattern after 1999. This leads us to break down the Mediterranean into 6 regions as done in figure 1.2. The change in trend before and after 1999 is about 0.7 cm/year, agreeing with those found in figure 1.1a and table 1.1 above.

The first two EOF/PC modes of SST in the Mediterranean for the whole pe-

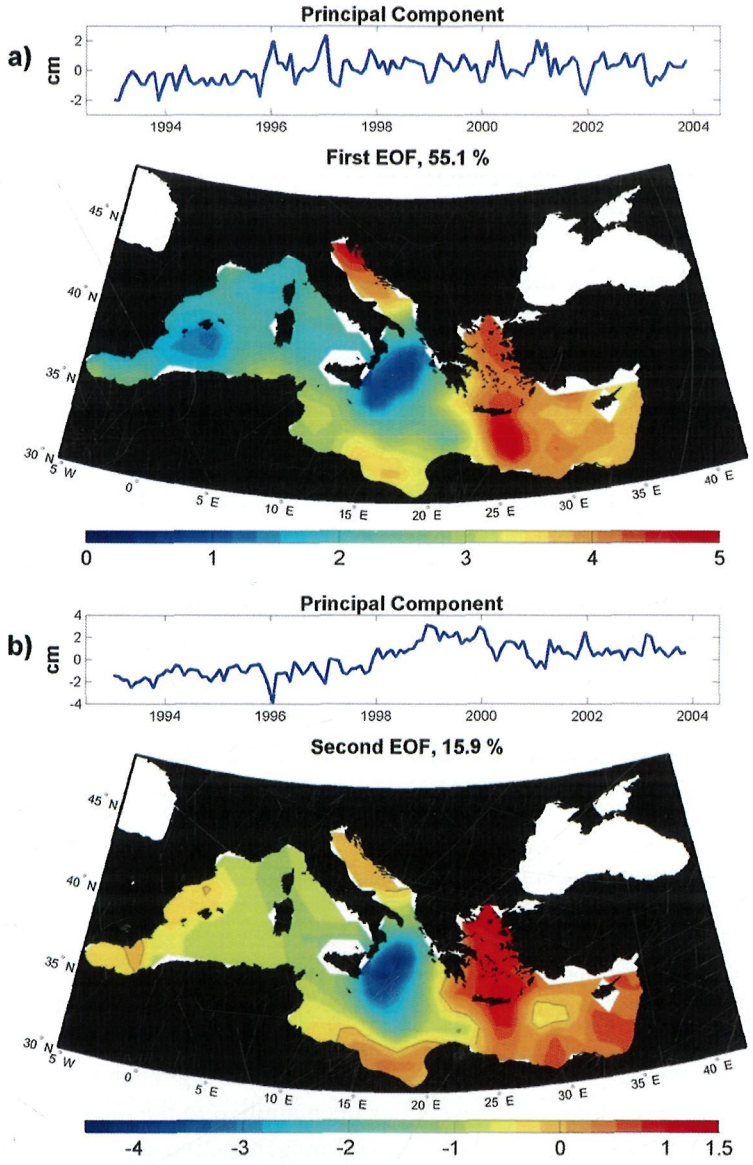

Figure 1.8: EOF/PC modes of SLV in the Mediterranean for the whole period of 01/1993 - 11/2003: (a) First mode explains 55% of the variance of the data, (b) Second mode explains 16%.

riod explain 54.1% and 22.7% of the variance, respectively (figure 1.9). In the first mode, a positive trend is observed in the time series with a positive pattern, meaning that SST has been rising in the Mediterranean for that period, and in the second mode the PC time series does not undergo any significant trending. In neither case does the EOF map pattern correlate well with the rate-of-change maps of SST. These results agree with those reported by Cazenave et al. (2001), who also found a positive linear trend in the first mode of the SST (without any signal shorter than 1 year) for the period 1993 - 1999, with no spatial correlation with SL behavior in the first two EOF/PC modes.

Unlike the Mediterranean, it is the first EOF/PC mode of SLV in the Black Sea (explaining as much as 90% of the variance, see figure 1.10a) that agrees quite well with the rate-of-change map for the whole period, since both maps show a focus in the southeastern part of the basin. This EOF has a positive value in the whole basin and the PC time series has a positive trend till mid-1999 and a negative one afterwards, agreeing with that found earlier in figure 1.1b. The second EOF/PC mode (figure 1.10b), which only explains 3% of the variance, divides the basin in two symmetric parts and executes an east-west seesaw of (presumably) mass transport.

The first EOF/PC mode of SST in Black sea (figure 1.11) explains 80% of the variance, the second one explains 9%, and both are very well correlated, respectively, with the first and second EOF of SLV. The PC time series show a lower correlation, except for the second PC time series.

1.2.3 Tide gauge (TG) data analysis

The available TG data, from PSMSL, with sufficient time span to study the change of trend in 1999 are described in table 1.3 and located in figure 1.2. We examine the TGs in the North Ionian Sea, Adriatic Sea, Levantine Basin, Aegean Sea and Black Sea, where the change of trend is observed. In order to determinate the linear trends before and after mid-1999, the seasonal signals have been removed from the data and a linear regression has been applied to the data in both periods, see figure 1.12. The linear rates of change for each station are given in table 1.3.

Here we see that 8 TGs (Patrai, Kalamai, Thessaloniki, Leros, Erdek, Mentes/Izmir, Hadera and Tel Aviv) in the Mediterranean and 2 in the Black Sea (Tuapse and

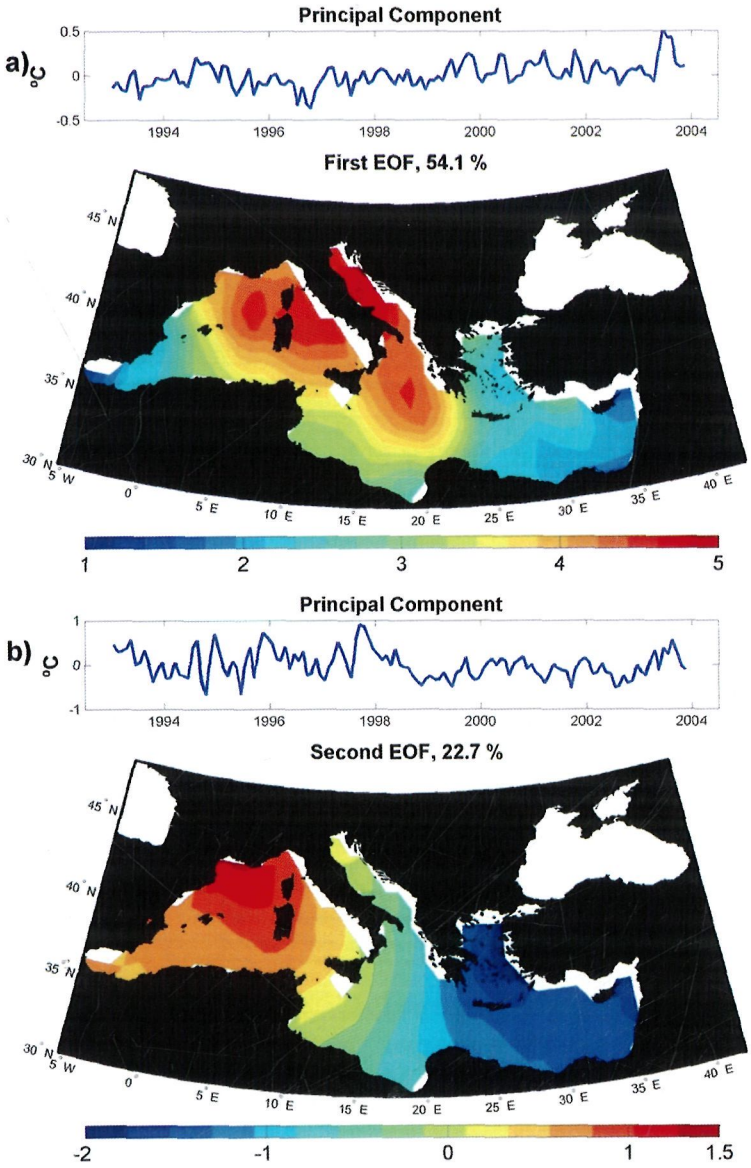

Figure 1.9: EOF/PC modes of SST in the Mediterranean for the whole period of 01/1993 - 11/2003: (a) First mode explains 54.1% of the variance of the data, (b) Second mode explains 22.7%.

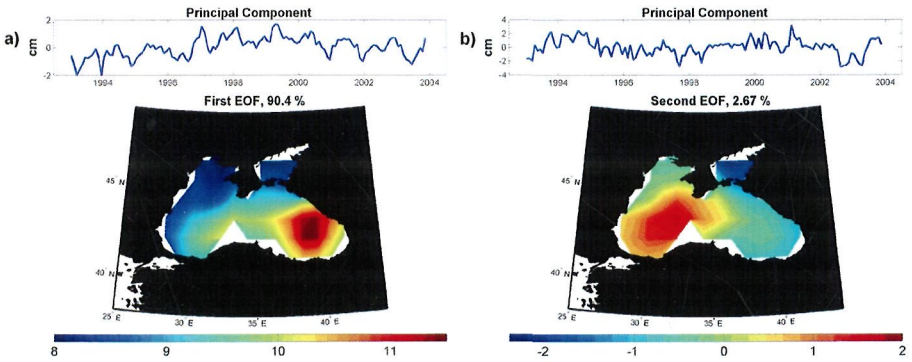

Figure 1.10: EOF/PC mode of SLV in the Black Sea for the whole period of 01/1993 - 11/2003: (a) First mode explains 90% of the variance of the data, (b) Second mode explains 2%.

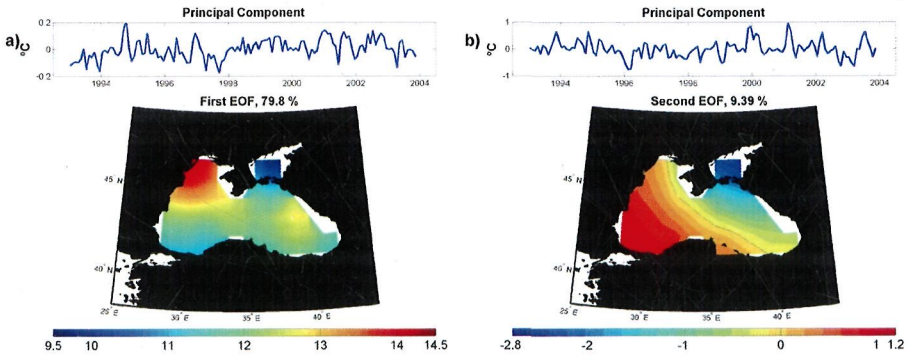

Figure 1.11: EOF/PC mode of SST in the Black Sea for the whole period of 01/1993 - 11/2003: (a) First mode explains 80% of the variance of the data, (b) Second mode explains 9%.

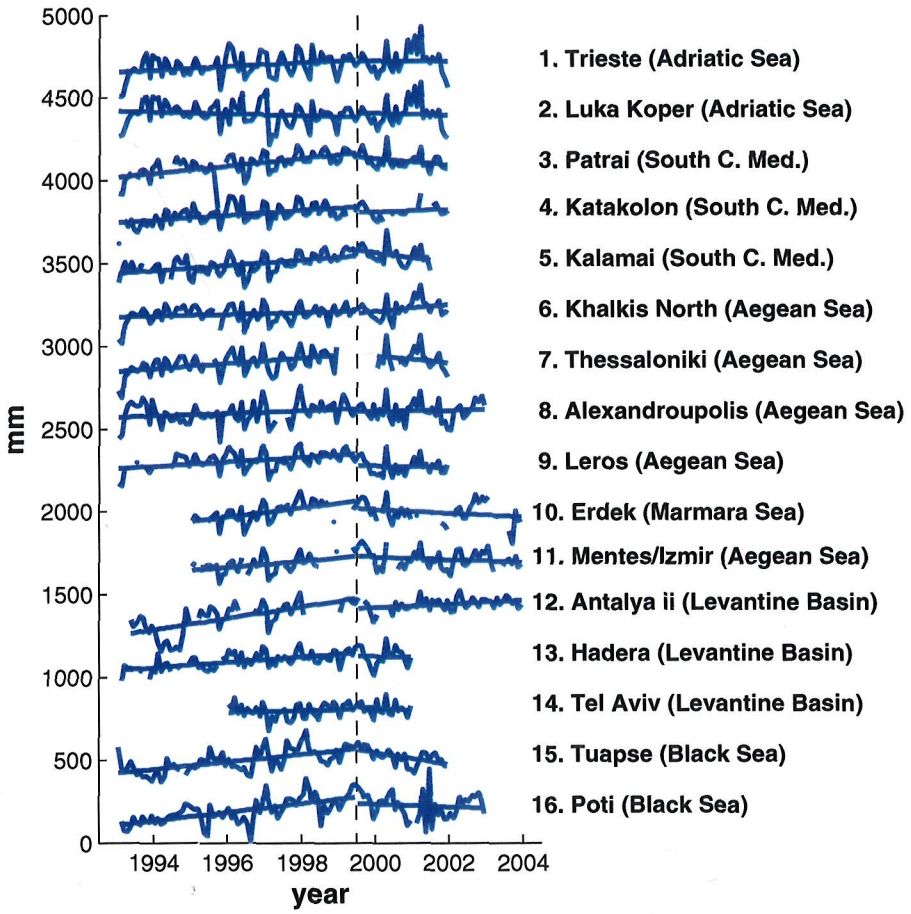

Figure 1.12: The non-seasonal sea level time series from the TGs. Separate linear regression is applied for periods before and after 1999, to indicate possible change in the linear trend, some are stronger than others.

			Linear rate of change (cm/year)	
		Mediterranean Sea		
	Name	Location	Pre-06/1999	Post-06/1999
1	Trieste	45 39 N 13 45 E	1.1 ± 0.4	0.0 ± 2.0
2	Luka Koper	45 34 N 13 45 E	-0.5 ± 0.4	-0.6 ± 2.0
3	Patrai	38 14 N 21 44 E	2.3 ± 0.3	-2.0 ± 1.2
4	Katakolon	37 38 N 21 19 E	1.5 ± 0.3	0.8 ± 1.1
5	Kalamai	37 01 N 22 08 E	1.6 ± 0.3	-3.1 ± 1.8
6	Khalkis North	38 28 N 23 36 E	0.5 ± 0.3	2.1 ± 1.4
7	Thessaloniki	40 37 N 23 02 E	1.6 ± 0.4	-2.2 ± 2.2
8	Alexandroupolis	40 51 N 25 53 E	0.8 ± 0.4	0.3 ± 0.9
9	Leros	37 05 N 26 53 E	1.4 ± 0.3	-0.4 ± 1.2
10	Erdek	40 23 N 27 51 E	2.8 ± 0.6	-1.1 ± 0.8
11	Mentes/Izmir	38 26 N 26 43 E	1.9 ± 0.6	-0.8 ± 0.6
12	Antalya ii	36 50 N 30 37 E	3.5 ± 0.5	1.1 ± 0.4
13	Hadera	32 28 N 34 53 E	1.6 ± 0.2	-0.4 ± 3.2
14	Tel Aviv	32 05 N 34 46 E	0.6 ± 0.7	-1.3 ± 2.3
		Black Sea		
15	Tuapse	44 06 N 39 04 E	2.3 ± 0.3	-3.6 ± 1.0
16	Poti	42 10 N 41 41 E	2.6 ± 0.4	-0.8 ± 1.2

Table 1.3: Linear rate of change for every TG before and after 06/1999. The error corresponds to 1 standard deviation estimated from equation 1.4

Poti) show a reverse change of trend in 1999, while the rest in the Mediterranean present different situation: Antalya does not show a reverse of trend but a reduced trend; Trieste shows a reduction in the rate of change, whereas the neighboring Luka Koper shows no change; neither do the 3 TGs at Katakolon, Khalkis North and Alexandroupolis. Thus, overall most of the available TG data show a change of trend in 1999, corroborating the results from altimetry. One of course recognizes that in general the TG measures the local sea level which is largely influenced by local conditions. For example, vertical crustal motions in the TG site may produce spurious sea level variations [Cazenave et al., 1999; Nerem and Mitchum, 2002; chapter 4]. It should also be noted that all TGs do not span the same period of time, hence introducing extra discrepancies in these estimates.

1.3 Discussion and conclusions

An abrupt change of linear trend of SLV that occurred in the Mediterranean and Black Seas in mid-1999 has been identified. The rate of change of the overall MSL, positive in Period I of the altimetry data (01/1993 - 06/1999), abruptly changed into a negative trend afterwards, producing a kink in the MSL temporal trend for both Mediterranean and Black Seas. Sub-regions of the Mediterranean individually exhibit similar kinks but with differing characteristics, with the North Ionian Sea doing the reverse trending. MSL has been dropping in the North Ionian up to mid-1999, where even an acceleration can be observed from early 1996, unlike the rest of Mediterranean and the Black Seas where the sea level was rising; after 1999 this pattern was reversed.

During Period I the Mediterranean SL's linear rate-of-change map correlates well with the SST counterpart, in sharp contrast with Period II (07/1999 - 11/2003) when this correlation virtually disappeared. We can conclude that the abrupt change in the Mediterranean in 1999 caused the steric effects to become less important as a forcing factor of SLV. EOF/PC analysis has further revealed more details of the SLV in Mediterranean and the Black Seas, as well as their relationships with the SST variation.

Whether the changes in trends are related to the change of state in the thermohaline circulation or part of some decadal fluctuation in sea level is a key ques-

tion. Hydrographic data in the eastern Mediterranean show that the main source of deep water in the last century was the Adriatic Sea. A change of that pattern occurred between 1987 and 1995 when a new source of deep water, called the *Eastern Mediterranean Transient* (EMT), appeared in the Aegean Sea [Roether et al., 1996]. As predicted by Klein et al. (2000), after some extremely cold winters, the Adriatic restored its role as main deep water source in the 1997-1999 period [Manca et al, 2003]. Manca et al. (2003) also confirmed the recovery of the westward transit of Levantine Intermediate Waters, through the Cretan Passage into the Ionian. The open thermohaline cell circulation was restored in 1999. The change in SLV reported here is stronger in the regions related to the restitution of pre-EMT situation, namely Adriatic sea, Ionian sea, Levantine basin and Aegean sea. Larnicol et al. (2002) already suggested that the changes observed in the SL during 1995-1999 in the Levantine and during 1997-1999 in the Ionian are related to variations in the deep and intermediate water masses distributions in the whole Eastern basin.

Therefore it is reasonable to hypothesize that the SLV change in the Mediterranean Sea in 1999 is related to the return to the pre-EMT situation. The Black Sea has been largely controlled by an interannual or decadal steric effect according to the 11-year long data, not agreeing with Tsimplis et al. (2004) who reported that the long-term SLV for the last 40 years was not driven by steric variations but probably by P-E variations. We can conclude that the cause and effect of the SLV in Mediterranean and Black Seas is not straightforward and highly time-dependent; our findings represent only a short segment in the longer-term fluctuations. As far as our results are concerned, the Mediterranean and Black Seas appear to be two separate and distinct dynamic systems. Despite their close geographical proximity, this is conceivable because they are under different meteorological and hydrological regime, and their physical connection, via the Straits of Dardanelles and Bosphorus, is quite restricted. It is of high interest to understand the meteorological and oceanographic conditions that led to the recent evolution of the SLV, and particularly the 1999 event and its evolution and consequences. The present study is done based on the analysis of surface data, and from the surface we can already tell something is going on, for a deeper study further investigations are needed incorporating in situ water column data (such as from XBT or drift ARGO buoys), and particularly oceanographic models.

Chapter 2

Annual Sea Level Variations in the Mediterranean Sea

2.1 Introduction

Accordingly to equation 1, the absolute total sea level variation (SLV) consists of two contributions: steric and mass-induced:

$$SLV_{total} = SLV_{steric} + SLV_{mass}.$$

Here the SLV is defined as in chapter 1, that is as the temporal anomaly as a function of geographical location relative to the "static" mean geoid and in reference to the terrestrial reference frame of the Earth. We consider timescales longer than monthly; on such timescales, the SLV is a critical indicator of the oceanographic and climatic processes. In that regards it is desirable to know the exact share, or relative importance, of the two SLV contributions as a function of location and time. Such knowledge will lead to valuable understanding about ocean dynamics as well as global climatic changes.

SLV_{steric} results from the volumetric expansion or contraction induced by variations of water temperature T and salinity S in the water column, basically a baroclinic phenomenon. SLV_{mass}, on the other hand, is simply a result of the addition (e.g., precipitation, river run-off, melting of land ice) or subtraction (e.g.,

evaporation, dam impoundment on land) of water mass to or from the water column, basically a barotropic effect. The relative share of the two SLV contributions is a strong function of location and time. For example, subject to large temperature swings in the course of the year, mid- and low-latitudes often see relatively larger steric contribution in the SLV_{total}. At higher latitudes and locations where dynamic variability is strong, the mass-induced effect can become the major contributor in SLV_{total}. In general, at any given location the two contributions superimpose at their own seasonal phasing; they can augment or oppose each other depending on meteorology and ocean dynamics. There are also large non-seasonal phenomena that manifest both in steric and mass-induced SLV, such as ENSO and Pacific Decacal Oscillation in the Pacific, and the North Atlantic Oscillation. Both SLV contributions presumably have long-term trends as well due to climate changes that result in global warming and melting of land ices.

SLV_{total} has been monitored by radar altimetry from the vantage point of artificial satellites for over two decades now. In particular, TOPEX/Poseidon (T/P) has acquired continuous and near-global coverage of SLV_{total} at a precision of 2-3 cm since 1992, and its successor Jason-1 is now achieving comparable data, if not of even higher precision [Luthcke et al., 2003]. SLV_{steric} can be estimated using the *equation of state for sea water* [Gill, 1982] when T and S observations are available, typically through in situ CTD and XBT casts collected from ships during oceanographic surveys, as well as the Argo floats (for detail information see <www.argo.ucsd.edu>). At seasonal time scales, the steric effect is felt mostly in the upper layer of the ocean. SLV_{steric} only involves volume changes of the same amount of water, and hence has virtually zero gravitational signature.

On the other hand, SLV_{mass} is accompanied by direct gravitational signature according to its temporal and spatial variations, and hence can be observed gravitationally. Since its launch in March 2002, the NASA/DLR dual-satellite space mission GRACE (Gravity Recovery And Climate Experiment) has mapped the time-variable gravity (TVG) signals globally with a monthly temporal resolution and a spatial resolution of about 1500 km [Tapley et al., 2004a; Wahr et al., 2004]. From the TVG one can readily and uniquely determine the mass variation that produce the TVG signal, assuming it comes from the Earth's surface (e.g., Wahr et al., 1998; Chao, 2005). The SLV_{mass} follows immediately from the surface mass variation (and the known density of sea water).

Ideally, if we had perfect determination of SLV_{total} (e.g., from satellite altimetry), SLV_{steric} (e.g., from in situ measurements), and SLV_{mass} (e.g., from TVG measurement), they should obey the simple Equation 1. Alternatively, then, knowing any two quantities perfectly, the third can be determined. The reality is of course far from the case. The data involved are noisy, contaminated, and incomplete (if not sparse) under limited sampling in time and space. Conceivably, the use of an ocean general circulation model (GCM) can serve as a tool to enforce Equation 1 by assimilating available data of all three data types into a theoretical framework based on physics. In fact, in this chapter we make use of the SLV_{steric} estimated from such a GCM, namely the ECCO ocean model [Lee and Fukumori, 2003].

The target subject of this chapter is the Mediterranean Sea. A semi-enclosed basin, the Mediterranean Sea exchanges water with the open sea only through the narrow Strait of Gibraltar, with the Black Sea through the even narrower Dardanelles and Bosphorus Straits, and with the land by the moderate runoff of rivers such as the Nile. If the fluxes through these waterways are closely monitored or modeled, then the only other water exchange is with the atmosphere in the form of *P-E* (precipitation minus evaporation), which can be modeled given sufficient meteorological data. Thus, the Mediterranean water budget can in principle be quite tractable. We will examine a host of direct and indirect measurement data to estimate the various SLV in the Mediterranean with respect to Equation 1. Because of the short time span of the GRACE TVG data (for estimating SLV_{mass}), we will concentrate on the seasonal variability, which is dominant in all observables.

To first order, it is not clear to what extent the total Mediterranean water budget undergoes a seasonal cycle [García-Lafuente et al., 2002; Bouzinac et al., 2003]. Such a cycle implies an out-of-phase exchange of water through the air-sea interface (*P-E*) and through the Straits and rivers. In the long term, the latter compensates the fresh water deficit produced by the former in order to preserve the water mass of the Mediterranean, but the compensation does not have to happen on a short-term basis, hence a seasonal signal of the mass budget in the Sea. Up to now, the seasonal mass imbalance at basin scale has been estimated in indirect ways; these data had been too noisy to elucidate on the weak signals at hand [García-Lafuente et al., 2002; Bouzinac et al., 2003; Larnicol et al., 1995].

2.2 Data and Processing

2.2.1 Total SLV

For SLV_{total}, we use the same combined monthly solution from T/P, Jason-1, ERS and ENVISAT altimetry missions than in chapter 1 (see section 1.2). However, the time span is 01/1993 - 07/2004. All standard corrections were applied to the altimetry data, including the IB effect applied to reduce aliasing errors, although it may introduce slight errors of its own by violating water mass conservation in the semi-enclosed sea. In order to estimate these errors and for comparison purposes, T/P data non corrected for the IB effect have also been analyzed [Brian Beckley, personal communication, 2004].

2.2.2 Steric term

To estimate SLV_{steric}, the temperature T and salinity S fields from two ECCO ocean model[1] products are used – the JPL-simulation and the JPL-adjoint-smoothed wind driven. The simulation uses the NCEP reanalysis as forcing except their time-means were replaced with those of COADS (Comprehensive Ocean-Atmosphere Data Set) (for details see Lee and Fukumori, 2003). The smoothed wind-driven run is based on a correction to this NCEP wind forcing estimated by assimilating altimetry data from T/P and Jason-1, and temperature profiles available on GTS (Global Telecommunication System from in-situ measurements by XBT, CTD, and Argo floats). Other components of the forcing are the same as the simulation (i.e., NCEP plus COADS correction). Although both simulation and assimilation products have been processed, only the former are shown here as both produce nearly exactly the same results. Data profiles are from surface to the (non-uniform) sea bottom at each point on a 1° x 1° regular grid, and the time span used is 01/1997 - 06/2004 with a time step of ten days. These data can be converted in density anomalies at each standard level using the classical expression for the *equation of state of sea water* [Gill, 1982]. The SLV_{steric} is then obtained by vertically integrating density anomalies at each grid point, (θ,λ) = (colatitude,

[1] <http://www.ecco-group.org>

longitude), and each time step, t, according to

$$SLV_{steric}(\theta,\lambda) = \int_{-H}^{0} \frac{\rho_0(\theta,\lambda,z) - \rho(\theta,\lambda,z,t)}{\rho_0(\theta,\lambda,z)}\, dz, \tag{2.1}$$

where $\rho_0(\theta,\lambda,z)$ is the reference density (T=35°C and S=35.0), $\rho(\theta,\lambda,z,t)$ is the instantaneous density and H is the maximum depth. The state-law algorithm for computing the corresponding SLV_{steric} is adopted from Pond and Pickard (1986).

2.2.3 Eustatic term

To estimate SLV_{mass}, we use the Level-2 (L-2) GRACE data provided by the GRACE Project for the period 04/2002 - 07/2004, which consists on 22 monthly sets of fully normalized spherical harmonic Stokes coefficients (see appendix A). Note that several monthly solutions are missing (June 2002, July 2002, December 2002, January 2003 and June 2003). The data include Stokes coefficients $\bar{C}_{nm}$ and $\bar{S}_{nm}$ up to degree 120 but among them only harmonic solutions up to degree 15 are sufficiently well determined for TVG [Tapley et al., 2004a; Wahr et al., 2004], corresponding to a spatial resolution of about 1500 km (see below). The monthly spherical harmonic TVG field is readily converted into surface mass variations by:

$$\Delta\sigma(\theta,\lambda) = \frac{a\rho_E}{3}\sum_{n=0}^{\infty}\sum_{m=0}^{n}\frac{2n+1}{1+k'_n}\bar{P}_{nm}(\cos\theta)\left(\Delta\bar{C}_{nm}\cos m\lambda + \Delta\bar{S}_{nm}\sin m\lambda\right) \tag{2.2}$$

assuming the latter only occur on the Earth surface [Wahr et al., 1998; Chao, 2005], where $\Delta\sigma$ is the estimated mass variation, ρ_E is the mean density of the Earth, k'_n is the nth load potential Love number, $\bar{P}_{nm}$ is the 4π-normalized associated Legendre function of degree n and order m, and $\Delta\bar{C}_{nm}$ and $\Delta\bar{S}_{nm}$ are the time-variable Stokes coefficients. The symbol Δ is to denote that L-2 GRACE data represents the geopotential anomalies with respect to a background gravity model [Bettadpur, 2004b]. Mass variations are further converted into "water thickness equivalent" (WTE) in units of mm by dividing with the water density assumed to be 1000 kg/m^3 (thus each kg/m^2 is equivalent to 1 mm WTE). Note that, however, a factor of 1/1.029 should be applied to the WTE to convert it into the observed SLV owing to the ocean water density of 1029 kg/m^3.

A mass variation in the water column produces a deformation in the sea bottom. As a consequence, a mass redistribution arises producing a variation of the potential. In Equation 2.2, the division by the factor undoes that variation of the potential and hence the original mass variation is recovered. Furthermore, when SLV_{mass} is indirectly estimated from Equation 1, the deformation produced by mass change is implicitly observed. For that reason, to fairly compare with SLV_{mass} estimated through Equation 2.2, the sea bottom deformation should be corrected, which can be estimated by:

$$\Delta H(\theta,\lambda) = a\sum_{n=0}^{\infty}\sum_{m=0}^{n}\frac{h'_n}{1+k'_n}\bar{P}_{nm}(\cos\theta)\left(\Delta\bar{C}_{nm}\cos m\lambda + \Delta\bar{S}_{nm}\sin m\lambda\right), \tag{2.3}$$

where h'_n is the nth load deformation Love number [Munk and Macdonald, 1960]. This effect proves to be negligible numerically, although important from a theoretical point of view and adopted in our computations.

The GRACE TVG data have beforehand been corrected for the following: the atmospheric loading effect according to the ECMWF (European Centre for Medium-Range Weather Forecast) GCM surface pressure output, the high-frequency ocean mass variations computed with a mass-conserving barotropic ocean model driven by high-frequency winds and atmospheric pressure [Flechtner, 2003], the solid Earth tides (including solid pole tide), ocean tides (including the ocean pole tide as a consequence of the solid pole tide via an equilibrium response [Wahr, 1985; Aviso, 1996], but not including the effects of loading and self-gravitation of the ocean pole tide [Desai, 2002]), as well as the routine satellite orbit perturbations of secular polar motion, N-body and general relativistic effects. In order to compare GRACE TVG and altimetry data, these differences should be considered, as have been in previous studies (e.g. Chambers et al., 2004).

Thus, we first add back the barotropic ocean GCM effect, which corrects among others for the IB response of the ocean, to the GRACE TVG field as recommended by Flechtner (2003). Then, GRACE TVG data should be compared to non-IB corrected altimetry. However, the IB correction does not change the annual amplitude and phase of the Mediterranean MSL, as can be seen in figure 1.3a, where the altimetry merged data is compared to T/P non-IB corrected data [Brian Beckley, personal communication, 2004]. Then, we will use the al-

timetry merged data in order to take advantage of the better space and temporal sampling than one single altimetry satellite. Secondly, while zero in GRACE data (because the center of mass of the Earth is taken to be the origin of the reference frame), the degree-1 terms are non-zero in altimetry data. Thus we add to the GRACE TVG field the estimated degree-1 terms calculated from an estimation of the annual and semiannual motion of the mass center of the Earth according to Chen et al. (1999). See section A.8 for further details. Thirdly, the degree-2 order-1 GRACE TVG coefficients have been corrected for secular variations but not corrected in altimetry data. Therefore, we add back the secular variations to those coefficients. Besides, as the degree-2 order-0 coefficient, which represents Earth's oblateness [Cox and Chao, 2002], is not well observed by GRACE [Tapley et al., 2004a], we have replaced it for a more accurate time series estimated from Satellite Laser Ranging (SLR) (updated from Cox and Chao, 2002; Cox, personal communication, 2005). In order to remove the atmospheric effect in the latter, we subtract the degree-2 order-0 coefficients of the atmospheric correction applied to GRACE data [Flechtner, 2003]. Finally, the only disturbing potential related to the polar motion assumed in altimetry correction is that produced by the solid earth pole tide. The disturbing potential produced by the latter leads to an equilibrium response of the sea level, called ocean pole tide, which is corrected in altimetry [AVISO, 1996]. However, the water mass displaced by that response produces extra effects of loading and self-gravitation, which are not corrected in altimetry [Desai, 2002]. In GRACE data, the solid earth pole tide is corrected, so no ocean response is observed due to the related disturbing potential, but the effects of loading and self-gravitation of the ocean pole tide are not corrected. Therefore, altimetry and GRACE partially correct the ocean pole tide in the same way and no inconsistency arises when comparing both datasets (see also section A.9).

Ancillary sources of data are processed in order to examine the water mass exchange fluxes in the Mediterranean Sea. In particular, we shall use the monthly *P-E* field derived from the proxy atmospheric humidity data as provided by the NCEP atmospheric GCM [Chao and Au, 2006], on a 2.5° x 2.5° grid for the period 01/2002 - 07/2004. These data are later combined with GRACE TVG data to estimate the water mass exchange through the Gibraltar Strait neglecting the moderate river runoffs. This result will be compared with historical data of

the net Gibraltar flux (GF) of water, as estimated from current-meter observations taken during the CANIGO (Canary Islands Azores Gibraltar Observations) project between 10/1995 and 5/1998 [García-Lafuente et al., 2002].

2.3 Results

2.3.1 The different contributions to the annual Mediterranean sea level signal

We shall first examine the spatial distribution of the seasonal signals. The annual signal can be extracted by least-squares fitting a given signal with seasonal sinusoids in terms of amplitude (A) and phase (ϕ):

$$signal = A\cos(\omega_a t - \phi), \tag{2.4}$$

where ω_a is the annual frequency and t denotes the time in months. Note that by this definition the phase ϕ corresponds to the time of the maximum positive amplitude during the year. An alternative form of Equation 2.4 that includes an additional semiannual harmonic has also been examined, which shows that semiannual amplitudes are an order of magnitude smaller than annual signals while the latter remain virtually unmodified. Thus, for the present purpose, Equation 2.4 is adequate to study the seasonal cycle and is used throughout this chapter. Figures 2.1a and 2.1b show the resultant annual A and ϕ estimates for SLV_{total} (altimetry) and SLV_{steric} (ECCO ocean GCM), respectively. The studied period depends on the availability of each data set.

Figure 2.1a shows a SLV_{total} annual amplitude of roughly 60-80 mm except for the Adriatic Sea (with $\backsim$50 mm) and four regions (the southern Levantine Basin, the Tyrrhenian Sea, the Ionian Sea and the central part of the Western Mediterranean Basin) where values up to 80-100 mm are reached. This spatial pattern is similar to Figure 2.1b that shows the annual amplitude of SLV_{steric} with values of $\backsim$90 mm, except for the same four regions of enhanced amplitude as in Figure 2.1a where values around 130-160 mm are observed. Besides, low amplitudes less than 60 mm are observed in the Adriatic and Aegean seas and near the Tunisian coast. The maximum positive amplitude of SLV_{total} occurs

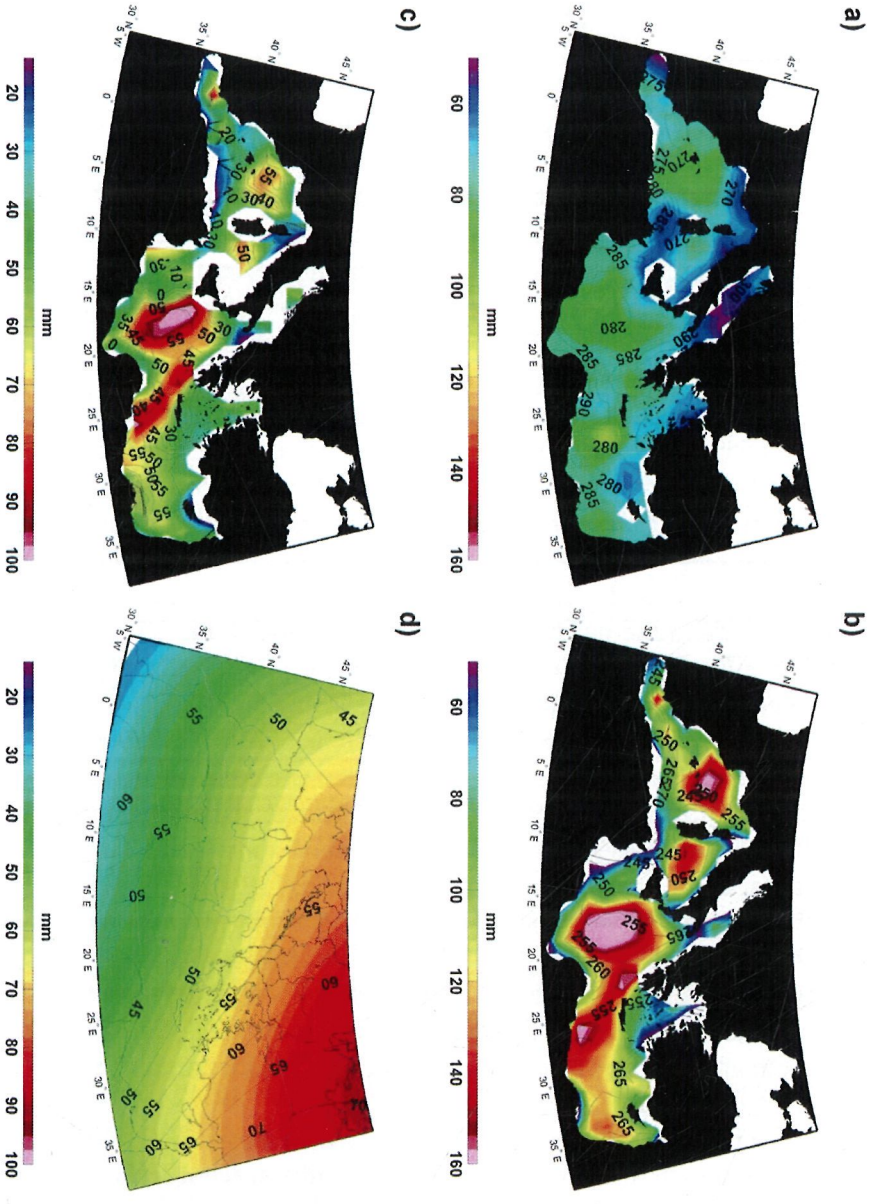

Figure 2.1: Annual amplitude A (color scale in mm) and phase ϕ (contour lines in degrees) from equation 2.4 for different datasets: (a) SLV_{total} from altimetry; (b) SLV_{steric} from ECCO model; (c) SLV_{mass} = (a) - (b); (d) SLV_{mass} from GRACE data.

between 270° and 285° (first half of October) in the whole basin and ∽300° in the Adriatic Sea (Figure 2.1a), while that of SLV_{steric} takes place around one month earlier (values between 240° and 260°, that is, the first half of September). Both of them are, not surprisingly, rather homogeneous. A noteworthy feature in these Figures is the west-to-east propagation of both sea level signals, with the Western Mediterranean Basin leading the Eastern Basin by 15 days (10° to 20°) or so.

From these Figures, it is clear that SLV_{total} and SLV_{steric} do not match each other. Not only SLV_{steric} has greater amplitude on average, but its phase also leads that of SLV_{total} by around 30°. Their difference, $SLV_{total} - SLV_{steric}$, which is an indirect estimate of SLV_{mass} according to Equation 1, is clearly non-vanishing, as shown in Figure 2.1c. Its annual amplitude is 30-60 mm, with two localized regions showing more than 90 mm, and its annual phase is between 10° and 55° (mid January and late February), except for a localized region in the Western Basin with a phase of 330° (or -30°). Now compare it with Figure 2.1d, which gives SLV_{mass} estimated from GRACE. Its annual amplitude is ∽50 mm and its phase range from 45° to 65° (second half of February), which propagates northeastward in the Levantine Basin and is quite homogeneous in the Western Basin. Aside from the much lower spatial resolution of the GRACE map, which does not allow the detection of the small features observed in figure 2.1c, the agreement between both approaches is reasonably good in general (or more precisely in average), considering that (i) they are completely independent data types with uncorrelated noises; and (ii) Figure 2.1c is a residual signal between two large varying fields. Particularly notable is the large phase difference of SLV_{mass} with SLV_{total} or SLV_{steric}. We conclude that the three data sets tell a consistent story as far as the annual variability is concerned.

To proceed, we examine only the mean annual signal averaged over the entire Mediterranean Sea region. We do so because all datasets are to be studied in conjunction with GRACE data and GRACE can barely resolve the detail within the Mediterranean Sea due to its relatively low spatial resolution. Thus we average both altimetry and steric height data in the Mediterranean Sea to obtain the mean time series variations (Figure 2.2).

In order to isolate the Mediterranean area to calculate its mean TVG signal from the GRACE data and to minimize the spectral leakage and data error for higher degrees, a Gaussian filter as described by Swenson and Wahr (2002) is

	A (mm)	ϕ
GRACE	55 ± 15	$52^o \pm 15^o$
Alt - ECCO steric	38 ± 16	$16^o \pm 27^o$
Altimetry	83 ± 13	$281^o \pm 10^o$
ECCO steric	94 ± 5	$258^o \pm 3^o$
$P - E$ (NCEP)	31 ± 8 /month	$7^o \pm 17^o$
F (Eq. 2.6)	17 ± 16 /month	$263^o \pm 76^o$

Table 2.1: Annual amplitude (A) and phase (ϕ) of the different spatially averaged monthly time series and the period covered by the datasets. The uncertainty indicates 95% formal error. The period of time is 04/2002 - 07/2004 for all data sets, except for the estimate of F whose period is 09/2002 - 07/2004.

applied to obtain the estimated mean mass anomaly in the Mediterranean Sea as follows:

$$\Delta\widetilde{\sigma}_{Med} = \frac{1}{\Omega_{Med}} \int \Delta\sigma(\theta,\lambda)\bar{W}(\theta,\lambda)d\Omega, \tag{2.5}$$

where $d\Omega = \sin\theta \, d\theta \, d\lambda$ is an element of solid angle, Ω_{Med} denotes the Mediterranean solid angle, $\bar{W}(\theta,\lambda)$ mimics value 1 over the Mediterranean Sea and 0 otherwise, changing smoothly (taken as 1000 km) at the boundary and truncating $\Delta\sigma(\theta,\lambda)$ at degree 30 (see equation 2.2 and section A.7). For each month of data this leads to a single $\Delta\widetilde{\sigma}_{Med}$ value obtained by weighted-sum of all the coefficients up to degree 30 (see figure A.2). The end product, when converted into WTE, is a monthly time series for mean SLV_{mass}.

Figure 2.2 presents all the monthly mean time series over the Mediterranean Sea, while Table 1 shows the numerical estimates of the spatially averaged (A,ϕ) from Equation 2.4. The uncertainty estimates are those of the 95% formal error during the least-squares fit procedure.

Figure 2.2 and Table 2.1 show the same good agreement between SLV_{total} and SLV_{steric} observed in Figure 2.1 in both annual amplitude and phase. We notice (i) the amplitude of SLV_{total} is $\backsim$10 mm lower and peaks $\backsim$23 days later than SLV_{steric}; (ii) the SLV_{mass} estimated from GRACE shows an annual am-

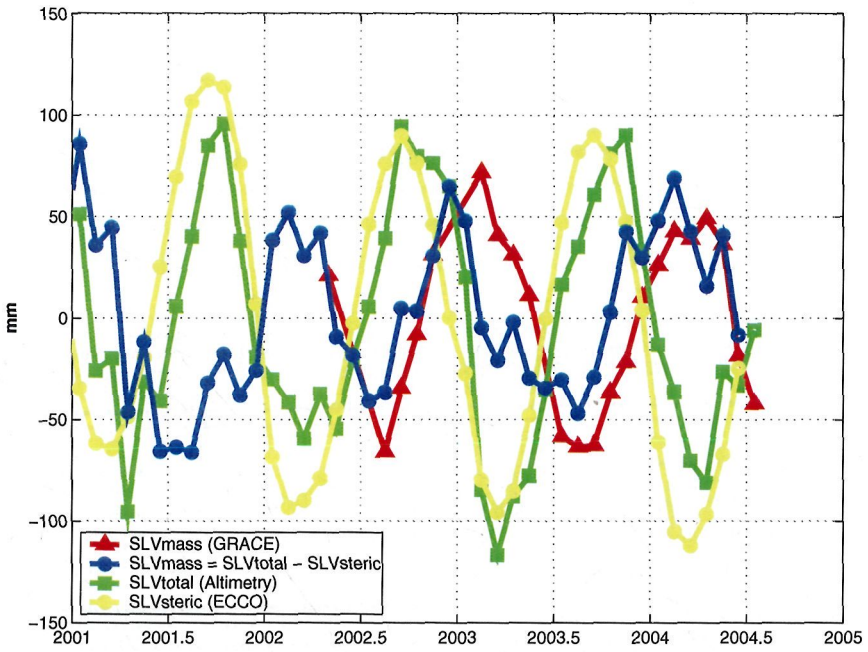

Figure 2.2: The time series represent the monthly mean values over the Mediterranean Sea for several datasets. Red curve: SLV_{mass} from GRACE data; green curve: SLV_{total} from altimetry data; yellow curve: SLV_{steric} from ECCO assimilation model; blue curve: SLV_{mass} estimated according to equation 1, $SLV_{mass} = SLV_{total} - SLV_{steric}$.

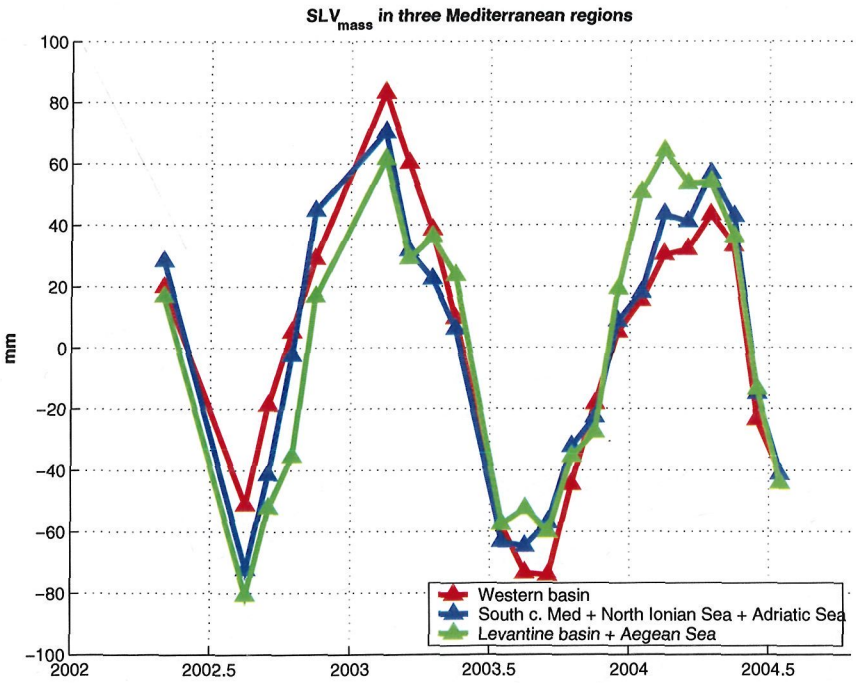

Figure 2.3: The time series represent the monthly mean values of SLV_{mass} over three Mediterranean regions. Accordingly to Figure 1.2, red curve: Western basin; blue curve: South central Mediterranean + North Ionian Sea + Adriatic Sea; green curve: Levantine basin + Aegean Sea.

plitude of 55 mm and a phase of 52° (mid February) which are noticeably different from those of SLV_{total} and SLV_{steric}; (iii) the estimation of SLV_{mass} as $SLV_{total} - SLV_{steric}$ from Equation 1 agrees very well with GRACE-derived SLV_{mass}. Thus, the annual SLV_{mass} in the Mediterranean is $\backsim$230° (8 months) ahead or $\backsim$130° (4 months) lagging with respect to SLV_{total}. The similitude of SLV_{steric} and SLV_{total} curves in Figure 2.2 indicates clearly that Mediterranean sea level is mainly driven by the steric changes, while SLV_{mass} amounts to about one third of SLV_{total} but having a quite different phase. For the first time it is shown how annual steric and mass-induced changes in the Mediterranean Sea counteract each other to produce the net sea level variation.

We have experimented with the same scheme but breaking down the Mediterranean Sea into three regions: (i) Western Basin, (ii) Central Mediterranean (including Ionian Sea) and Adriatic Sea, (iii) Levantine Basin and Aegean Sea. The individual mean SLV_{mass} (Figure 2.3) show that the annual signals are quite similar in all regions, and almost identical to that of the whole Mediterranean in Figure 2.2. This is consistent with the fact that the annual SLV_{mass} is homogeneous in the whole basin (see Figure 2.1) with little exchange among the regions. However, it is interesting to point out a possible gaining of water in region (iii) at the expense of region (i) on an interannual timescale. At present the data span is still too short to tell.

2.3.2 The mass signal and the water fluxes

Besides the above indirect scheme of determine SLV_{mass} by subtracting SLV_{total} (altimetry) with SLV_{steric} (ocean GCM) according to Equation 1 (see also Bouzinac et al., 2003; Larnicol et al., 1995), one can alternatively observe the net barotropic flow through the Strait of Gibraltar from in situ sensors and compare it with the P - E estimates in the area [García-Lafuente et al. (2002). Conversely, now that SLV_{mass} can be directly measured by GRACE, we can deduce this mass signal arising as the balance between the "horizontal" water mass flux F and the vertical flux P - E, taking the form:

$$\delta(SLV_{mass}) = F + (P - E), \tag{2.6}$$

where δ indicates the month-to-month incremental change which is calculated from GRACE data. Only 18 monthly values of $\delta(SLV_{mass})$ have been obtained subject to the availability of GRACE product. They are shown in Figure 2.4.

On the other hand, the monthly $P - E$ field as estimated by Chao and Au (2006) (see Section 2) are averaged over the Mediterranean Sea. The annual signal (A,ϕ) obtained according to Equation 2.4 is A = 31 mm/month and ϕ = 7° (early January) during the period of Figure 2.4. It is interesting to note that the mean $P-E$ in the Mediterranean is negative in general, with no more than three positive monthly values per year. The mean value is -15.7 mm/month during the time period in Figure 2.4, amounting to a total of 19 cm/year of net loss of water, which is considerably less severe than the historically reported values [Bryden et al., 1994; Boukthir and Barnier, 2000].

An estimate of the water mass flux F follows immediately from Equation 2.6, see Figure 2.4. F comes primarily from the flux through the Gibraltar Strait, while the river run-off and the exchange with the Black Sea are negligible in comparison [Bethoux and Gentili, 1999]. Its estimated annual signals are A = 17 mm/month and ϕ = 263° (late September). The yearly mean value of F cannot be readily estimated using GRACE data because there are only 18 months of $\delta(SLV_{mass})$. Nevertheless, as long as the interannual variability and trends are insignificant, the Mediterranean mean mass content does not vary much from year to year and the mean F should be completely offset by $P - E$ flux.

The F estimate can be compared with historical results as reported by García-Lafuente et al. (2002), who estimated the main contributor of F (the flux through the Gibraltar Strait) from measurements of three arrays of current-meters situated in the East side of Gibraltar between October 1995 and May 1998. They give an annual influx amplitude of 0.077 $\pm$ 0.044 Sv (1 Sv = 10^6 m^3/s), with annual phase 234° $\pm$ 33° (late August). For a Mediterranean Sea area of 2.57 x 10^{12} m^2, this amplitude is equivalent 78 $\pm$ 44 mm/month. Our estimate for F above has a much lower annual amplitude; it is not clear which estimate is more accurate but the different period of time should be noted. However, they agree remarkably well in phase, which is encouraging because of the very different procedure and datasets used.

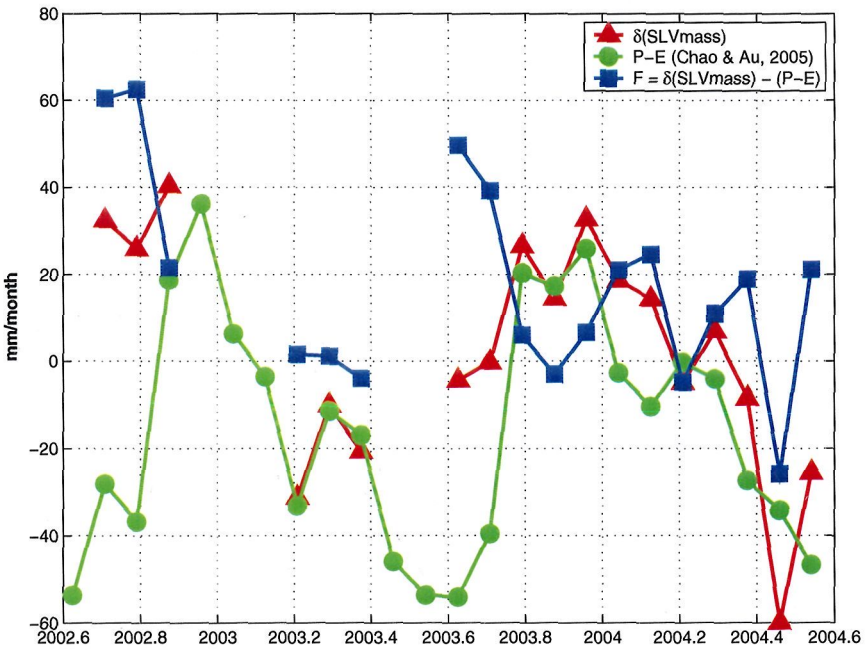

Figure 2.4: The time series represent the monthly mean values over the Mediterranean Sea for several datasets. Red curve: $\delta(SLV_{mass})$ from GRACE data; green curve: $P-E$ field from Chao and Au [2005]; blue curve: water mass flux F from the difference between the above two curves according to Equation 2.6.

2.4 Discussion and Conclusions

We have demonstrated the combined application of several remote sensing data types to understand the behavior of SLV in the Mediterranean Sea. We have produced monthly time series of the total SLV from altimetry (SLV_{total}), which has an annual amplitude of 83 mm and peaks in mid-October. We have also estimated monthly steric SLV from T and S outputs of ECCO ocean model (SLV_{steric}), with amplitude of 94 mm and peak phase at mid-September, differing not much from those of SLV_{total}. To close this (secondary) difference calls for a mass signal SLV_{mass}, according to Equation 1. The similar behavior between SLV_{total} and SLV_{steric} indicates that the Mediterranean annual SLV_{total} is mainly driven by steric changes and only moderately offset by mass-induced changes. This SLV_{mass} contribution is found to match remarkably well with that detected independently by GRACE, which has an annual amplitude of 55 mm and the peak phase at mid-February, the latter is almost half a cycle later than SLV_{total} or SLV_{steric}. These results confirm previous indirect measurements [García-Lafuente et al., 2002; Bouzinac et al., 2003; Larnicol et al., 1995] which indicated the existence of an annual signal in the Mediterranean mass budget. Overall our results show that, during the annual cycle, when the sea level is rising (falling) in the Mediterranean Sea, it is also losing (gaining) mass. Such a phase difference is not surprising (another recent indication was reported in Chao et al. (2003) in the Pacific), as SLV_{steric} and SLV_{mass} are governed by different processes.

Previous studies of global mass variations based on GRACE observations show that the annual amplitude in the open ocean is significantly lower (at 7-9 mm) [Chambers et al., 2004] than the values found here in the Mediterranean Sea (55 mm), while certain land values can be quite larger ($\backsim$150 mm in the Amazon River basin and the Bay of Bengal) [Wahr et al., 2004]. We note that several studies have revealed that the Mediterranean Sea usually undergoes a different behavior than the global ocean as it has already been highlighted in chapter 1.

While providing an effective means toward the understanding of the geophysical processes that are responsible for ocean dynamic behaviors, the low spatial resolution of the standard GRACE data product proves to be an impediment to our present study, thereby little TVG detail within the Mediterranean can be revealed. Alternative GRACE data processing approaches aimed at improving spatial and

Volver al índice/Tornar a l'índex

temporal resolutions are currently explored. For example, Rowlands et al. (2005) demonstrated a factor of 3 improvements in both temporal and spatial resolutions through a "mascon" analysis of GRACE orbit data. Future studies taking advantage of such higher-resolution data can potentially yield much refined conclusions.

Chapter 3

Annual Sea Level Variations in the Global Ocean

3.1 Introduction

In this chapter, we extend the study of the annual SLV from the Mediterranean Sea to the global ocean. Then, equation 1 and the previous notation are still valid:

$$SLV_{total} = SLV_{steric} + SLV_{mass}.$$

In that case, variations of ocean mass are due to water exchange with atmosphere, continental water reservoirs and land ice bodies.

Long-term sea level rise measured by tide gauges over the past decades (e.g., Church et al., 2004; Holgate and Woodworth, 2004) and satellite altimetry since 1993 (e.g., Nerem and Mitchum, 2001a; Leuliette et al., 2004) has been interpreted in terms of thermal expansion and ocean mass change using models and various observations (see Church et al., 2001; and Cazenave and Nerem, 2004, for reviews). Other studies, focusing on the annual mean sea level [Chen et al., 1998; Minster et al., 1999; Cazenave et al., 2000; Milly et al., 2003], showed that the non steric annual SLV based on T/P altimetry corrected for thermal expansion, is well explained by seasonal variations in atmospheric water vapor content and total land water storage (as estimated from outputs of global land surface models).

As aforementioned, the newly launched GRACE mission, devoted to measure tiny variations of the Earth's gravity field [Tapley et al., 2004a, 2004b; Wahr et al., 2004; Schmidt et al., 2005], now allows direct estimates of land water storage change over continental areas as well as ocean mass change over oceanic areas. The latter application has been recently presented by Chambers et al. (2004) who showed that the GRACE data averaged over the global ocean closely follow the altimetry-derived SLV after correcting for steric effects, thus represent the ocean mass component due to change in atmospheric water, land hydrology and land ice mass. In the present study, we propose a step further, consisting of improving Chambers et al.'s estimate in three points: i) monthly altimetric and T profiles will be used to estimate SLV_{total} and SLV_{steric}, respectively, instead of averaged years as done in Chambers et al. (2004); ii) an accurate estimate of the degree-2 order-0 Stokes coefficients from SLR will be used (see section 2.2.3); iii) the mean sea level pressure over the whole ocean is accounted for. On the other hand, we will estimate, over a short time span (April 2002-December 2003), the SLV_{steric} by combining GRACE data over the oceans with T/P-derived SLV_{total}.

3.2 Data and processing

3.2.1 Total SLV

SLV_{total} is estimated from T/P altimetry data (distributed by the AVISO data centre). We consider the period 04/2002 - 12/2003. Usual geophysical and atmospheric corrections (tides, wet and dry tropospheric corrections, ionospheric correction, sea state bias as well as instrumental drifts and bias) are applied to the data, as recommended by AVISO. We also apply the inverted barometer (IB) correction to account for atmospheric loading on sea surface, using the time-variable mean surface pressure averaged over the oceanic domain (e.g., Minster et al., 1999). The IB correction, at latitude ϕ, longitude λ and time t, is expressed as:

$$-0.9948 \cdot [P(\phi, \lambda, t) - P(t)], \tag{3.1}$$

where $P(\phi, \lambda, t)$ is the instantaneous local surface pressure and $P(t)$ is the mean surface pressure spatially averaged over the whole oceanic domain[1]. In this equation, the IB correction is in cm if pressure is in mbar. IB-corrected T/P sea level data are interpolated onto $1° \times 1°$ regular grids at 10-day interval (the duration of the T/P orbital cycle), then spatially averaged between latitudes 60°S and 60°N, using *equi-area weighting*, and further expressed as monthly means between April 2002 and December 2003. For a general $\mathrm{d}\theta^{\mathrm{o}} \times \mathrm{d}\lambda^{\mathrm{o}}$ (latitude $\times$ longitude) regular grid, the spatial average of a region R using an equi-area weighting is estimated as

$$SLV_{total} = \sum_{i \in R} \frac{\mathrm{d}\theta \, \mathrm{d}\lambda \cos\theta_i}{S} h_i, \tag{3.2}$$

where θ_i is the latitude of the point i in R, and S is the surface of R,

$$S = \sum_{i \in R} \mathrm{d}\theta \, \mathrm{d}\lambda \cos\theta_i. \tag{3.3}$$

Errors associated with 10-day T/P SLV values are estimated to $\backsim$4 mm [Nerem and Mitchum, 2001a]. For monthly values, we assume that the uncertainty is $\frac{4}{\sqrt{3}}$, thus $\backsim$2.5 mm.

3.2.2 Eustatic term

As aforementioned, the GRACE mission measures spatio-temporal gravity variations, providing direct monitoring of water mass change in the Earth system [Tapley et al., 2004a, 2004b; Wahr et al., 2004]. Here we focus on the ocean mass component that can be determined by considering the GRACE data over the oceanic domain. We use the same L-2 GRACE data than in chapter 2, but from April 2002 through December 2003. Note that several monthly solutions are still missing (June 2002, July 2002, December 2002, January 2003 and June 2003).

[1]This IB correction has been implemented by K. Dominh from LEGOS. The IB correction applied to the altimetric merged solution, which has been used in the rest of the chapters, takes $P(t) = 1013.3$ mbar as constant value [AVISO, 1996]. This fact is relevant in the global ocean, but not in the Mediterranean Sea where the IB response of the ocean is constrained by the narrow Strait of Gibraltar and the IB corrected MSL closely follows the non-IB corrected MSL (figure 1.3).

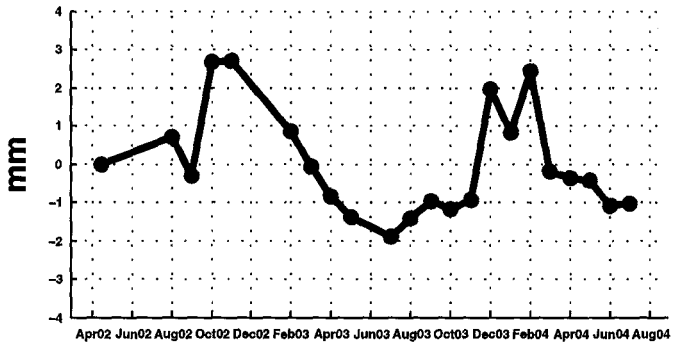

Figure 3.1: Water thickness equivalent average over the oceanic domain between 60°S and 60°N of the barotropic ocean model applied to L-2 GRACE data.

During the GRACE data processing, a number of effects are modelled (see section 2.2.3). Since we are interested into the total ocean mass signal, we restored the barotropic ocean model removed during the GRACE data processing, as recommended in Flechtner (2003). As mentioned in Chambers et al. (2004), the barotropic model is mass-conserving. Thus it cannot introduce parasitic signal to GRACE SLV_{mass} as far as global average is concerned. However, we checked that missing the high-latitude ocean domain above 60°N/S, has a small, but non negligible effect on the SLV_{mass} curve (figure 3.1). We also restored the atmospheric loading model. Thus, over the ocean, the total GRACE signal, which now includes both atmospheric and oceanic loads, accounts for the IB effect (i.e., locally, any atmospheric pressure anomaly is cancelled by a corresponding ocean mass anomaly). However, for comparison with the IB-corrected sea level change based on T/P altimetry, we have to remove, from the GRACE signal, the $P(t)$ term (i.e., mean atmospheric surface pressure averaged over the whole oceanic domain). In effect, this term is removed from the altimetry data when applying the IB correction. This is unlike the GRACE data: when averaged over the oceanic domain, the sum of the restored atmosphere plus ocean loads, while cancelling locally the ocean response to atmospheric mass anomalies, leads to a non zero term, equal to $P(t)$. It has thus to be removed to the GRACE data too.

As already mentioned in chapter 2: i) GRACE data do not include degree-1 spherical harmonic coefficients. Then, to be consistent with the reference frame used for T/P, an estimate of those coefficients are added to GRACE data (see section 2.2.3 and A.8). ii) The degree-2, order-0 coefficient, representing the Earth's oblateness [Cox and Chao, 2002], is not well observed by GRACE [Tapley et al., 2004a]. Therefore, we use an accurate estimate of the degree-2, order-0 coefficient based on SLR observations (updated from Cox and Chao, 2002; Cox, personal communication, 2005). iii) For a discussion about consistency between the pole tide corrections applied to altimetry and GRACE data, see section 2.2.3.

Assuming that the gravity changes observed by GRACE are produced by mass changes at the surface of the Earth, the GRACE monthly geoid data can be converted into surface mass variations and expressed into equivalent water height [Wahr et al., 1998; Chao, 2005]. In order to minimize the leakage error due to land water mass signal over the continents, a Gaussian filter as described by Swenson and Wahr (2002) was applied to the GRACE data over the 60°S-60°N ocean domain for each month from April 2002 through December 2003 (see section A.7). We tested two Gaussian filter radius, 300 km and 1000 km. In principle, the smaller the radius, the smaller the leakage. However, because of noise affecting higher degree spherical harmonic coefficients of the current GRACE solutions [Tapley et al., 2004a; Wahr et al., 2004], we choose the 1000 km radius, which by definition removes all signal beyond degree 30 (see figure A.2). Alternative approaches to process the GRACE data that aim at reducing the noise at high degrees, in order to improve spatial resolution, are currently explored by several groups. For example, Rowlands et al. (2005) reported a factor of 3 improvement in both temporal and spatial resolutions through a "mascon" analysis of GRACE data.

Errors associated to each spherical harmonics coefficient are released with the GRACE L-2 data. These errors are weighted similarly to the coefficients during the Gaussian filter processing. Then, the error associated to GRACE-derived SLV_{mass} estimate is computed as described in Swenson and Wahr (2002), which is estimated around $\backsim$2 mm.

3.3 Results

3.3.1 Combining GRACE and T/P altimetry data

Figures 3.2a, 3.2b and 3.2c presents the observed T/P SLV_{total}, GRACE SLV_{mass} and the differences between the two time series (noted $SLV_{total} - SLV_{mass}$). These curves are based on a spatial averaging between 60°S and 60°N. The least-squares fitted annual amplitudes and phases of the three time series are presented in Table 3.1. The SLV_{total} has an annual amplitude of 6.1±1.2 mm, and a phase of 309.7°±11.3° (maximum signal in early November). The GRACE SLV_{mass} has an annual amplitude is 10.9±1.1 mm and a phase of 276.5°±7.8° (maximum signal in early-October). Note that the GRACE SLV_{mass} computed over the whole oceanic domain, which represents the total water budget exchanged between the ocean and the atmosphere/continents, has an annual amplitude of 10.0±2.3 mm and a phase of 282.1°±16.3° (maximum signal in mid-October). Accounting for the global ocean surface, this signal represents a water mass variation of $6.86 \cdot 10^{12}$ m^3 from peak to peak.

The annual amplitude of the difference curve is 6.4±2.1 mm, with a phase of 72.7°±22.3° (maximum signal on 15 March). In principle this difference curve represents the steric contribution to SLV. The annual amplitude and phase of the residual curve compare well with published estimates of the steric annual sea level based on climatologies. For example, Chen et al. (1998), using World Ocean Atlas 1994 (WOA94) objectively analyzed temperature fields [Levitus et al., 1994a, 1994b], report an amplitude of 5.5 mm and a phase of 79° (corresponding to 20 March) for the annual steric sea level cycle. Minster et al. (1999) and Cazenave et al. (2000), also using the Levitus et al. (1994a, 1994b) climatology, found an amplitude of 5 mm and a maximum signal on March 12. Thus the result reported here by combining T/P SLV_{total} and GRACE ocean mass appears quite comparable with values based on ocean data climatologies.

3.3.2 Steric sea level data

We have compared the residual ($SLV_{total} - SLV_{mass}$) time series with the steric sea level computed using Ishii et al. (2006)' global ocean temperature data. The

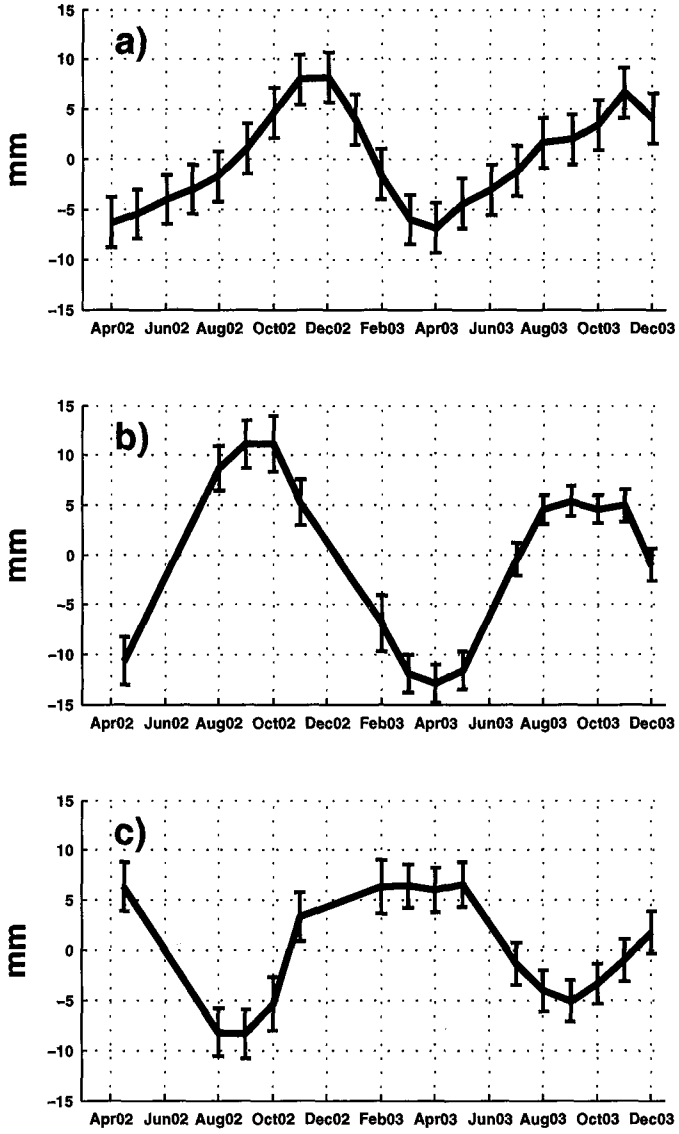

Figure 3.2: Sea Level Variations (SLV) over 2002-2004. (a) T/P SLV_{total}. (b) GRACE SLV_{mass}. (c) $SLV_{total} - SLV_{mass}$

	Period (month/year)	A (mm)	ϕ
SLV_{total} ($\pm 60^o$)	04/02 - 12/03	6.1 ± 1.2	$309.7^o \pm 11.3^o$
SLV_{mass} ($\pm 60^o$)	04/02 - 12/03	10.9 ± 1.1	$276.5^o \pm 7.8^o$
$SLV_{total} - SLV_{mass}$($\pm 60^o$)	04/02 - 12/03	6.4 ± 2.1	$72.7^o \pm 22.3^o$
SLV_{steric} ($\pm 60^o$)	04/02 - 12/03	5.3 ± 1.0	$101.4^o \pm 11.3^o$

Table 3.1: Annual amplitude (A) and phase (ϕ) of the different spatially averaged monthly time series and the period covered by the datasets. The uncertainty indicates 95% formal error.

latter data set consists of $1^\circ \times 1^\circ$ gridded temperature fields given as monthly means down to 700 m, from 1945 to 2003 (see Ishii et al. 2003,2006; for detailed description). Unless using an ocean temperature climatology (i.e., based on data averaged over many years) as done in Chambers et al. (2004), the Ishii et al. data base is the only one providing monthly mean temperatures suitable for the short time span of overlap with the GRACE data (April 2002 through December 2003). Indeed other available global ocean data bases (e.g., Levitus et al., 2005; Willis et al., 2004) provide only yearly-mean temperatures. We have computed monthly steric sea level maps by vertically integrating density anomalies based on the Ishii et al. (2006) temperature anomalies, through the equation of state of sea water (see Lombard et al., 2005). The monthly steric sea level data were further spatially averaged between 60°S and 60°N, using equi-area weighting. The resultant time series is denoted SLV_{steric} and is shown in figure 3.3. Error bars of the monthly values are crudely estimated to ± 5 mm, based on the errors provided in Ishii et al. (2006), for the annual means. The corresponding best fitting annual sinusoid has an amplitude of 5.3 ± 1.0 mm and a phase of $101.4^\circ \pm 11.3^o$ (maximum on 10 April). The amplitude agrees very well with that of the WOA94 climatology, while a 22° phase difference is noted. The latter difference can easily be explained by the difference in time span between the two different data sets.

On figure 3.3 is superimposed the ($SLV_{total} - SLV_{mass}$) curve (i.e., figure 3.2c). We observed a good agreement between the two curves, within the error bars, for all studied months, with two exceptions: November 2002 and February 2003. The annual amplitudes of the two signals also show a very good agreement,

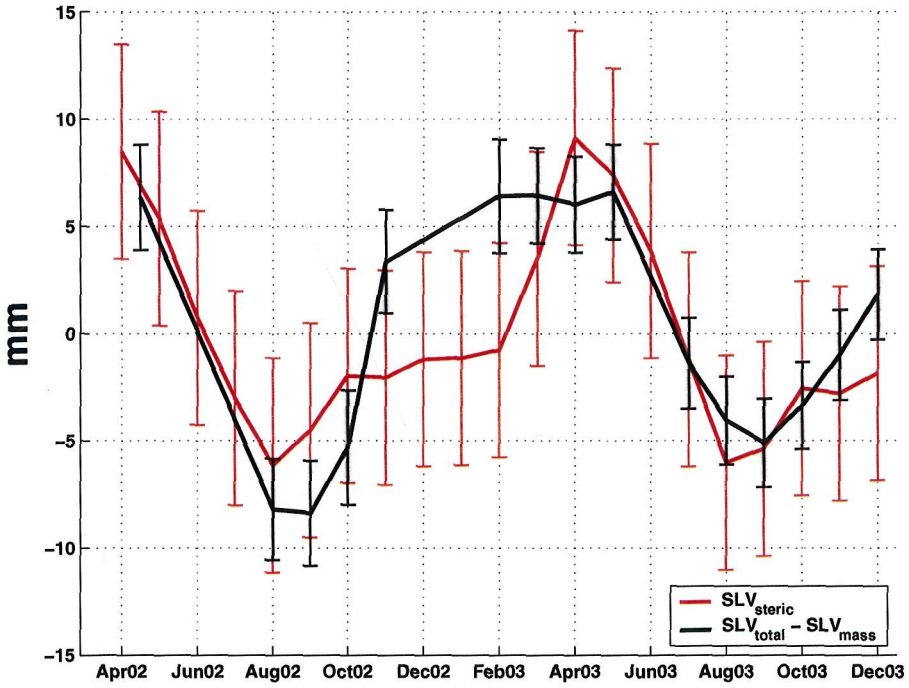

Figure 3.3: Red curve: SLV_{steric} (based on Ishii et al. (2006) data); Black curve: $SLV_{total} - SLV_{mass}$.

with only 1 mm difference (see Table 3.1). As far as the phases are concerned, we note a 30° difference, with the phase of $(SLV_{total} - SLV_{mass})$ closely coinciding with the phase of the steric sea level deduced from the WOA94 climatology. This result validates the applied methodology, which allows us to estimate steric sea surface height variations independently from in situ hydrographic data.

3.4 Discussion and conclusions

In this study, we combined global mean sea level data from T/P altimetry and GRACE data averaged over the same oceanic domain (60°N-60°S) and compared the difference time series to the steric sea level estimated over the same time span (and same oceanic domain) from in situ hydrographic data. An overall good agreement between the two data sets has been noticed. However the observed steric sea level and that deduced from T/P-GRACE do not exactly coincide. Several reasons may be invoked: (1) errors of the different data sets, (2) Deep ocean contribution, not accounted in the thermal expansion curve (based on the upper 700 m ocean layer), and (3) effect of salinity. However, the annual cycle of thermal expansion mainly occurs in the upper ocean layers (0-500 m), so that unaccounted deep thermal expansion is unlikely to be large. The effect of salinity on the global SLV is negligible compared to thermal expansion, on interannual to decadal time scales [Antonov et al., 2002; Ishii et al., 2006]. To check whether at annual time scale, the salinity contribution to sea level is also negligible in terms of global mean, we have also estimated the SLV_{steric} signal accounting for both temperature and salinity, using for the latter, the monthly salinity variations of a standard year based on the WOA01 climatology. In that case, a negligible difference of 0.2 mm and 1.2° was observed in the annual amplitude and phase, respectively. Besides, the salinity curve does not show any annual signal. Finally data errors, both in GRACE data and in the steric sea level, may be the dominant factors explaining the phase difference between the $SLV_{total} - SLV_{mass}$ curve and the steric sea level. For the latter, under sampling of the southern oceans may be the largest source of uncertainty. The fact that the phase of the $SLV_{total} - SLV_{mass}$ curve agrees well with the mean steric sea level curves based on ocean temperature climatologies (which provide better coverage of the oceans over the long time spans of data averaging) suggests that this is indeed the case.

It is important to emphasize that the maximum of the ocean mass and steric annual SLV cycles are shifted by about 150°-180° (5-6 months). A similar behaviour has also been observed in previous studies of the global ocean [Chen et al., 1998; Minster et al., 1999; Cazenave et al., 2000], as well as in local studies like the Mediterranean Sea (see chapter 2). This difference in phase means that the water budget of the ocean is minimum when the steric sea level, and then the

heat content in the ocean, is maximum. Depending on the estimate, the maximum SLV_{steric} is reached between 72.7° (mid-Mars) and 101.4° (early-April), following the austral summer when the heat stored is maximum in the southern ocean. The annual cycle of the ocean mass variation results mainly from land water storage variations, plus a small contribution from the atmospheric water vapour [Chambers et al., 2004; Chen et al., 1998; Minster et al., 1999; Cazenave et al., 2000; Milly et al., 2003]. These studies, based on comparisons between T/P SLV_{total} (corrected for steric effects) and global land models outputs, showed that seasonal change in the snow pack is the main driver of the annual ocean mass variation. But in addition, Ngo-Duc et al. (2005a, 2005b), showed that underground water stored in the major tropical basins (Amazon, Congo, etc.) in response to seasonal precipitation plays a non negligible role.

The present study is limited to a very short time span of less than 2 years. However when the GRACE time series extend in the future, this approach will provide new information on the global ocean heat content change, with important perpectives on a better estimate of the oceans contribution to the net radiative imbalance of the Earth's climate system [Levitus et al., 2005] and to sea level rise.

Chapter 4

Another altimetric application: Vertical Crustal Motion estimates

4.1 Introduction

The altimetry measurement of the SLV is relative to a reference ellipsoid, and then is given in a absolute geocentric reference frame. On the other hand, the TG measurement gives the SLV relative to the solid ground on which the TG is fixed. Hence any vertical ground motion, for whatever reasons, will masquerade as an apparent sea level variation: An apparent sea level rise would be added to the absolute sea level motion as the land sinks, and conversely. Therefore, in principle the difference between the two data types, altimetry and TG, is the absolute vertical ground motion [Nerem and Mitchum, 2002; Cazenave et al., 1999]. Let $TG(t)$ denote the time series of the TG record of SLV, and $Alt(t)$ be that measured by altimetry at the closest point to the TG site. Ideally, apart from measurement noise and the fact that the actual locations are not exactly the same (especially when coastal geometry influences are significant), $Alt(t)$ and $TG(t)$ should be found to fluctuate in unison in a linear approach, the only difference would be the actual vertical ground motion at the TG site. At places where the latter is known or negligible, this has been the basis for the in-situ calibration/validation for altimetric measurements [Chambers et al., 1998; Mitchum, 1994, 1998, 2000]. In this paper

we will form the difference time series $Alt(t) - TG(t)$ and examine its long-term behaviour on at least decadal timescales, where the local/geographic differences become less important and the effect of measurement noise can also be greatly reduced by averaging. It is hoped that a decade long record of $Alt(t) - TG(t)$ should be able to give unequivocal information about the long-term vertical ground motion in the absolute sense. We will not be concerned about timescales shorter than interannual and seasonal periods, for which $Alt(t) - TG(t)$ signifies primarily the surface mass loading effects on the ground, both tidal and non-tidal.

We shall estimate the linear trend, or slope, of the $Alt(t) - TG(t)$ record for each of the available TG locations along the northern coast of the Mediterranean Sea and the Black Sea. In this region, the post-glacial rebound effect in the vertical ground motion is minimal according to geophysical models, around $\pm 0.1/0.2$ mm/year [Peltier, 2001], so our result reflects the vertical ground motion arising primarily from tectonics, except at the sites where local 'noises' are evident, for example ground subsidence due to land settlement or groundwater extraction. This provides for regional tectonics studies source information that is independent of, and complementary to, other data types such as gravity and GPS. In fact, the series of vertical motion recorded at various continuous GPS stations will be compared with our results for further insight.

4.2 Data

Figure 4.1 shows the locations of all data used in this study as described below. The numbering of the TG sites, which is in the west-to-east order along the coast, corresponds to the numbering in Tables 4.1 and 4.2; the same goes with the GPS stations with respect to Table 4.3. In figure 4.1 the altimetry grid points are indicated by the dots; those closest to each TG are indicated by the larger dots; and circles correspond to TG locations.

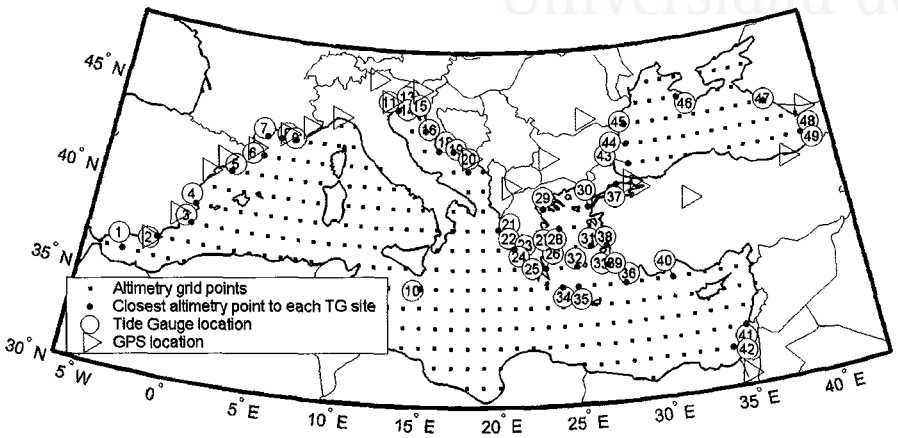

Figure 4.1: Data locations used in this study.

4.2.1 Altimetry Data

The altimetry data sets used in this study were provided by NASA's Ocean Altimeter Pathfinder Project prior to 2003. In particular, we use the multi-mission altimetry data for the 9-year period of 1993 - 2001, where the source data come from the T/P and ERS-1 and -2 satellites. The data are given on continuous monthly 1 degree by 1 degree grided. All "standard" corrections have been applied to the data, including the T/P instrument drifts, the solid-Earth, ocean and pole tides, and the inverse barometer (IB) correction. The region we examine for the Mediterranean and Black seas is between 5°W and 42°E in longitude, 30°N and 48°N in latitude. We select the altimetry measurement at the closest point to the tide gauge as stated.

4.2.2 Tide Gauge Data

In this study we use TG data available from the Permanent Service for Mean Sea Level (PSMSL) [Spencer and Woodworth, 1993]. For the present study we choose, for 42 gauges along the northern coast of Mediterranean and 7 along the

Black Sea coast, the so-called RLR (Revised Local Reference) series that provide precise information about the TG benchmark. Data are monthly time series that cover most of the 9-year altimeter period of this study (see figure 4.2 for the data availability of each tide gauge station). Barring some limited earlier TG activities in Egypt (pre-dating our study period), no data are available from the southern coast of Mediterranean. Neither are the many TG records from the Italian peninsula reported to PSMSL in recent years [Tsimplis and Spencer, 1997] (but see Fenoglio-Marc, 2004; for analysis of the Italian records). Otherwise, the spatial distribution of the TG that we use (those with data after 1993 in PSMSL) is quite dense and homogeneous along the Mediterranean and Black Sea coasts, as shown in Figure 4.1.

4.3 Analysis and Results

It is clear that all the data series above are dominated by very strong seasonal signals, primarily annual and semi-annual. There are of course various meteorological as well as geophysical reasons why this is so, but whatever the reasons, they are outside of our present interest. It is thus desirable to remove the seasonal signals from our data series, as their presence would skew our later estimates in various ways and render our statistics intractable due to the strong departure from broad-band or "white" statistics.

We remove the seasonal signals from the original time series by simple subtraction of estimates obtained by least-squared fitting of seasonal sinusoids with annual and semiannual periods. We then compare the altimetry observed SLV, $Alt(t)$, at the closest grid point to a TG location with the given $TG(t)$. In general, a good agreement can be observed between the two time series, showing a same temporal behaviour in much of the SLV. In particular, for example, in chapter 1 the prominent and abrupt change in the slope of the Mediterranean and Black Sea SLV during 1999 was found to exist in both $Alt(t)$ and $TG(t)$. However, when examining the long-term behaviour of SLV, discrepancies between the two data sets, which are our sought signal, arise. In Figure 4.3, three examples of such comparison are shown, – Marseille and Trieste in the Mediterranean, and Tuapse in the Black Sea. The time series on the left are the original observation data

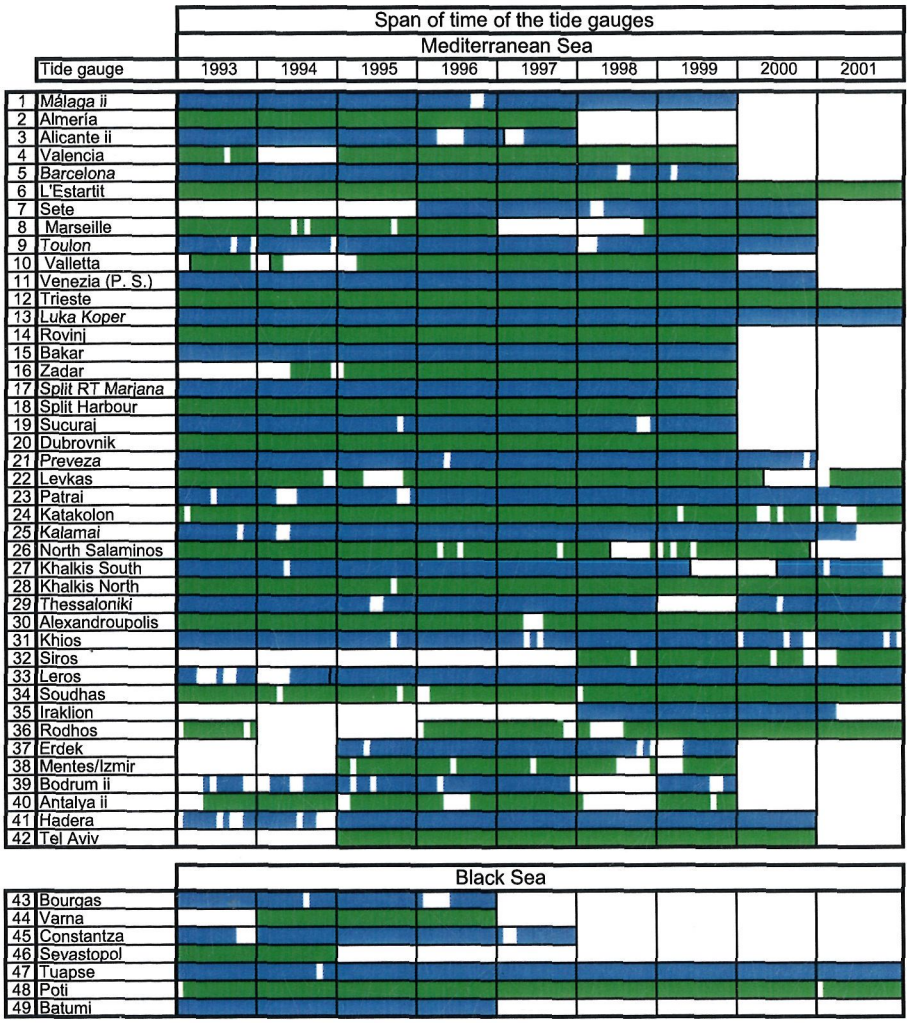

Figure 4.2: Span of time of the tide gauge data.

from the two sources; the middle column those after the removal of the nominal seasonal signals as just described. The right column shows the respective non-seasonal $Alt(t) - TG(t)$ difference series.

As stated, a TG measures the SLV relative to the ground on which the TG sits, whereas the altimetry measures the absolute SLV relative to the terrestrial reference frame with respect to which the satellite orbit is defined. Their difference then contains all information about the vertical ground motion of the tide gauge location in the terrestrial frame. We form the (non-seasonal) $Alt(t) - TG(t)$ for the 49 PSMSL TG sites as described above and estimate their slopes using least-squares linear fit - a positive slope means land uplift while a negative slope land subsidence. Such linear slopes are plotted in the right columns of Figure 4.3.

Tables 4.1 and 4.2 shows our estimates for the $Alt(t) - TG(t)$ linear slopes for all stations in the Mediterranean and Black Sea, respectively. As the seasonal signal has been removed from all time series, we can assume a linear relation as in equation 1.1. Positive values are in red (land up-lift), negative values in blue (land subsidence), while uncolored indicates values statistically indistinguishable from zero within 1 standard deviation (given in the last column), which has been estimated with equation 1.4. Figure 4.4 gives a map view of the same results as Tables 4.1 and 4.2, where the "up" triangles represent land uplift, the "down" triangles represent land subsidence, circle means indistinguishable from zero, all color-scaled. It is seen that, except for a few near-zero ones and those that are known to have large local influences, the uplift-subsidence has definite spatial grouping, signifying regional patterns that are most likely of tectonic origin. This will be discussed below.

Several error sources are considered in estimating vertical land movements from the Alt-TG time series. For one thing, we compare SLV at geographical points that are not exactly the same locale but are the closest grid point where the seasonal and shorter responses can be significantly different depending on the coastal geometry. Also, corrections for the solid-Earth and ocean tides, solid-Earth pole tides, and the equilibrium inverted barometer effects are all applied in the altimetry data, but not in the TG data. However, errors due to such differences are insignificant as far as the long-term trend is concerned and in any case small in magnitude. On the other hand, errors have been made also in the preparation and processing of data. Further errors come from the secular drift of the T/P

Mediterranean Sea: Linear rate of change (mm/year)				
	Tide Gauge site (country)	Location	Trend	Sigma
1	Málaga ii (Spain)	36 43 N 04 25 W	-3.1	2.4
2	Almería (Spain)	36 50 N 02 29 W	-8.5	3.2
3	Alicante ii (Spain)	38 20 N 00 29 W	-18.9	3.9
4	Valencia (Spain)	39 28 N 00 20 W	**1.2**	3.1
5	Barcelona (Spain)	41 21 N 02 10 E	5.2	2.4
6	L'Estartit (Spain)	42 03 N 03 12 E	**-0.4**	1.6
7	Sete (France)	43 24 N 03 42 E	6.2	5.2
8	Marseille (France)	43 18 N 05 21 E	-2.3	2.0
9	Toulon (France)	43 07 N 05 55 E	**1.6**	1.9
10	Valletta (Malta)	35 54 N 14 31 E	-8.9	2.8
11	Venezia P.S. (Italy)	45 26 N 12 20 E	-5.5	2.4
12	Trieste (Italy)	45 39 N 13 45 E	-4.9	2.2
13	Luka Koper (Slovenia)	45 34 N 13 45 E	5.7	2.5
14	Rovinj (Croatia)	45 05 N 13 38 E	-6.0	2.8
15	Bakar (Croatia)	45 18 N 14 32 E	-9.5	3.2
16	Zadar (Croatia)	44 07 N 15 14 E	**-0.2**	5.0
17	Split RT Marjana (Croatia)	43 30 N 16 23 E	-3.6	2.6
18	Split Harbour (Croatia)	43 30 N 16 26 E	-3.9	2.6
19	Sucuraj (Croatia)	43 08 N 17 12 E	-5.7	3.4
20	Dubrovnik (Croatia)	42 40 N 18 04 E	-5.0	2.3
21	Preveza (Greece)	38 57 N 20 46 E	-18.0	2.3
22	Levkas (Greece)	38 50 N 20 42 E	-16.2	1.9
23	Patrai (Greece)	38 14 N 21 44 E	-13.7	2.3
24	Katakolon (Greece)	37 38 N 21 19 E	-13.9	2.1
25	Kalamai (Greece)	37 01 N 22 08 E	**-0.1**	1.6
26	North Salaminos (Greece)	37 57 N 23 30 E	9.4	2.0
27	Khalkis South (Greece)	38 28 N 23 36 E	8.9	2.2
28	Khalkis North (Greece)	38 28 N 23 36 E	4.5	1.7
29	Tessaloniki (Greece)	40 37 N 23 02 E	**1.5**	1.7
30	Alexandroupolis (Greece)	40 51 N 25 53 E	6.5	1.6
31	Khios (Greece)	38 23 N 26 09 E	4.5	2.2
32	Siros (Greece)	37 26 N 24 55 E	**0.1**	4.2
33	Leros (Greece)	37 05 N 26 53 E	12.1	1.9
34	Soudhas (Greece)	35 30 N 24 03 E	4.0	1.4
35	Iraklion (Greece)	35 20 N 25 08 E	**-5.6**	6.7
36	Rodhos (Greece)	36 26 N 28 14 E	-7.8	1.6
37	Erdek (Turkey)	40 23 N 27 51 E	**0.2**	5.2
38	Mentes/Izmir (Turkey)	38 26 N 26 43 E	-11.8	4.0
39	Bodrum ii (Turkey)	37 02 N 27 25 E	22.3	5.1
40	Antalaya ii (Turkey)	36 50 N 30 37 E	-18.7	4.1
41	Hadera (Israel)	32 28 N 34 53 E	-3.2	1.8
42	Tel Aviv (Israel)	32 05 N 34 46 E	**-3.5**	3.6

Table 4.1: Linear Rate of Change, or slope, (mm / year) of the Alt-TG Series in the Mediterranean Sea. Negative values (highlighted in blue) indicate land subsidence, positive values (in red) indicate land uplift, the uncolored are values indistinguishable from zero within 1 sigma. The numbering of the sites corresponds to Figure 4.1.

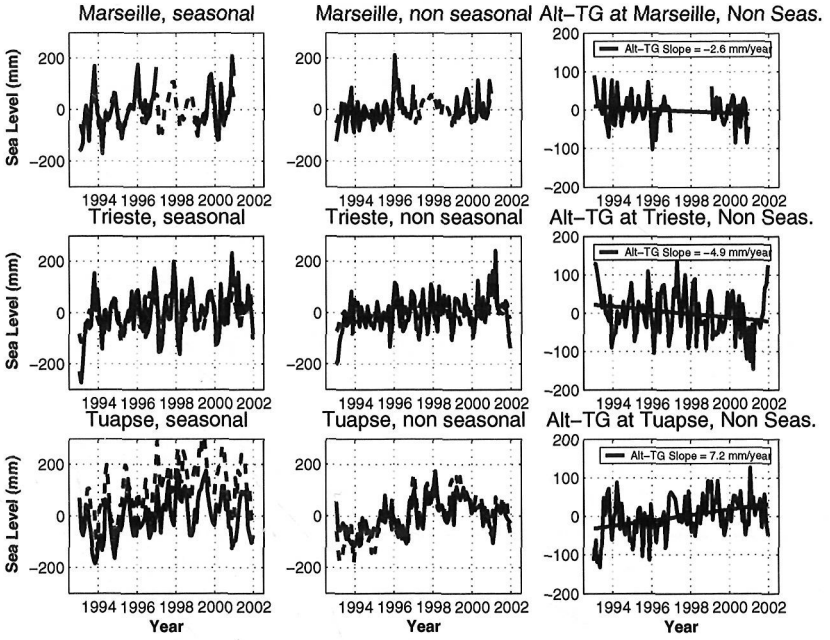

Figure 4.3: The first and second columns show seasonal and not seasonal Alt (solid line) and TG (dashed line) time series at Marseille (first row), Trieste (second row) and Tuapse (third row). The third column shows the non-seasonal Alt-TG time series and the least-squared linear fit to give the slope.

instruments (altimeter as well as radiometer for atmospheric correction) although such drifts have been corrected to the extent possible by the T/P Projects based on in-situ calibrations [Ruf, 2000; Keihm et al., 2000]. These error sources mainly impact our estimates of the vertical land movement that are close to zero, which we have indicated in our results.

For gaining more insight and for further validation we can compare our linear trend estimates for the vertical ground motion derived from $Alt(t) - TG(t)$ with corresponding data from permanent, continuous GPS stations that are reasonably nearby in location to the TG stations. About 150 GPS stations from the EUREF

Black Sea: Linear rate of change (mm/year)				
	Tide Gauge site (country)	Location	Trend	Sigma
43	Bourgas (Bulgaria)	42 29 N 27 29 E	-12.1	8.2
44	Varna (Bulgaria)	43 11 N 27 55 E	-30.8	8.5
45	Constanza (Romania)	44 10 N 28 40 E	**-1.5**	6.1
46	Sevastopol (Ukraine)	44 37 N 33 32 E	**3.3**	14
47	Tuapse (Russian Federation)	44 06 N 39 04 E	7.1	1.8
48	Poti (Georgia)	42 10 N 41 41 E	4.7	2.9
49	Batumi (Georgia)	41 38 N 41 42 E	27.7	8.5

Table 4.2: The same as 4.1 but for the Black Sea.

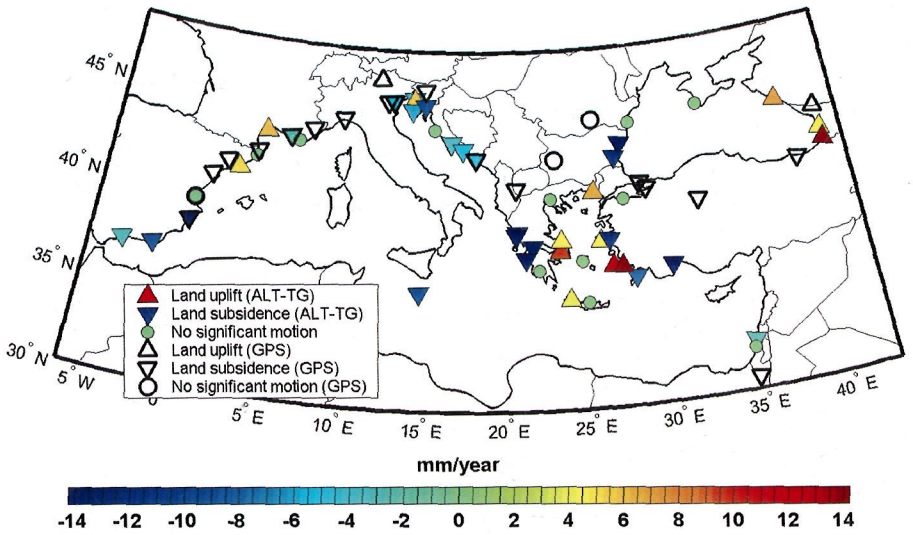

Figure 4.4: Vertical land movement along the Mediterranean and Black Sea coasts derived from Alt-TG time series

Permanent Network (EPN)[1], distributed over 32 European countries, acquire high quality GPS data in near real-time. In particular we use the cleaned GPS time series for 22 stations, close to the TG (Figure 4.1), produced by the EPN Time Series Monitoring Project [A. KENYERES, personal communication, 2005]. These GPS time series did not start until late 1990s or early 2000s, so they generally only have limited overlap with the available TG data (see figure 4.2). For that reason, we only use the GPS data (till late 2002) in a rudimentary comparison with respect to the sign of the vertical velocity, where a general good agreement in sign is observed. This result is shown in Figure 4.4, whereas the numerical values are given in Table 4.3.

We also compared our linear trend estimates for the vertical ground motion with those obtained via several GPS campaigns from the SELF (Sea Level Fluctuations) projects during the years 1993 - 1998 as reported by Becker et al. (2002). We note the following: (i) Becker et al. (2002) found no significant vertical motion in Spain, whereas our $Alt(t) - TG(t)$ result in face value indicates a coastal subsidence in Southern Spain. The reason is presently unclear (but see Section 4). (ii) Becker et al. (2002) reported a slight uplift at Venice and a subsidence at Trieste in Italy, whereas we found significant subsidence at both sites. (iii) In Greece, a general agreement is observed at Katakolon, Patrai, Preveza and Rodhos where subsidence is reported, unlike the disagreement at North of Crete (Soudhas) and Alexandroupolis where we found uplift, and at Kalamai, Siros and Iraklion where we found no significant motion with little TG data available in the two latter. (iv) In the Black Sea, a good agreement in subsidence is found at Varna and Bourgas.

4.4 Discussions and Conclusions

The absolute rates of vertical ground motion obtained in this work (Figure 4.4 and Tables 4.1 and 4.2) are in accord with the general notion that the Mediterranean is a location of plate subduction boundary, and the seismicity is more active in the eastern Mediterranean and gets quieter towards the north. Here in order to establish the framework to draw farther conclusions, we need to delve deeper

[1] <http://www.epncb.oma.be>

Vertical velocities at GPS stations (mm/year)				
	Mediterranean Sea			
	GPS site (country)	Location	Trend	Sigma
1	Alicante (Spain)	38 20 N 00 29 W	-3.21	0.19
2	Valencia (Spain)	39 29 N 00 20 W	**-0.68**	0.91
3	Ebre (Spain)	41 49 N 00 30 E	-1.33	0.10
4	Bellmunt (Spain)	41 36 N 01 24 E	-0.22	0.18
5	Cap de Creus (Spain)	42 19 N 03 18 E	-0.44	0.31
6	Marseille (France)	43 17 N 05 21 E	-2.35	0.16
7	Calern (France)	43 45 N 06 55 E	-0.78	0.11
8	Genova (Italy)	44 25 N 08 55 E	-1.66	0.21
9	Bolzano (Italy)	46 29 N 11 20 W	1.33	0.23
10	Venezia (Italy)	45 26 N 12 20 E	-5.95	0.74
11	Padova (Italy)	45 24 N 01 15 E	-6.32	0.75
12	Geoservis GR.1 (Slovenija)	46 03 N 14 33 E	-1.18	0.96
13	Dubrovnik (Croatia)	42 39 N 18 07 E	-5.31	0.52
14	Orhid (Macedonia)	41 08 N 20 48 E	-0.68	0.47
15	Sofia (Bulgaria)	42 33 N 23 24 E	**-0.17**	0.18
16	Mitzpe Ramon (Israel)	30 36 N 34 46 E	-2.25	0.48
	Black Sea			
17	Bucuresti (Romania)	44 28 N 26 08 E	**0.11**	0.18
18	Istambul (Turkey)	41 06 N 29 01 E	-0.52	0.28
19	Gebze (Turkey)	40 47 N 29 27 E	-4.33	0.23
20	Ankara (Turkey)	39 53 N 32 46 E	-1.70	0.17
21	Trabzon (Turkey)	41 00 N 39 47 E	-3.27	0.48
22	Zelenchukskaya (Russia)	43 17 N 41 34 E	0.68	0.26

Table 4.3: Vertical velocities (mm / year) of the GPS time series up to $\backsim$1199 GPS week (late 2002). Negative values indicate land subsidence, positive values indicate land uplift. The sign of these values is represented in Figure 4.4.

into the complexity of the Mediterranean tectonics. Prior to that, however, we should assess the impact of the glacial isostatic adjustment (GIA) on the vertical ground motion. Model of GIA by Peltier (2001) puts the vertical ground motion at around $\pm 0.1/0.2$ mm/year in the Mediterranean and Black Sea region. That amounts to just a small fraction of the land uplift/subsidence rates reported here. Thus, the vertical ground motion due to GIA does add to or subtract from the otherwise tectonic ground motion detected in our results, but the magnitude of that "contamination" is relatively small and has generally little, if any, impact on the sign of our results. Therefore we shall ignore the GIA influence in the discussion on tectonics below.

Figure 4.5 depicts the main tectonic processes in the Mediterranean and Black Seas. In the Mediterranean the collisions between the African, Eurasian and Arabic plates have produced a very complex tectonic regime of microplates that is far from resolved, especially with respect to vertical motions [R. Sabadini, H. Drewes, personal communication, 2003]. Some of the present plate boundaries, especially in the eastern Mediterranean, appear to be so diffuse and so anomalous that they cannot be categorized into the three classical types of plate boundaries - subduction, spreading, and transform. The global tectonic models NUVEL1 [Demets et al., 1990] and geodetic data establish that the Eurasian and African plates converge along NW-SE direction, both rotating anticlockwise [Jimenez-Munt et al., 2002].

Being one of the most seismically active and rapidly deforming continental regions in the world, the Aegean Sea area in the eastern Mediterranean should be taken in special consideration. In this area, including western Turkey and Greece, many destructive earthquakes have occurred throughout history. The Crete island situates in the north side of the Hellenic Arc, which is the result of the ongoing collision between the African and Eurasian plates, causing Anatolian plate (Turkey) to move westward [McKenzie, 1972; Jimenez-Munt and Sabadini, 2002]. As a result, the African block is subducted northward, producing an uplift in Crete island [Rahl et al., 2004], which is in agreement with our results found in Soudhas. It may seem in contradiction with the fact that we do not find any vertical motion at Iraklion. However, the results in the former are more reliable because its time series is 3 times longer that the one in the latter (see figure 4.2).

A general and distinct land subsidence in the west coast of Greece and the

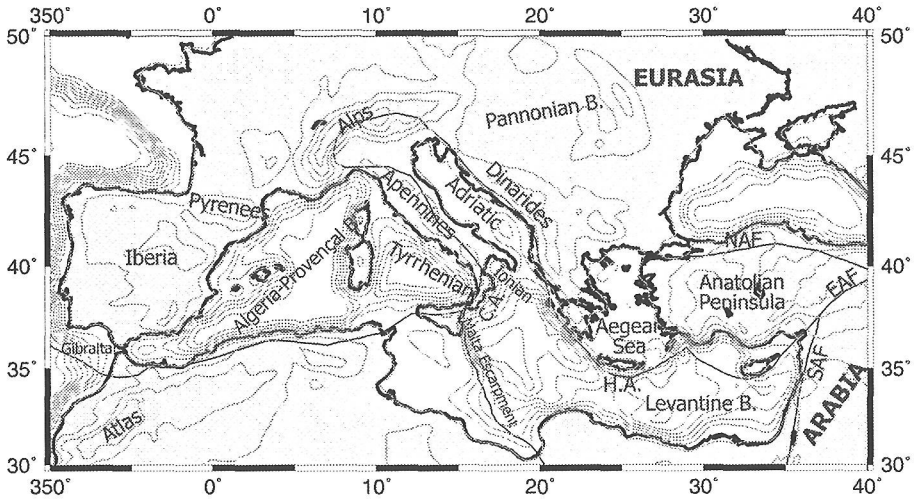

Figure 4.5: Plates boundaries in the Mediterranean and Black Seas from Jimenez-Munt et al. (2002). H. A., Hellenic Arc; C. A. Calabrian Arc; B., Basin; NAF, North Anatolian Fault; SAF, South Anatolian Fault; EAF, East Anatolian Fault.

north-east coasts of the Adriatic Sea, is reported in this study. This finding may be related to the Adriatic lithosphere subducting beneath the Eurasian plate along the Dinarides fault (Figure 4.5). In particular, Venice has seen geological evidences of subsidence (due to the rollback of the Apennines subduction, the contemporary effect of the load of the Alpine belt on its foreland and the river sediments, and the exploitation of subsurface water) [Rutigliano et al., 2000]. Similarly, the uplift in the eastern coast of Greece may be explained as a consequence of the same but converse associated movements.

On the other hand, we find conflicting behaviour (in terms of uplift versus subsidence) in the TGs located on the eastern (Turkish) coast of the Aegean Sea. It is unclear whether or how much of it is due to data errors, local motions, or any interesting regional tectonics. This awaits further studies. Similarly, towards the west, noteworthy is the fact that our study reflects opposite behaviour in the case

of Sete and Marsella, on the French coast. Given their geographical proximity and if the results are correct, it might be related to the existence of a tectonic fault separating the two sites, although the exact location might not be clearly identified.

Finally, the western Mediterranean basins are almost totally surrounded by mountain belts that for the most part remain tectonically and seismically active. The three sub-basins of different ages reflect different stages in the development of the western Mediterranean by back-arc spreading in response to subduction of the African lithosphere beneath southern Europe. Our finding that the general area in southern Spain is subsiding is in odds with this subducting African plate model because such subduction should predict an uplift for the region. This appears quite interesting, but we should note that in the case of Alicante our estimate is strongly contaminated by the settling of the harbour construct on which the TG is situated.

In summary, in spite of several error sources in the Alt-TG series, with a sufficiently long time span up to 9 years we are able to obtain reliable estimates for the vertical ground motion at the TG sites along the northern Mediterranean and Black Sea coast. These results provide useful source data for studying, contrasting, and constraining tectonic models of the region.

Appendix A

Potential theory and GRACE data

This appendix is mainly based on Heiskanen and Moritz (1967) and Hofmann-Wellenhof and Moritz (2005).

A.1 Potential of a solid body

Accordingly to Newton's law of gravitation, two points of masses m_1 and m_2, separated by a distance l, attract each other with a force:

$$F = G\frac{m_1 m_2}{l^2}, \tag{A.1}$$

where G is the Newton's gravitational constant $G = 66.7 \cdot 10^{-9}\text{cm}^3\text{g}^{-1}\text{seg}^{-2}$.

For simplicity, we call one of the masses the attracting mass, denoted hereafter m, and the other the attracted mass, which will be equal to the unity. Then,

$$F = G\frac{m}{l^2} \tag{A.2}$$

expresses the force exerted by the mass m on a unit of mass located at P at distance l from m. In a rectangular coordinate system xyz, a such force is represented

as a vector from P to m and with magnitud F, denoted as $\mathbf{F}$. The latter can be obtained as

$$\mathbf{F} = \left(\frac{\partial V}{\partial x}, \frac{\partial V}{\partial y}, \frac{\partial V}{\partial z}\right) = grad(V), \tag{A.3}$$

where

$$V = \frac{Gm}{l} \tag{A.4}$$

is the called *potential of gravitation* of the mass m.

The potential of a system formed by n masses, $\{m_1, m_2, \ldots, m_n\}$, is the sum of the individual contributions:

$$V = \frac{Gm_1}{l_1} + \frac{Gm_2}{l_2} + \ldots + \frac{Gm_n}{l_n}, \tag{A.5}$$

where l_i is the distance between m_i and the attracted mass, $\forall i = 1, 2, \ldots, n$.

In the case of a solid body, we can consider a system of masses distributed continuously over its volume v. Then, the sum A.5 becomes the integral

$$V = G \iiint_v \frac{dm}{l} = G \iiint_v \frac{\rho}{l} dv, \tag{A.6}$$

where l is the distance between the mass element dm and the attracted point, which must be outside the body. The second identity comes from the relation $\rho = \frac{dm}{dv}$, where ρ is the density of a differential of mass with volume dv. This integral is known as *Newton's integral.*

The potential V is continuous when it is defined, that is outside the body, and vanishes at infinity like $1/l$ for $l \to \infty$. Then, for very large distances, the body acts approximately like a point mass, with the result that its attraction is then approximately given by A.4. Consequently, in Celestial Mechanics the planets are usually considered as point masses.

The first derivatives of V, that is, the force components, are also continuous throughout space, but not so the second derivatives. At points where the density changes discontinuously, some second derivatives have a discontinuity. This is evident because the potential V satisfies *Poisson's equation*

$$\Delta V = -4\pi G\rho, \tag{A.7}$$

where Δ is the *Laplacian operator*

$$\Delta V = \frac{\partial^2 V}{\partial x^2} + \frac{\partial^2 V}{\partial y^2} + \frac{\partial^2 V}{\partial z^2}. \tag{A.8}$$

Outside the attracting body, in empty space, the density ρ is zero and A.7 becomes

$$\Delta V = 0, \tag{A.9}$$

which is called *Laplace's equation* . Its solutions are called *harmonic functions*. More precisely, a function is called *harmonic* in a region Ω of space if it satisfies Laplace's equation at every point in Ω. If the region is the exterior of a certain closed surface, then it must vanish like $1/l$ for $l \to \infty$. Hence, the potential of gravitation is a harmonic function outside the attracting masses, but not inside the masses: there it satisfies Poisson's equation. Moreover, it can be shown that every harmonic function is *analytic* in Ω, that is, it is continuous and has continuous derivatives of any order.

A.2 Spherical harmonics

The Laplace's equation can be written in *spherical coordinates*, (r, θ, λ)=(radius, colatitude, longitude), which are related to the rectangular coordinates, (x, y, z), by (see figure A.1)

$$\begin{aligned} x &= r \sin\theta \cos\lambda, \\ y &= r \sin\theta \sin\lambda, \\ z &= r \cos\theta, \end{aligned} \tag{A.10}$$

or inversely by

$$\begin{aligned} r &= \sqrt{x^2 + y^2 + z^2}, \\ \theta &= \tan^{-1} \frac{\sqrt{x^2 + y^2}}{z}, \\ \lambda &= \tan^{-1} \frac{y}{x}. \end{aligned} \tag{A.11}$$

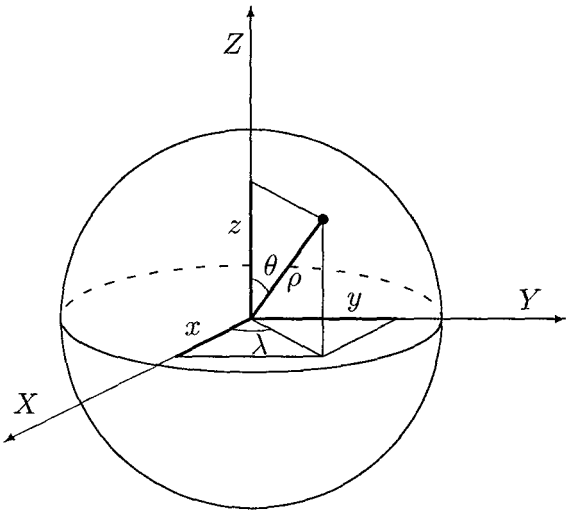

Figure A.1: Rectangular (x, y, z) and spherical (r, θ, λ) coordinates.

Then, Laplace's equation can be solved by separating the variables. In that case, the potential of a solid body can be written, at its exterior, like a power series of $1/r$,

$$V(r,\theta,\lambda) = \sum_{n=0}^{\infty} \frac{1}{r^{n+1}} \sum_{m=0}^{\infty} \left[a_{nm} P_{nm}(\cos\theta)\cos m\lambda + b_{nm} P_{nm}(\cos\theta)\sin m\lambda\right], \tag{A.12}$$

where a_{nm} and b_{nm} are the coefficients of the expansion, and P_{nm} are the *associated Legendre functions* of degree n and order m. P_{nm} is defined as

$$P_{nm}(t) = \frac{1}{2^n n!}(1-t^2)^{m/2}\frac{d^{n+m}}{dt^{n+m}}(t^2-1)^n. \tag{A.13}$$

If $n = 0$, we obtain the *Legendre's polynomials*:

$$P_n(t) = P_{n0}(t) = \frac{1}{2^n n!}\frac{d^n}{dt^n}(t^2-1)^n. \tag{A.14}$$

We denote

$$\mathcal{R}_{nm}(\theta,\lambda) = P_{nm}(\cos\theta)\cos m\lambda, \quad \text{(A.15)}$$

$$\mathcal{S}_{nm}(\theta,\lambda) = P_{nm}(\cos\theta)\sin m\lambda, \quad \text{(A.16)}$$

and these functions are called the *surface spherical harmonics* of degree n and order m. With this notation, A.12 can be written

$$V(r,\theta,\lambda) = \sum_{n=0}^{\infty}\frac{1}{r^{n+1}}\sum_{m=0}^{\infty}\left[a_{nm}\mathcal{R}_{nm}(\theta,\lambda) + b_{nm}\mathcal{S}_{nm}(\theta,\lambda)\right]. \quad \text{(A.17)}$$

With the following scalar product

$$< g,h >:= \int_0^{2\pi}\int_0^{\pi} g(\theta,\lambda)h(\theta,\lambda)\sin\theta\, d\theta d\lambda = \iint_\sigma g(\theta,\lambda)h(\theta,\lambda)\, d\sigma, \quad \text{(A.18)}$$

where σ represents the unit sphere, the surface spherical harmonics obeys the *orthogonality relations*:

$$< \mathcal{R}_{nm},\mathcal{R}_{rs} > = \iint_\sigma \mathcal{R}_{nm}(\theta,\lambda)\mathcal{R}_{sr}(\theta,\lambda)d\sigma = 0 \quad \text{si } s\neq n \text{ ó } m\neq r,$$

$$< \mathcal{S}_{nm},\mathcal{S}_{rs} > = \iint_\sigma \mathcal{S}_{nm}(\theta,\lambda)\mathcal{S}_{sr}(\theta,\lambda)d\sigma = 0 \quad \text{si } s\neq n \text{ ó } m\neq r,$$

$$< \mathcal{R}_{nm},\mathcal{S}_{rs} > = \iint_\sigma \mathcal{R}_{nm}(\theta,\lambda)\mathcal{S}_{sr}(\theta,\lambda)d\sigma = 0 \quad \text{in any case.} \quad \text{(A.19)}$$

For the product of two equal functions $\mathcal{R}_{nm}$ and $\mathcal{S}_{nm}$, we have, for $m=0$,

$$< \mathcal{R}_{n0},\mathcal{R}_{n0} >= \iint_\sigma [\mathcal{R}_{n0}(\theta,\lambda)]^2 d\sigma = \frac{4\pi}{2n+1}, \quad \text{(A.20)}$$

and for $m\neq 0$,

$$< \mathcal{R}_{nm},\mathcal{R}_{nm} >=< \mathcal{S}_{nm},\mathcal{S}_{nm} >=$$
$$= \iint_\sigma [\mathcal{R}_{nm}(\theta,\lambda)]^2 d\sigma = \iint_\sigma [\mathcal{S}_{nm}(\theta,\lambda)]^2 d\sigma = \frac{2\pi}{2n+1}\frac{(n+m)!}{(n-m)!}. \quad \text{(A.21)}$$

The *expansion theorem* states that an arbitrary (at least in a very general sense) function $f(\theta, \lambda)$ on the surface of the sphere can be expanded into a series of surface spherical harmonics:

$$f(\theta,\lambda) = \sum_{n=0}^{\infty}\sum_{m=0}^{\infty}\left[a_{nm}\mathcal{R}_{nm}(\cos\theta) + b_{nm}\mathcal{S}_{nm}(\cos\theta)\right]. \tag{A.22}$$

According to the orthogonality relations, the coefficients of the expansion can be isolated from

$$< f, \mathcal{R}_{rs} > = a_{rs} < \mathcal{R}_{rs}, \mathcal{R}_{rs} >, \tag{A.23}$$
$$< f, \mathcal{S}_{rs} > = b_{rs} < \mathcal{S}_{rs}, \mathcal{S}_{rs} > . \tag{A.24}$$

More explicitly, for $m = 0$,

$$a_{n0} = \frac{2n+1}{4\pi}\iint_{\sigma} f(\theta,\lambda)P_n(\theta,\lambda)d\sigma, \tag{A.25}$$

and for $m \neq 0$,

$$a_{nm} = \frac{2n+1}{2\pi}\frac{(n-m)!}{(n+m)!}\iint_{\sigma} f(\theta,\lambda)\mathcal{R}_{nm}(\theta,\lambda)d\sigma, \tag{A.26}$$

$$b_{nm} = \frac{2n+1}{2\pi}\frac{(n-m)!}{(n+m)!}\iint_{\sigma} f(\theta,\lambda)\mathcal{S}_{nm}(\theta,\lambda)d\sigma. \tag{A.27}$$

A.3 Fully normalized spherical harmonics

The spherical harmonics defined in equations A.15 and A.16, are usually replaced by others which differ by a constant factor and are easier to handle. They are called the *fully normalized harmonics* and defined, for $m = 0$

$$\bar{\mathcal{R}}_{n0}(\theta,\lambda) = \sqrt{2n+1}\,\mathcal{R}_{n0}(\theta,\lambda) \equiv \sqrt{2n+1}P_n(\cos\theta), \tag{A.28}$$

and for $m \neq 0$,

$$\bar{\mathcal{R}}_{nm}(\theta,\lambda) = \sqrt{2(2n+1)\frac{(n-m)!}{(n+m)!}}\,\mathcal{R}_{nm}(\theta,\lambda), \tag{A.29}$$

$$\bar{\mathcal{S}}_{nm}(\theta,\lambda) = \sqrt{2(2n+1)\frac{(n-m)!}{(n+m)!}}\,\mathcal{S}_{nm}(\theta,\lambda). \tag{A.30}$$

Obviously, the orthogonal relations are still valid for $\bar{\mathcal{R}}_{nm}$ and $\bar{\mathcal{S}}_{nm}$, and besides,

$$< \bar{\mathcal{R}}_{nm}, \bar{\mathcal{R}}_{nm} >=< \bar{\mathcal{S}}_{nm}, \bar{\mathcal{S}}_{nm} >= 4\pi. \tag{A.31}$$

This means that the average square of any fully normalized harmonic is unity, the average being taken over the sphere (the average corresponds to the integral divided by the area 4π). This is the reason why the fully normalized harmonics are also called the *4π-normalized harmonics*.

The *expansion theorem* is still valid for fully normalized harmonics. Then, if we expand an arbitrary function $f(\theta,\lambda)$ into a series of fully normalized harmonics, analogously to A.22,

$$f(\theta,\lambda) = \sum_{n=0}^{\infty}\sum_{m=0}^{n}\left[\bar{a}_{nm}\bar{\mathcal{R}}_{nm}(\theta,\lambda) + \bar{b}_{nm}\bar{\mathcal{S}}_{nm}(\theta,\lambda)\right]. \tag{A.32}$$

And the coefficients $\bar{a}_{nm}$ and $\bar{b}_{nm}$ are given by:

$$\bar{a}_{nm} = \frac{1}{4\pi}\iint_{\sigma} f(\theta,\lambda)\bar{\mathcal{R}}_{nm}(\theta,\lambda)\,d\sigma, \tag{A.33}$$

$$\bar{b}_{nm} = \frac{1}{4\pi}\iint_{\sigma} f(\theta,\lambda)\bar{\mathcal{S}}_{nm}(\theta,\lambda)\,d\sigma. \tag{A.34}$$

The simplicity of these formulas constitutes the main advantage of the fully normalized spherical harmonics and make them useful in many respects, even though the functions $\bar{\mathcal{R}}_{nm}$ and $\bar{\mathcal{S}}_{nm}$ are a little more complicated than the conventional $\mathcal{R}_{nm}$ and $\mathcal{S}_{nm}$.

There are relations between the coefficients $\bar{a}_{nm}$ and $\bar{b}_{nm}$ for fully normalized harmonics and the coefficients a_{nm} and b_{nm} for conventional harmonics that are inverse to those in A.28, A.29 and A.30. Then, for $m = 0$,

$$\bar{a}_{n0} = \frac{a_{n0}}{\sqrt{2n+1}}, \tag{A.35}$$

and for $m \neq 0$,

$$\bar{a}_{nm} = \sqrt{\frac{1}{2(2n+1)}\frac{(n+m)!}{(n-m)!}}\, a_{nm}, \tag{A.36}$$

$$\bar{b}_{nm} = \sqrt{\frac{1}{2(2n+1)}\frac{(n+m)!}{(n-m)!}}\, b_{nm}. \tag{A.37}$$

A.4 Geopotential

Accordingly to Newton's integral (A.6), the potencial of the earth, denoted V and called *geopotential*, is

$$V = G \iiint_{earth} \frac{dm}{l}. \tag{A.38}$$

The inverse of the distance between two points, (θ, λ, r) and (θ', λ', r'), is an harmonic function that can be expanded as

$$\frac{1}{l} = \sum_{n=0}^{\infty}\sum_{m=0}^{n} \frac{1}{2n+1}\left(\frac{\bar{\mathcal{R}}_{nm}(\theta,\lambda)}{r^{n+1}} r'^{n} \bar{\mathcal{R}}_{nm}(\theta',\lambda') + \frac{\bar{\mathcal{S}}_{nm}(\theta,\lambda)}{r^{n+1}} r'^{n} \bar{\mathcal{S}}_{nm}(\theta',\lambda')\right), \tag{A.39}$$

which is called the *decomposition formula*. Substituting this relation into A.38, we obtain

$$V(r,\theta,\lambda) = \sum_{n=0}^{\infty}\sum_{m=0}^{\infty}\left[\bar{A}_{nm}\frac{\bar{\mathcal{R}}_{nm}(\theta,\lambda)}{r^{n+1}} + \bar{B}_{nm}\frac{\bar{\mathcal{S}}_{nm}(\theta,\lambda)}{r^{n+1}}\right], \tag{A.40}$$

where the constant coefficients $\bar{A}_{nm}$ and $\bar{B}_{nm}$ are given by

$$\bar{A}_{nm} = \frac{1}{2n+1} G \iiint_{earth} r'^n \bar{\mathcal{R}}_{nm}(\theta', \lambda') dm, \tag{A.41}$$

$$\bar{B}_{nm} = \frac{1}{2n+1} G \iiint_{earth} r'^n \bar{\mathcal{S}}_{nm}(\theta', \lambda') dm. \tag{A.42}$$

Recalling the relations between conventional and fully normalized spherical harmonics (A.35, A.36 and A.37), the geopotential can also be expressed in terms of conventional harmonics

$$V(r, \theta, \lambda) = \sum_{n=0}^{\infty} \sum_{m=0}^{\infty} \left[A_{nm} \frac{\mathcal{R}_{nm}(\theta, \lambda)}{r^{n+1}} + B_{nm} \frac{\mathcal{S}_{nm}(\theta, \lambda)}{r^{n+1}} \right], \tag{A.43}$$

where, for m=0,

$$A_{n0} = G \iiint_{earth} r'^n P_n(\cos\theta') dm, \tag{A.44}$$

and for $m \neq 0$,

$$A_{nm} = 2 \frac{(n-m)!}{(n+m)!} G \iiint_{earth} r'^n \bar{\mathcal{R}}_{nm}(\theta', \lambda') dm, \tag{A.45}$$

$$B_{nm} = 2 \frac{(n-m)!}{(n+m)!} G \iiint_{earth} r'^n \bar{\mathcal{S}}_{nm}(\theta', \lambda') dm. \tag{A.46}$$

On the other hand, applying the change

$$\bar{A}_{nm} = GMa^n \bar{C}_{nm}, \tag{A.47}$$

$$\bar{B}_{nm} = GMa^n \bar{S}_{nm}, \tag{A.48}$$

to A.40, we get the usual expression of the geopotential in satellite dynamics

$$V(\theta, \lambda, r) = \frac{GM}{r} \left[1 + \sum_{n=1}^{\infty} \sum_{m=0}^{n} \left(\frac{a}{r} \right)^n \left(\bar{C}_{nm} \bar{\mathcal{R}}_{nm}(\theta, \lambda) + \bar{S}_{nm} \bar{\mathcal{S}}_{nm}(\theta, \lambda) \right) \right], \tag{A.49}$$

where GM is the product of the gravitational constant and the mass of the earth, $GM = 3.986004418 \cdot 10^{14}\ \mathrm{m^3 s^{-2}}$, and a is the equatorial radius of the earth, $a = 6378136.6$ m [McCarthy and Petit, 2003]. $\bar{C}_{nm}$ and $\bar{S}_{nm}$ are called *Stoke coefficients*. Note the difference between the coefficients $\bar{C}_{nm}$ and $\bar{S}_{nm}$, and the functions $\bar{\mathcal{R}}_{nm}$ and $\bar{\mathcal{S}}_{nm}$. The C_{n0} coefficients are usually denoted by $-J_n$.

A.5 Low degree Spherical Harmonics

We are going to calculate the spherical harmonics coefficients A_{nm} and B_{nm} up to degree 2. Then, we firstly estimate the surface spherical harmonics (A.15 and A.16):

$$\begin{aligned}
\mathcal{R}_{00} &= 1, & \mathcal{S}_{00} &= 0,\\
\mathcal{R}_{10} &= \cos\theta, & \mathcal{S}_{10} &= 0\\
\mathcal{R}_{11} &= \sin\theta\cos\lambda, & \mathcal{S}_{11} &= \sin\theta\sin\lambda,\\
\mathcal{R}_{20} &= \frac{3}{2}\cos\theta^2 - \frac{1}{2}, & \mathcal{S}_{20} &= 0,\\
\mathcal{R}_{21} &= 3\sin\theta\cos\theta\cos\lambda, & \mathcal{S}_{21} &= 3\sin\theta\cos\theta\sin\lambda,\\
\mathcal{R}_{22} &= 3\sin\theta^2\cos(2\lambda), & \mathcal{S}_{22} &= 3\sin\theta^2\sin(2\lambda).
\end{aligned} \tag{A.50}$$

The corresponding *solid harmonics* $r^n\bar{\mathcal{R}}_{nm}(\theta,\lambda)$ and $r^n\bar{\mathcal{S}}_{nm}(\theta,\lambda)$ are simply polynomials in the rectangular coordinates xyz (A.10). For instance,

$$\begin{aligned}
r^2\mathcal{S}_{22} = r^2 3\sin\theta^2\sin(2\lambda) = 6r^2\sin\theta^2\sin\lambda\cos\lambda =\\
= 6(r\sin\theta\cos\lambda)(r\sin\theta\sin\lambda) = 6xy.
\end{aligned} \tag{A.51}$$

In this way, we obtain

$$\begin{aligned}
\mathcal{R}_{00} &= 1, & \mathcal{S}_{00} &= 0,\\
r\mathcal{R}_{10} &= z, & r\mathcal{S}_{10} &= 0\\
r\mathcal{R}_{11} &= x, & r\mathcal{S}_{11} &= y,\\
r^2\mathcal{R}_{20} &= -\frac{1}{2}x^2 - \frac{1}{2}y^2 + z^2, & r^2\mathcal{S}_{20} &= 0,\\
r^2\mathcal{R}_{21} &= 3xz, & r^2\mathcal{S}_{21} &= 3yz,\\
r^2\mathcal{R}_{22} &= 3x^2 - 3y^2, & r^2\mathcal{S}_{22} &= 6xy.
\end{aligned} \tag{A.52}$$

Substituting these functions in A.44, A.45 and A.46, yields for the 0-degree term

$$A_{00} = G\iiint_{earth} dm = GM, \tag{A.53}$$

and obviously $B_{00} = 0$. Then, the 0-degree term accounts for the mass of the earth.

For the 1-degree coefficients, we get

$$A_{10} = G\iiint_{earth} z'dm, \tag{A.54}$$

$$A_{11} = G\iiint_{earth} x'dm, \tag{A.55}$$

$$B_{11} = G\iiint_{earth} y'dm, \tag{A.56}$$

and obviously $B_{10} = 0$. Then, 1-degree terms are related to the center of mass of the earth, the so-called *geocenter*, since it is known from mechanics:

$$x_{cm} = \frac{1}{M}\iiint x'dm, \tag{A.57}$$

$$y_{cm} = \frac{1}{M}\iiint y'dm, \tag{A.58}$$

$$z_{cm} = \frac{1}{M}\iiint z'dm, \tag{A.59}$$

where (x_{cm}, y_{cm}, z_{cm}) are the rectangular coordinates of the geocenter. If the origin of the coordinate system coincides with the center of mass, then these coordinates and, hence, the 1-degree coefficients are zero.

For 2-degree terms, we get

$$A_{20} = \frac{1}{2}G\iiint_{earth}(-x'^2 - y'^2 + 2z'^2)dm, \tag{A.60}$$

$$A_{21} = G\iiint_{earth} x'z'dm, \tag{A.61}$$

$$A_{22} = \frac{1}{4}G\iiint_{earth}(x'^2 - y'^2)dm, \tag{A.62}$$

$$B_{21} = G\iiint_{earth} y'z'dm, \tag{A.63}$$

$$B_{22} = \frac{1}{2}G\iiint_{earth} x'y'dm, \tag{A.64}$$

and obviously $B_{20} = 0$. A_{20} is proportional to $\bar{C}_{20} = -J_2$ (A.47). The J_2 term represents the oblateness of the earth and the study of its variations has been related to earthquakes, variations of the length of the day and water mass redistribution in the earth system [Cox and Chao, 2002]. The coefficients A_{21}, B_{21} and B_{22} are proportional to the *products of inertia*,

$$G\iiint x'y'dm, \qquad G\iiint y'z'dm, \qquad G\iiint z'x'dm. \tag{A.65}$$

They are zero if the coordinate axes coincide with the principal axes of inertia. If the z-axis is identical with the mean rotational axis of the earth, which coincides with the axis of maximum inertia, at least the second and third of these products of inertia must vanish. Hence, A_{21} and B_{21} will be zero, but not so B_{22}, which is proportional to the first product of inertia. B_{22} would vanish only if the earth had complete rotational symmetry or if a principal axis of inertia happened to coincide with the Greenwich meridian.

A.6 GRACE data

The geopotential is not fixed, but it is depending on the mass distribution of the Earth, as it can be inferred from Newton's integral (A.6). Then, any mass redistribution may potentially change the geopotential. The GRACE mission has been designed to detect such changes, and in particular, those produced by water mass movement and exchange between the ocean, the continents and the atmosphere. Then, in the process of Level-2 (L-2) GRACE data, many geophysical processes producing geopotential changes, which are not related with water mass movement and/or can be more accurately estimated from other techniques different from GRACE, have been eliminated. So, L-2 GRACE data represent geopotential variations with respect to the so-called *background gravity model*. The latter is formed by the *a priori* best-known geopotential static model and the mathematical models of the eliminated geophysical processes.

Before GRACE, the best geopotential static model was EGM96 [Lemoine et al., 1998]. However, GRACE is also being used to improve the geopotential static model.Tapley et al. (2004a) calculated the GGM01S model from GRACE data, which improves the accuracy of the EGM96 in one order of magnitude. The EGM96 model was developed by combining data from over a thirty-year period of tracking near-Earth satellites, satellite altimeter data over the oceans and an extensive set of land-based measurements, whereas the GGM01S model was developed from only 111 selected days of GRACE data. The different time periods used and the accuracy obtained show the great potential of the GRACE mission.

The known geopotential variations that have been eliminated from L-2 GRACE data are: 1) Secular variations of the degree-2 harmonics; 2) Solid Earth, ocean and pole tides; 3) Non-tidal load variability in the atmosphere and the ocean; 4) N-body perturbations; 5) General relativistic perturbations. Further information about these corrections can be found at Bettadpur (2004a, 2004b).

L-2 GRACE data consist of monthly Stoke coefficients of A.49, which will be denoted $\Delta\bar{C}_{nm}(t)$ and $\Delta\bar{S}_{nm}(t)$, where n and m are the degree and the order respectively, and t denotes the time dependency of the coefficients. The symbol Δ is to show that the data represent the gravity anomalies with respect to the background gravity model. Then, the time variable gravity (TVG) anomalies detected

by GRACE will be

$$\Delta V(r,\theta,\lambda,t) = \\ = \frac{GM}{r}\left[\sum_{n=1}^{\infty}\sum_{m=0}^{n}\left(\frac{a}{r}\right)^n\left(\Delta\bar{C}_{nm}(t)\bar{\mathcal{R}}_{nm}(\theta,\lambda)+\Delta\bar{S}_{nm}(t)\bar{\mathcal{S}}_{nm}(\theta,\lambda)\right)\right]. \tag{A.66}$$

Note that the 1 term outside the series expansion is not included in this expression. This is because that term accounts for the mass of the earth system, which is constant, and has been included in the background gravity model. It is clear that GRACE data will contain real TVG signals as well as errors in the background gravity model.

Knowing the mass (or density) distribution of the earth, it is possible to uniquely determine the geopotential following Newton's integral (A.6). On the other hand, to determine the mass distribution of the Earth knowing the geopotential has not an unique solution [Chao, 2005]. This problem is known as the *inverse problem of potential theory*. However, the inverse problem has an unique solution assuming that all the mass is distributed on the surface of the Earth. Of course, this assumption is not true. Nevertheless, in the case of the GRACE TVG data, it can be assumed that the gravity variations are produced by water mass redistribution in the surface of the earth. This assumption is possible after the applied corrections and is quite realistic in the annual frequencies.

Then, assuming that the TVG is produced at the surface of the earth, the surface mass variations, $\Delta\sigma$, can be estimated by [Chao, 2005; Wahr et al, 1998]

$$\Delta\sigma(\theta,\lambda,t) = \frac{a\rho}{3}\sum_{n=2}^{\infty}\sum_{m=0}^{n}\frac{2n+1}{1+k'_n}\left(\Delta\bar{C}_{nm}(t)\bar{\mathcal{R}}_{nm}(\theta,\lambda)+\Delta\bar{S}_{nm}(t)\bar{\mathcal{S}}_{nm}(\theta,\lambda)\right), \tag{A.67}$$

where ρ is the mean density of the earth, $\rho = 5517$ kg/m^3 [Yoder, 1995], and k'_n is the nth load Love number.

The series presented in A.66 or A.67 have infinity terms. However, L-2 GRACE data consists of all Stokes coefficients up to degree 120. This truncation produces a limitation in the spatial resolution of the expansion. In general, a

truncation at degree N produces an spatial resolution of

$$\frac{20000}{N} \text{ km}. \tag{A.68}$$

It means that L-2 GRACE data should have an spatial resolution of $\backsim$ 166 km. However, the Stoke coefficients are very noisy beyond degree 15 [Wahr et al., 2004]. Then, the actual spatial resolution is $\backsim$ 1300 km.

A.7 Gaussian filter for GRACE data

This section is based on Swenson and Wahr (2002). If all spherical harmonics Stokes coefficients, $\Delta\bar{C}_{nm}$ and $\Delta\bar{S}_{nm}$, were available for any degree and order, the surface mass variation at a given region would be estimated by

$$\Delta\bar{\sigma}_{region} = \frac{1}{\Omega_{region}} \int \Delta\sigma(\theta,\lambda)\vartheta(\theta,\lambda)d\Omega, \tag{A.69}$$

where $d\Omega = \sin\theta\, d\theta\, d\lambda$ is an element of solid angle, $\vartheta(\theta,\lambda)$ is the exact averaging kernel describing the region

$$\vartheta(\theta,\lambda) = \begin{cases} 0 & \text{outside the region} \\ 1 & \text{inside the region} \end{cases}$$

and Ω_{region} denotes the solid angle of the region

$$\Omega_{region} = \int \vartheta(\theta,\lambda)d\Omega. \tag{A.70}$$

Using equation A.67, equation A.69 can be expressed as

$$\Delta\bar{\sigma}_{region} = \frac{a\rho}{3\Omega_{region}} \sum_{n=2}^{\infty}\sum_{m=0}^{n} \frac{2n+1}{1+k'_n} \left(\vartheta^c_{nm}\Delta\bar{C}_{nm} + \vartheta^s_{nm}\Delta\bar{S}_{nm}\right), \tag{A.71}$$

where ϑ^c_{nm} and ϑ^s_{nm} are the fully normalized Stokes coefficients describing $\vartheta(\theta,\lambda)$ (see the expansion theorem in section A.3):

$$\vartheta(\theta,\lambda) = \sum_{n=0}^{\infty}\sum_{m=0}^{n} \left[\vartheta^c_{nm}\bar{\mathcal{R}}_{nm}(\theta,\lambda) + \vartheta^s_{nm}\bar{\mathcal{S}}_{nm}(\theta,\lambda)\right], \tag{A.72}$$

which can be estimated by

$$\bar{\vartheta}^c_{nm} = \frac{1}{4\pi}\int \vartheta(\theta,\lambda)\bar{\mathcal{R}}_{nm}(\theta,\lambda)\,d\Omega, \tag{A.73}$$

$$\bar{\vartheta}^s_{nm} = \frac{1}{4\pi}\int \vartheta(\theta,\lambda)\bar{\mathcal{S}}_{nm}(\theta,\lambda)\,d\Omega. \tag{A.74}$$

However, as aforementioned the GRACE Stokes coefficients are truncated at degree 120 and they are noisy after degree 15. For that reason, we use an approximate averaging kernel that smooths with a Gaussian filter the high degree Stokes coefficients. We define an averaging kernel, $\bar{W}$, that changes smoothly from a value of 1 inside the region to a value of 0 outside over a horizontal distance of approximately r km. Then, if

$$\bar{W}(\theta,\lambda) = \sum_{n=0}^{N}\sum_{m=0}^{n}\left[\bar{W}^c_{nm}\bar{\mathcal{R}}_{nm}(\theta,\lambda) + \bar{W}^s_{nm}\bar{\mathcal{S}}_{nm}(\theta,\lambda)\right], \tag{A.75}$$

the coefficients $\bar{W}^c_{nm}$ and $\bar{W}^s_{nm}$ are defined as

$$\bar{W}^c_{nm} = W_n\vartheta^c_{nm}, \tag{A.76}$$

$$\bar{W}^s_{nm} = W_n\vartheta^c_{nm}, \tag{A.77}$$

where W_n is computed recursively by the following relation[1]:

$$W_0 = 1, \tag{A.78}$$

$$W_1 = \frac{1+e^{-2b}}{1-e^{-2b}} - \frac{1}{b}, \tag{A.79}$$

$$W_{n+1} = -\frac{2n-1}{b}W_n + W_{n-1}, \tag{A.80}$$

where

$$b = \frac{\ln(2)}{1-\cos\frac{r}{a}}. \tag{A.81}$$

[1]The relation $W_{n+1} = -\frac{2n+1}{b}W_n + W_{n-1}$ given in Swenson and Wahr (2002) is erroneous.

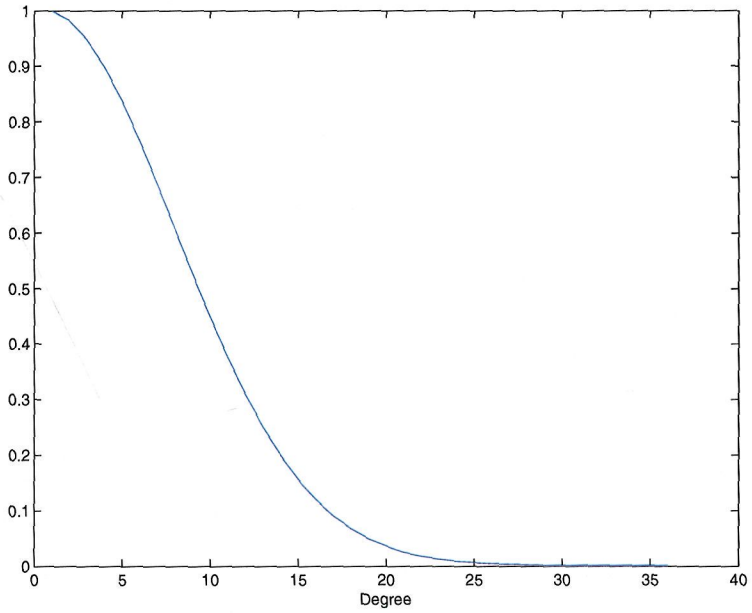

Figure A.2: Smoothing of the Stokes coefficients using a Gaussian filter with $r = 1000$ km.

Using this Gaussian filter we will obtain an approximate of the surface mass variation of the region,

$$\widetilde{\sigma}_{region} = \frac{a\rho}{3\Omega_{region}} \sum_{n=2}^{\infty} \sum_{m=0}^{n} \frac{2n+1}{1+k'_n} \left(\bar{W}^c_{nm} \Delta \bar{C}_{nm} + \bar{W}^s_{nm} \Delta \bar{S}_{nm} \right). \quad \text{(A.82)}$$

Then, using an smoothing radius of $r = 1000$ km, the GRACE Stokes coefficients will be smoothed as shown in figure A.2. It can be observed that all coefficients vanish after degree 30 and they are greatly reduced after degree 15.

A.8 Geocenter variations

The *geocenter* is defined as the center of mass of the earth system, i. e., including the solid earth, the ocean and the atmosphere. In an inertial reference frame, as for instance the International Terrestrial Reference Frame (ITRF), the geocenter is not fixed, but its location varies due to redistributions of mass. Space geodetic techniques such as SLR or GPS have shown that the geocenter varies between mm and cm at frequencies between diary and inter-seasonal.

The origin of the reference frame of GRACE satellites is defined to coincide with the geocenter, and then 1-degree coefficients vanish (see section A.5), unlike altimetry. Then, when comparing both datasets an inconsistency appears. There are two possible solutions: i) to correct the geocenter motion in altimetry, or ii) include it in GRACE data. We are interested in the mass redistribution during the water cycle, which produces variations in the geocenter location. Then, to keep as information as possible in the data, we choose option ii).

To add the geocenter variations to GRACE data, we must relate them to the 1-degree Stoke's coefficients (A.5). Assuming the ITRF as reference frame, we can define $R_{cm} = (x_{cm}, y_{cm}, z_{cm})$ as the location vector of the geocenter. Now, we substitute the expressions of x_{cm}, y_{cm} and z_{cm} (A.57, A.58 and A.59) in the those of A_{11}, B_{11} and A_{10} (A.55, A.56 and A.54), respectively, and we get:

$$\begin{aligned} A_{10} &= GMz_{cm}, \\ A_{11} &= GMx_{cm}, \\ B_{11} &= GMy_{cm}. \end{aligned} \tag{A.83}$$

Applying the relations A.47 and A.48, we obtain

$$\begin{aligned} C_{10} &= \frac{A_{10}}{GMa} = \frac{z_{cm}}{a}, \\ C_{11} &= \frac{A_{11}}{GMa} = \frac{x_{cm}}{a}, \\ S_{11} &= \frac{B_{11}}{GMa} = \frac{y_{cm}}{a}. \end{aligned} \tag{A.84}$$

These expressions can be expressed in terms of fully normalized Stoke's coeffi-

cients through A.35, A.36 and A.37). Then we get:

$$\begin{aligned} \bar{C}_{10} &= \frac{1}{\sqrt{3}} C_{10} = \frac{z_{cm}}{a\sqrt{3}} \\ \bar{C}_{11} &= \sqrt{\frac{2}{6}} C_{11} = \frac{x_{cm}}{a\sqrt{3}} \\ \bar{S}_{11} &= \sqrt{\frac{2}{6}} S_{11} = \frac{y_{cm}}{a\sqrt{3}} \end{aligned} \tag{A.85}$$

From these relations, it is easy to estimate the 1-degree Stoke's coefficients from variations of the geocenter. However, accurate estimation of the latter are not available. For that reason, we will use an estimation of the annual and semi-annual variation of the geocenter made by Chen et al. (1999).

This estimation is based on the surface load variations produced by the mass variations of the ocean, atmosphere and continental hydrology. In spherical coordinates, the load mass variations in a rigid earth produce the following geocenter variations:

$$R_{cm} = \frac{1}{M} \iint R\, L(\theta, \lambda)\, ds, \tag{A.86}$$

where M is the mass of the earth, $L(\theta, \lambda)$ is the load mass variation (in units of mass/surface) in the surface point $R = (x, y, z) = (a \sin\theta \cos\lambda, a \sin\theta \sin\lambda, a \cos\theta)$, $ds = a^2 \sin\theta\, d\theta d\lambda$ is the surface differential, and a is the mean radius of the earth. Coordinate by coordinate we get

$$\begin{aligned} x_{cm} &= \frac{a}{M} \iint \sin\theta \cos\lambda\, L(\theta, \lambda)\, ds, \\ y_{cm} &= \frac{a}{M} \iint \sin\theta \sin\lambda\, L(\theta, \lambda)\, ds, \end{aligned} \tag{A.87}$$

$$z_{cm} = \frac{a}{M} \iint \cos\theta\, L(\theta, \lambda)\, ds. \tag{A.88}$$

The load mass variation, $L(\theta, \lambda)$, from ocean, atmosphere and continental hydrology is estimated as follows:

- Ocean: SLV are estimated from T/P for the span of time 10/1992 - 04/1997, where all usual corrections have been applied, including IB correction. The steric SLV, estimated from temperature data from NOAA World Ocean Atlas 1994 (WOA94), is corrected from T/P-derived SLV. Then, from the non-steric SLV, $\Delta H(\theta, \lambda)$, we get

$$L_{ocn}(\theta, \lambda) = \Delta H(\theta, \lambda)\, \rho_w,$$

where $\rho_w = 1.03$ g/cm^3 is the mean density of the sea water.

- Atmosphere: pressure variations at the surface, $\Delta P(\theta, \lambda)$, are estimated from the NCEP-NCAR Climate Data Assimilation System I (CDAS-1) atmospheric GCM, for the period 1974-1999. The load mass variation is inferred from

$$L_{atm}(\theta, \lambda) = \frac{\Delta P(\theta, \lambda)}{g},$$

where the acceleration of gravity $g = 978.03$ cm/s^2 is assumed to be constant. A standard IB correction is applied in computing atmospheric contribution, i.e., only the pressure variation is included on land and it is assumed to be constant over the ocean. The rason to do that is that the same IB assumption has been done in altimetry.

- Continental hydrology: to estimate continental water storage changes, assimilated soil moisture fields and water equivalent snow depth fields in the NCEP-NCAR CDAS-1 hydrological models. The monthly soil moisture fields contain two layers, which cover the top 2 m of soil (0-10 cm and 10-200 cm). Water content is represented by volumetric fraction, and total water storage changes (in g/cm^2) for a given point are estimated by integrating water content in the two soil moisture layers ($\eta_1(\theta, \lambda)$ and $\eta_2(\theta, \lambda)$), and the equivalent water content in snow depth fields ($\Delta N(\theta, \lambda)$), as

$$\begin{aligned} L_{soil}(\theta, \lambda) &= \sum_{i=1,2} \eta_i(\theta, \lambda) h_i\, \rho_0, \\ L_{snow}(\theta, \lambda) &= \Delta N(\theta, \lambda), \end{aligned}$$

where $\rho_0 = 1$ g/cm^2 is water density, $h_1 = 10$ cm, and $h_2 = 190$ cm.

		Annual		Semi-annual	
		Amplitude, mm	Phase, degree	Amplitude, mm	Phase degree
Ocean	x_{cm}	0.96	73	0.86	187
	y_{cm}	0.97	52	0.73	173
	z_{cm}	0.49	3	0.25	232
Atmosphere	x_{cm}	0.37	116	0.16	100
	y_{cm}	1.26	94	0.41	217
	z_{cm}	0.80	100	0.75	252
Soil moisture + Snow	x_{cm}	1.28	44	0.15	331
	y_{cm}	0.52	182	0.56	312
	z_{cm}	3.30	43	0.50	75
Total	x_{cm}	2.38	64	0.75	181
	y_{cm}	2.00	90	0.89	221
	z_{cm}	4.10	48	0.50	238

Table A.1: Annual and semi-annual variations of the geocenter produced by the ocean, atmosphere and continental hydrology [Chen et al., 1999].

As a result of these computations, Chen et al. (1999) obtained an estimation of the annual and the semi-annual geocenter variations produced by the ocean, atmosphere and continental hydrology (see table A.1).

A.9 Pole tide

This section is mainly based on Wahr (1985), Desai (2002) and Munk and Macdonald (1960).

The earth is more nearly an ellipsoid than a perfect sphere because of its response to the centrifugal force associated with its diurnal rotation. Variations in either the rate of rotation or in the geocentric position of the rotation axis (i.e., polar motion) will perturb the centrifugal force and so will further deform the earth.

We assume that the earth is attached to a coordinate system of axes XYZ. We orient Z along the earth's mean rotation axis, denoted as ω_0, X along the Greenwich meridian, and Y along the 90°E meridian. Then, we can write

$$\omega_0 = (0, 0, \Omega), \tag{A.89}$$

where Ω is the mean angular velocity of rotation of the earth. The instantaneous position of the earth's rotation vector is

$$\omega(t) = \Omega(m_1(t), m_2(t), 1 + m_3(t)) \tag{A.90}$$

where $m_1(t)$ and $m_2(t)$ describe the polar motion in radians with respect to the reference system XYZ, and $m_3(t)$ describes the variations in the rotation rate.

The instantaneous centrifugal potential, $V_c(x, y, z, t)$, at an arbitrary point with coordinates $r = (x, y, z)$ at an instant t, is

$$V_c(x, y, z, t) = \frac{1}{2}\left[|\omega(t)|^2|r|^2 - (\omega(t) \cdot r)^2\right], \tag{A.91}$$

which, to first order in the $\{m_i\}_{i=1}^3$, is

$$V_c(x, y, z, t) = \frac{\Omega^2}{2}\left[(1 + 2m_3(t))(x^2 + y^2) - 2z(x\, m_1(t) + y\, m_2(t))\right]. \tag{A.92}$$

The centrifugal potential produced by the mean rotation vector, ω_0, is

$$V_{\omega_0}(x, y, z) = \frac{\Omega^2}{2}\left[x^2 + y^2\right] \tag{A.93}$$

Then, the instantaneous centrifugal potential can be seen as the addition of the mean centrifugal potential, $V_{\omega_0}(x, y, z)$, and a disturbing potential, $\Delta V(x, y, z, t)$, produced by the polar motion, $m_1(t)$ and $m_2(t)$, and changes in the variations in the rotation rate, $m_3(t)$. Note that $\{m_i\}_{i=1}^3$ are time dependent. Then, the instantaneous centrifugal potential can be written as

$$V_c(x, y, z, t) = V_{\omega_0}(x, y, z) + \Delta V(x, y, z, t), \tag{A.94}$$

where

$$\Delta V(x,y,z,t) = \frac{\Omega^2}{2}\big[2m_3(t)(x^2+y^2) - 2z(x\,m_1(t) + y\,m_2(t))\big], \quad \text{(A.95)}$$

and it is referred to as the *pole tide potential.*

Variations in the rotation rate, $m_3(t)$, are at least two orders of magnitude smaller than variations in the pole location, $m_1(t)$ and $m_2(t)$, and cause radial deformations that are below the millimeter level, and can be neglected [Wahr, 1985].

The pole tide potential can be written in spherical coordinates (accordingly to equation A.10) as

$$\begin{aligned} \Delta V(\rho,\theta,\lambda,t) &= \frac{\Omega^2}{2}\big[-2\rho\cos\theta(\rho\sin\theta\cos\lambda\; m_1 + \rho\sin\theta\sin\lambda\; m_2)\big] = \\ &= -\Omega^2\rho^2\sin\theta\cos\theta(\cos\lambda\; m_1 + \sin\lambda\; m_2) = \\ &= \frac{-\Omega^2\rho^2}{2}\sin 2\theta(\cos\lambda\; m_1 + \sin\lambda\; m_2). \end{aligned} \quad \text{(A.96)}$$

To estimate ΔV at the surface of the earth, ρ can be assumed to be the equatorial radius of the earth, a_E = 6378136.6 m, and Ω = 7.292115 $\cdot 10^{-5}$ rad/s. These values are taken from *International Earth Rotation and Reference System Service (IERS) Conventions (2003)* [McCarthy and Petit, 2003]. For the values of m_1 and m_2, a daily solution can be found at the *Earth Orientation Parameters (EOP) Combined Series, EOP_C04*, delivered by IERS (<http://www.iers.org>). With this estimation, the potential pole tide can be corrected in altimetry and TVG GRACE data.

Solid earth and ocean pole tides. Consider the response of the earth to a general disturbing potential, $U(r)$, of degree 2 (tidal forces of the moon and sun, and centrifugal forces arising from rotation can be written as gradients of such a potential U). The resulting deformation defines the *Love numbers*, h_2 and k_2, as follows [Munk and Macdonald, 1960]: the ground is lifted by

$$h_2\frac{U_{surface}}{g}, \quad \text{(A.97)}$$

where g is the gravity, and the additional gravitational potential at the (displaced) surface arising solely from this redistribution of mass is

$$k_2 U. \tag{A.98}$$

Thus $1 + k_2$ is a factor allowing for the attraction of the bulge by itself, and the response by

Then, at the displaced point the total variation of the potential (that is accounting for the original disturbing potential U and for the one produced by the redistribution of mass) is given by

$$(1 + k_2)U. \tag{A.99}$$

Note that the displacement $h_2 U/g$ takes this self-attraction into account. In addition to the vertical displacement of the solid surface by $h_2 U/g$ there is an horizontal displacement with components

$$\frac{1}{g}\frac{\partial U}{\partial \theta}, \quad \frac{1}{g}\frac{1}{\sin\theta}\frac{\partial U}{\partial \lambda}. \tag{A.100}$$

When the disturbing potential U is the pole tide potential, ΔV, the displacement of the earth surface is called *solid earth pole tide*. In the altimetry and TVG GRACE data used in this dissertation, the solid earth pole tide has been corrected accordingly to equation A.99.

The response of the oceans to a disturbing potential is somewhat more complicated. When the disturbing potential is the pole tide potential, such a response is called *ocean pole tide*. The oceans are a fluid surface covering the globe which would remain an equipotential surface, defining the *geoid*. Then any disturbing potential will produce a displacement of the sea surface. The equilibrium ocean pole tide response assumes that the displaced ocean surface is in equilibrium with the equipotential surface. Then, a disturbing potential, U, will lift the sea surface by

$$\frac{(1 + k_2)U}{g}, \tag{A.101}$$

relative to the center of the earth, and by

$$\frac{(1 + k_2 - h_2)U}{g}, \tag{A.102}$$

relative to the sea bottom.

On the other hand, this classical equilibrium response of the ocean ignores the effects of loading and self-gravitation of the ocean pole tide. As with the solid earth pole tide, an additional potential arises from the redistribution of (oceanic) mass. This additional potential is determined by scaling each degree n spherical harmonic component of the gravitational potential of the ocean pole tide, $U_n(\theta, \lambda, t)$, by the load Love numbers k'_n [Munk and Macdonald, 1960]. The total tide generating potential in the oceans is then

$$(1 + k_2)\Delta V + \sum_{n=0}^{\infty}(1 + k'_n)U_n \tag{A.103}$$

and the ocean bottom is displaced accordingly to this potential [Desai, 2002].

The ocean pole tide is corrected in altimetry following equation A.101. That displacement is a consequence of the solid earth pole tide described in equation A.99 which is corrected in TVG GRACE data. Therefore, even if the ocean pole tide is not completely corrected in both altimetry and TVG GRACE data, the correction applied to them is similar, and then, no inconsistency arises when comparing them.

References

Andersen, O. B., and J. Hinderer. Global inter-annual gravity changes from GRACE: early results. *Geophys. Res. Lett.*, Vol. 32, L01402, doi:10.1029/2004GL020948, 2005.

Antonov, J. I., S. Levitus, and T. P. Boyer. Steric sea level variations during 1957-1994: Importance of salinity. *J. Geophys. Res.*, 107(C12), 8013, doi:10.1029/2001JC000964, 2002.

Antonov, J. I., S. Levitus, and T. P. Boyer. Thermosteric sea level rise, 1955-2003. *Geophys. Res. Lett.*, 32, L12602, doi:10.1029/2005GL023112, 2005.

Au, A. Y. , B. F. Chao, M. Rodell and T. J. Johnson. Global land hydrology and its geodynamic effects. *Proceedings of Workshop on Hydrology from Space*, Toulouse, in press, 2005.

AVISO. User Handbook: Merged Topex/Poseidon Products. AVI-NT-02-101-CN, Edition 3.0, 1996. Online available from <http://www.jason.oceanobs.com/>. [Visited: 06/20/2004].

AVISO. User Handbook: Sea Level Anomalies. AVI-NT-011-312-CN, Edition 3.1, 1998. Online available from <http://www.jason.oceanobs.com/>. [Visited: 06/20/2004].

Becker, M., S. Zerbini, T. Baker, B. Brki, J. Galanis, J. Garate, I. Georgiev, H.-G. Kahle, V. Kotzev, V. Lobazov, I. Marson, N. Negusini, B. Richter, G. Veis and P. Yuzefovich. Assessment of height variations by GPS at Mediterranean

and Black Sea coast tide gauges from the SELF projects. *Global and Planetary Change* 34, 5-35, 2002.

Bethoux, J. P., and B. Gentili. Functioning of the Mediterranean Sea: past and present changes related to freshwater input and climate changes. *Journal of Marine Systems*, 20, 33-47, 1999.

Bettadpur, S. GRACE 327-734 (CSR-GR-03-01), Level-2 Gravity Field Product, User Handbook, 2004. Online available from <http://podaac.jpl.nasa.gov/grace/documentation>. [Visited: 09/15/2004]

Bettadpur, S. GRACE 327-742 (CSR-GR-03-03), UTCSR Level-2 Processing Standards Document, For Level-2 Product Release 0001, 2004. Online available from <http://podaac.jpl.nasa.gov/grace/documentation>. [Visited: 09/15/2004]

Boukthir, M., and B. Barnier. Seasonal and inter-annual variations in the surface freshwater flux in the Mediterranean Sea from the ECMWF re-analysis project. *Journal of Marine Systems*, 24, 343-354, 2000.

Bouzinac, C., J. Font and J. Johannessen. Annual cycles of sea level and sea surface temperature in the western Mediterranean Sea. *J. Geophys. Res.*, 108, C3, 3059, doi:10.1029/2002JC001365, 2003.

Bryden, H., J. Candela and T. H. Kinder. Exchange through the Strait of Gibraltar. *Progress in Oceanography*, 33, 201-248, 1994

Cabanes, C., A. Cazenave and C. Le Provost. Sea level rise during past 40 years determined from satellite and in situ observations. *Science*, Vol. 294, 840-842, 2001.

Candela, J., C. D. Winant and H. L. Bryden. Meteorologically forced subinertial flows through the Strait of Gibraltar. *J. Geophys. Res.*, 94(C9), 12, 667-12,679, 1989.

Cazenave, A., K. Dominh, F. Ponchaut, L. Soudarin, J. F. Cretaux and C. Le Provost. Sea level changes from Topex-Poseidon altimetry and tide gauges, and vertical crustal motions from DORIS. *Geophys. Res. Lett.*, 26, 2077-2080, 1999.

Cazenave, A., F. Remy, K. Dominh and H. Douville. Global ocean mass variations, continental hydrology and the mass balance of Antarctica ice sheet at seasonal timescale. *Geophys. Res. Lett.*, Vol. 27, No. 22, 3755-3758, 2000.

Cazenave, A., C. Cabanes, K. Dominh and S. Mangiarotti. Recent Sea Level Change in the Mediterranean Sea Revealed by Topex/Poseidon Satellite Altimetry. *Geophys. Res. Lett.*, Vol. 28, No. 8, 1607-1610, 2001.

Cazenave, A., P. Bonnefond, F. Mercier, K. Dominh and Toumazou. Sea level variations in the Mediterranean Sea and Black Sea from satellite altimetry and tide gauges. *Global and Planetary Change*, 34, 59-86, 2002.

Cazenave, A., and R. S. Nerem. Present-day sea level change: observations and causes. *Reviews of Geophysics*, 42, RG3001, 2004.

Chambers, D. P., J. C. Ries, C. K. Shum and B. D. Tapley. On the use of tide gauges to determine altimeter drift. *J. Geophys. Res.*, 103 (C6), 12, 885-12, 890, 1998.

Chambers, D. P., J. Wahr and R. S. Nerem. Preliminary observations of global ocean mass variations with GRACE. *Geophys. Res. Lett.*, Vol. 31, L13310, doi:10.1029/2004GL020461, 2004.

Chao, B. F., A. Y. Au, J-P Boy, and C. Cox. Time-variable gravity signal of an anomalous redistribution of water mass in extratropic Pacific during 1998-2002. *G-Cubed Geochemistry Geophysics Geosystems*, 4, 1096, doi:10.1029/2003GC00589, 2003.

Chao, B. F. On inversion for mass distribution from global (time-variable) gravity field. *Journal of Geodynamics*, 39, 223-230, doi:10.1016/j.jog.2004.11.001, 2005.

Chao, B. F., and A. Au. Global hydrological budget derived from atmospheric circulation model and GRACE time-variable gravity data. Submitted to *Earth Interactions*, 2006.

Chen, J. L., C. R. Wilson, D. P. Chambers, R. S. Nerem and B. D. Tapley. Seasonal global water mass budget and mean sea level variations. *Geophys. Res. Lett.*, 32, 19, 3555-3558, 1998.

Chen, J. L., C. R. Wilson, R. J. Eanes and R. S. Nerem. Geophysical interpretation of observed geocenter variations. *J. Geophys. Res.*, Vol. 104, No. B2, páginas 2683-2690, 1999.

Chen, J. L., C. R. Wilson, B. D. Tapley and J. Ries. Low degree gravitational changes from GRACE: Validation and interpretation. *Geophys. Res. Lett.*, Vol. 31, No. L22607,2004.

Cheng, M. K., and B. D. Tapley. Temporal variations in the Earth's Gravity Field from SLR and CHAMP GPS data. *Gravity and Geoid 2002*, edited by I. N. Tziavos, 424-431, Greece, 2002.

Church, J. A., J. M. Gregory, P. Huybrechts, M. Kuhn, K. Lambeck, M. T. Nhuan, D. Qin and P. L. Woodworth. Changes in Sea Level, Climate Change 2001: The Scientific Basis. Eds. Houghton and Ding, Cambridge Univ. Press, 2001.

Church, J. A., N. J. White, R. Coleman, K. Lambeck and J. Mitrovica. Estimates of the regional distribution of sea level rise over the 1950-2000 period. *J. Climate*, 17, 2609-2625, 2004.

Cox, C., and B. F. Chao. Detection of a large-scale mass redistribution in the terrestrial system since 1998. *Science*, 297, 2002.

Demets, C., R. G. Gordon, D. F. Argus and S. Stein. Current plate motions. *Geophysical Journal International*, 101, 425-478, 1990.

Desai, S. D. Observing the pole tide with satellite altimetry. *J. Geophys. Res.*, 107, C11, 3186, 2002.

Douglas, B. C. Global sea rise: a redetermination. *Surveys in Geophysiscs*, 18 (2-3), 279-292, 1997.

Douglas, B. C. Sea level change in the era of the recording tide gauge. Sea level rise: history and consequences. *International Geophysisc Series*, vol. 75, edited by B. Douglas, M. Kearney, and S. Leatherman, pp. 37-62, ed. Academic Press, 2001.

Douglas, B. C., and W. R. Peltier. The puzzle of global sea level rise. *Phys. Today*, 55, 35-40, 2002.

Ducet, N., P. Y. Le Traon and P. Gauzelin. Response of the Black Sea mean level to atmospheric pressure and wind forcing. *Journal of Marine Systems* 22, 311-327, 1999.

Fenoglio-Marc, L. Analysis and representation of regional sea-level variability from altimetry and atmospheric-oceanic data. *Geophys. J. Int.*, 145, 1–18, 2001.

Fenoglio-Marc, L. Long-term sea level change in the Mediterranean Sea from multi-satellite altimetry and tide gauges. *Physics and Chemistry of the Earth*, 27, 1419–1431, 2002.

Fenoglio-Marc, L., L. Dietz., and E. Groten. Vertical Land Motion in the Mediterranean Sea from Altimetry and Tide Gauge Stations. *Marine Geodesy*, 27, 1-19, 2004.

Flechtner, F. GRACE 327-750 (GR-GFZ-AOD-0001), AOD1B Product Description Document, 2004. Online available from <http://podaac.jpl.nasa.gov/grace/documentation>. [Visited: 01/15/2005].

Fu, L.-F. and A. Cazenave (Editors). Satellite altimetry and Earth sciences. *International Geophysisc Series*, Vol. 69, ed. Academic Press, 2001.

Fukumori, I., T. Lee, B. Tang, D. Menemenlis. A basin-oscillation of the Mediterranean Sea. *Ocean Sci. Meet. Suppl.*, Eos Trans. AGU, 84, 52, 2003.

Garcia-Lafuente, J., J. Delgado, J. M. Vargas, M. Vargas, F. Plaza and T. Sarhan. Low-frequency variability of the exchanged flow through the Strait of Gibraltar during CANIGO. *Deep-Sea Research II* 49, 4051-4067, 2002.

Gill, A. E. Atmosphere-ocean dynamics. *International Geophysical Series*, 30, Academic Press, 1982.

Heiskanen, W. A., and H. Moritz. *Physical Geodesy*. W. H. Freeman and Company, San Francisco and London, 1967.

Hofmann-Wellenhof, B., and H. Moritz. Physical Geodesy. Springer Wien New York, 2005, ISBN-10 3-211-23584-1.

Holgate, S. J., and P. L. Woodworth Evidence for enhanced coastal sea level rise during 1990s. *Geophys. Res. Lett.*, 31, L07305, doi:10.1029/2004GL019626, 2004.

Hurrell, J. W. Decadal Trend in the North Atlantic Oscillation: Regional Temperatures and Precipitation. *Science*, 269, 676-679, 1995.

IPCC, 2001: Climate change 2001: The scientific basis. Contribution of Working Group I to the Third Assessment Report of the Intergovernmental Panel on Climate Change. [Houghton, J. T., Y. Ding, D. J. Griggs, M. Noguer, P. J. van der Linden, X. Dai, K. Maskell and C. A. Johnson (editors)]. Cambridge University Press, 2001.

Ishii, M., M. Kimoto and M. Kachi. Historical ocean subsurface temperature analysis with error estimates. *Monthly Weather Rev.*, 131, 51-73, 2003.

Ishii, M., A. Shoji, S. Sugimoto and T. Matsumoto. Objective Analyses of Sea-Surface Temperature and marine meteorological variables for the 20th Century using ICOADS and the Kobe Collection. *Int. J. Climatol.*, 25, 865-879, 2005.

Ishii, M., M. Kimoto, K. Sakamoto and S.I. Iwasaki. Steric sea level changes estimated from historical ocean subsurface temperature and salinity analyses. *Journal of Oceanography*, 62 (2), 155-170, 2006.

Jekely, C. The determination of gravitational potential differences from satellite-to-satellite tracking. *Celestial Mechanics and Dynamical Astronomy* 75, 85-101, 1999.

Jimenez-Munt, I., and R. Sabadini. The block-like behavior of Anatolia envisaged in the modeled and geodetic strain rates. *Geophys. Res. Lett.*, 29(20), 1978, doi:10.1029/2002GL015995, 2002.

Jimenez-Munt, I., R. Sabadini, A. Gardi, and G. Bianco. Active deformation in the Mediterranean from Gibraltar to Anatolia inferred from numerical modeling and geodetic and seismological data. *J. Geophys. Res.*, 108(B1), 2006, doi:10.1029/2001JB001544, 2003

Kearney, M. S. Late holocene sea level variations. Sea level rise, history and consequences. *International Geophysisc Series*, Vol. 75, , edited by B. Douglas, M. Kearney, and S. Leatherman, pp. 13-36, ed. Academic Press, 2001.

Keihm, S. J., V. Zlotniki and C. S. Ruf. TOPEX Microwave Radiometer Performance Evaluation,1992-1998. *IEEE Trans. Geosci. Remote Sensing*, Vol. 38, pp. 1396-1386, 2000.

Kiehl, T. J., and K. E. Trenberth. Earth's annual global mean energy budget. *Bull. Am. Met. Soc.* 78, 197-208.

Klein, B., W. Roether, G. Civitarese, M. Gacic, B. B. Manca and M. Ribera d'Alcalà. Is the Adriatic returning to dominate the production of Eastern Mediterranean Deep Water? *Geophys. Res. Lett.*, 27 (20), 3377-3380, 2000.

Larnicol, G., P. Y. Le Traon, N. Ayoub, and P. De Mey. Mean sea level and surface circulation variability of the Mediterranean Sea from 2 years of TOPEX/POSEIDON altimetry. *J. Geophys. Res.*, 100, C12, 25163-25177, 1995.

Larnicol, G., N. Ayoub and P. Y. Le Traon,. Major changes in Mediterranean Sea level variability from 7 years of TOPEX/Poseidon and ERS-1/2 data. *Journal of Marine Systems* 33-34, 63-89, 2002.

Lee, T., and I. Fukumori. Interannual-To-Decadal Variations Of Tropical-Subtropical Exchange In The Pacific Ocean: Boundary Versus Interior Pycnocline Transports. *J. Climate*, 16 (24), 4022-4042, 2003.

Lemoine, F. G., S. C. Kenyon, J. K. Factor, R. G. Trimmer, N. K. Pavlis, D. S. Chinn, C. M. Cox, S. M. Klosko, S. B. Luthcke, M. H. Torrence, Y. M. Wang, R. G. Williamson, E. C. Pavlis, R. H. Rapp and T. R. Olson. The development of the joint NASA GSFC and NIMA geopotential model EGM96. Report TM-1998-206861, NASA, Greenbelt, MD, 1998.

Le Traon, P., and P. Gauzelin. Response of the Mediterranean mean sea level to atmospheric pressure forcing. *J. Geophys. Res.*, 102(C1), 973-984, 1997.

Leuliette, E. W., R. S. Nerem, and G. T. Mitchum. Calibration of TOPEX/Poseidon and Jason altimeter data to construct a continuous record of mean sea level change. *Marine Geodesy*, 27, 79- 94, 2004.

Levitus, S., R. Burgett and T. P. Boyer. World ocean atlas 1994 Volume 3: Salinity. *NOAA Atlas NESDIS* 3. 99 pp, 1994.

Levitus, S., and T. P. Boyer. World ocean atlas 1994 Vol. 4: Temperature. *NOAA Atlas NESDIS 4*. 117 pp, 1994.

Levitus, S., J. Antonov, T. P. Boyer, C. Stephens. Warming of the world ocean. *Science*, Vol. 287, 2000.

Levitus, S., C. Stephens, J. Antonov and T. P. Boyer. NOAA Atlas NESDIS 40. U.S. Government Printing Office, Washington, DC, 2000.

Levitus, S., J. Antonov, J. Wang, T. L. Delworth, K. W. Dixon and A. J. Broccoli. Anthropogenic warming of Earth's climate system. *Science*, Vol. 292, 267-270, 2001.

Levitus, S., J. Antonov and T. Boyer. Warming of the world ocean, 1955-2003. *Geophys. Res. Lett.*, 32, L02604, doi:10.1029/2004GL021592, 2005.

Lombard, A., A. Cazenave, P. Y. Le Traon and M. Ishii. Contribution of thermal expansion to present-day sea-level change revisited. *Global and planetary change*, 47, 1-16, 2005.

Luthcke, S. B., N. P. Zelensky, D. D. Rowlands, F. G. Lemoine and T. A. Williams. The 1-Centimeter Orbit: Jason-1 Precision Orbit Determination Using GPS, SLR, DORIS, and Altimetry Data. *Marine Geodesy*, 26, 399-421, 2003.

Manca, B. B., G. Budillon, P. Scarazzato, L. Ursella. 2003. Evolution of dynamics in the eastern Mediterranean affecting water mass structures and properties in the Ionian and Adriatic Seas. *J. Geophys. Res.*, 108 (C9), 8102, doi:10.1029/2002JC001664,m 2003.

McCarthy, D. D., and G. Petit (editors.) International Earth and Reference System Service (IERS) Conventions 2003. Technical note No. 32. Online available from <http://www.iers.org/iers/publications/tn/tn32/>. [Visited: 01/06/2005].

McKenzie, D. P. Active tectonics of the Mediterranean region. *Geophysical Journal of the Royal Astronomical Society* 30, 109-185, 1972.

Meier, M. F., and M. Dyurgerov. How Alaska affects the world. *Science*, 297, 350-351, 2002.

Mitchum, G. T. Comparison of TOPEX sea surface heights and tide gauge sea levels. *J. Geophys. Res.*, 99, 24, 541-24, 553, 1994.

Mitchum, G. T. Monitoring the stability of satellite altimeters with tide gauges. *J. Atmos. Oceanic Tech.*, 15, 721-730, 1998.

Mitchum, G. T. An improved calibration of satellite altimetric heights using tide gauge sea levels with adjustment for land motion. *Marine Geodesy*, 23, 145-166, 2000.

Miller, L., B. C. Douglas. Mass and volume contributions to twentieth-century global sea level rise. *Nature*, Vol. 428, 406-409, 2004.

Milly, P. C. D., A. Cazenave and M. C. Gennero. Contribution of climate-driven change in continental water storage to recent sea-level rise. *Proc. Natl. Acad. Sci. U.S.A.*, 100, 13,158-13,161, 2003.

Minster, J. F., A. Cazenave, Y. V. Serafini, F. Mercier, M. C. Gennero and P. Rogel. Annual cycle in mean sea level from Topex-Poseidon and ERS-1: inference on the global hydrological cycle. *Global and Planetary Change*, 20, 57-66, 1999.

Munk, W. H., and G. J. F. Macdonald. The rotation of the Earth. A geophysical discussion. Cambridge at the University Press, 1960.

Nerem R. S. and G. T. Mitchum. Observations of sea level change from satellite altimetry. Sea Level Rise: History and Consequences. *International Geophysisc Series*, vol. 75, edited by B. Douglas, M. Kearney, and S. Leatherman, pp. 121-164, Academic Press, 2001.

Nerem, R. S., and G. T. Mitchum. Sea Level Change. Satellite altimetry and Earth sciences. *International Geophysisc Series*, vol. 69, edited by L.-F. Fu and A. Cazenave, pp. 329-350, Academic Press, San Diego, 2001.

Nerem, R. S., and G. T. Mitchum. Estimates of vertical Crustal Motion Derived from Differences of TOPEX/Poseidon and Tide Gauge Sea Level Measurements. *Geophys. Res. Lett.*, Vol 29, Iss 19, art. no. 1934, 2002.

Ngo-Duc, T., K. Laval, J. Polcher, A. Lombard and A. Cazenave. Effects of land water storage on global mean sea level over the past half century. *Geophys. Res. Lett.*, 32, L09704, 2005.

Ngo-Duc, T., K. Laval, Y. Polcher and A. Cazenave. Analyses of the contribution of continental water to sea level variations during the 1997-1998 ENSO event; Comparison between the AMIP simulations and the Topex/Poseidon satellite data. *J. Geophys. Res.*, 110, D09103, doi:10.1029/2004JDO04940, 2005.

Peltier, W. Global glacial isostatic adjustment and modern instrumental records of relative sea level history. Sea Level Rise: History and Consequences. *International Geophysisc Series*, vol. 75, edited by B. Douglas, M. Kearney, and S. Leatherman, pp. 65-95, Academic Press, 2001.

Preisendorfer, R. W. Principal component analysis in Meteorology and Oceanography. Elsevier Sci., New York, 425pp, 1988.

Pond, S., and G. Pickard. Introductory Dynamical Oceanography. Pergamon Press Sydney, 1986.

Rahl, J. M., C. Fassoulas and M. T. Brandon. Exhumation of high-pressure metamorphic rocks within an active convergent margin Crete, Greece: A field guide. *32th International Geological Congress*, Vol. 2 - from B16 to B33, art. No B32, 2004.

Ramillien, G., F. Frappart, A. Cazenave and A. Güntner. Time variations of land water storage from an inversion of 2 years of GRACE geoids. *Earth and Planetary Science Letters*, 235, 283-301, 2005.

Revelle, R., W. Broecker, H. Craig, C. D. Keeling and J. Smagorinsky. Appendix Y4, in Restoring the quality of our enviroment - Report of the environment pollution panel. Pres. Sci. Advis. Comm., Washington, D. C., 112-133, 1965.

Reynolds, R. W. A real-time global sea surfuce temperature nalysis. *J. Climate*, 1, 75-86, 1988.

Reynolds, R. W., N.A. Rayner, T.M. Smith, D.C. Stokes, and W. Wang. An Improved In Situ and Satellite SST Analysis for Climate. J. Climate, 15, 1609-1625, 2002.

Rignot, E., G. Casassa, S. Gogineni, P. Kanagaratnam, W. Krabill, H. Pritchard, A. Rivera, R. Thomas, J. Turner and D. Vaughan. Recent ice loss from the Fleming and other glaciers, Wordie Bay, West Antarctic Peninsula. *Geophys. Res. Lett.*, 32, L07502, 2005.

Rodell, M., L. S. Famiglietti, J. Chen, S. I. Seneviratne, P. Viterbo, S. Holl and C. R. Wilson. Basin scale estimates of evapotranspiration using GRACE and other observations. *Geophys. Res. Lett.*, Vol. 31, L20504, doi:10.1029/2004GL020873, 2004.

Roether, W., B. B. Manca, B. Klein, D. Bregant, D. Georgopoulos, V. Beitzel, V. Kovacevic, A. Luchetta. Recent Changes in Eastern Mediterranean Deep Waters. *Science*, 271, 333- 335, 1996.

Rowlands, D. D., S. B. Luthcke, S. M. Klosko, F. R. Lemoine, D. S. Chinn, J. J. Mccarthy, C. M. Cox and O. B. Anderson. Resolving mass flux at high spatial and temporal resolution using GRACE intersatellite measurements. *Geophys. Res. Lett.*, Vol. 32, L04310, doi:10.1029/2004GL021908, 2005.

Ruf, C. S. Detection of calibration drifts in spaceborne microwave radiometers using a vicarious cold referenc. *IEEE Trans. Geosci. Remote Sensing*, vol 38, pp 44-52, 2000.

Rutigliano, P., C. Ferraro, R. Devoti, R. Lanotte, V. Luceri, A. Nardi, R. Pacione and C. Sciarretta . Vertical motions in the Western Mediterranean area from geodetic and geological data. *Proceedings of The Tenth General Assembly of the Wegener Project*, 2000.

Schmidt R., F. Flechtner, Ch. Reigber, P. Schwintzer, A. Gunter, P. Doll, G. Ramillien, A. Cazenave, S. Petrovic, H. Jochman and J. Wunsch. GRACE observations of changes in continental water storage. *Global and Planetary Change*, in press, 2005.

Spencer, N. E., and P. L. Woodworth. Data Holdings of the Permanent Service for Mean Sea Level. Bidston, Birkenhead: Permanent Service for Mean Sea Level. 81pp., 1993.

Steward, R. H. Introduction to physical oceanography. Online available from <http://oceanworld.tamu.edu/home/course_book.htm>, 2003. [Visited: 02/01/2003].

Swenson, S., and J. Wahr. Methods for inferring regional surface-mass anomalies from Gravity Recovery and Climate Experiment (GRACE) measurements of time-variable gravity. *J. Geophys. Res.*, 107, B9, 2193, doi:10.1029/2001JB000576, 2002.

Tapley, B. D., S. Bettadpur, M. Watkins, C. Reigber. The Gravity Recovery and Climate Experiment: Mission overview and early results. *Geophys. Res. Lett.*, Vol. 31, L09607, doi:10.1029/2004GL019920, 2004.

Tapley, B. D., S. Bettadpur, J. C. Ries, Paul F. Thompson, M. Watkins. GRACE Measurements of Mass Variability in the Earth System. *Science*, Vol. 305, 2004.

Tsimplis, M. N., and N. E. Spencer. Collection and Analysis of Monthly Mean Sea Level Data in the Mediterranean and Black Sea. *Journal of Coastal Research*, 13, 2, 534-544, Fort Lauderdale, Florida, 1997

Tsimplis, M. N., and T. F. Baker. Sea level drop in the Mediterranean Sea: An indicator of deep water salinity and temperature changes? *Geophys. Res. Lett.*, Vol. 27, No. 12, 1731-1734, 2000.

Tsimplis, M. N., and S. A. Josey. Forcing of the Mediterranean Sea by atmospheric oscillations over the North Atlantic. *Geophys. Res. Lett.*, 28 (5), 803–806, 2001.

Tsimplis, M. N., and M. Rixen. Sea level in the Mediterranean Sea: The contribution of temperature and salinity changes. *Geophys. Res. Lett.*, 29 (23), 2136, doi: 10.1029/2002GL015870, 2002.

Tsimplis, M. N., S. A. Josey, M. Rixen, and E. V. Stanev. On the forcing of sea level in the Black Sea. *J. Geophys. Res.*, 109, C08015, doi:10.1029/2003JC002185, 2004.

Velicogna, I., J. Wahr, E. Hanna and P. Huybrechts. Short term mass variability in Greenland, from GRACE. *Geophys. Res. Lett.*, Vol. 32, L05501, doi:10.1029/2004GL021948, 2005.

Vigo, I., D. García, and B. F. Chao. Change of sea level trend in the Mediterranean and Black seas. *Journal of Marine Research*, Vol. 63, N. 6, 2005.

Wahr, J. Deformation induced by polar motion. *J. Geophys. Res.*, Vol. 90, No. B11, 9363-9368, 1985.

Wahr, J., M. Molenaar and F. Bryan. Time variability of the Earth's gravity field: Hydrological and oceanic effects and their possible detection using GRACE. *J. Geophys. Res.*, 103, B12, 30205-30229, 1998.

Wahr, J., S. Swenson, V. Zlotnicki and I. Velicogna. Time-variable gravity from GRACE: First results. *Geophys. Res. Lett.*, Vol. 31, L11501, doi:10.1029/2004GL019779, 2004.

Willis, J. K., D. Roemmich, and B. Cornuelle. Interannual variability in upper ocean heat content, temperature, and thermosteric expansion on global scales. *J. Geophys. Res.*, 109, C12036, 2004.

Woolf, D. K., A. Shaw, and M. Tsimplis. The influence of the North Atlantic Oscillation on sea-level variability in the North Atlantic region. *The Global Atmosphere and Ocean System*, 9 (4), 145-167, 2003.

Yoder, C. F. Astrometric and Geodetic Properties of Earth and the Solar System. A Handbook of Physical Constants: Global Earth Physics (Vol.1). *AGU Reference Shelf Series*, edited by T. J. Ahrens, pp. 1-31, ISBN 0-87590-851-9, 1995.

Acronyms and abbreviations

°C: Celsius degree
AVHRR: Advanced Very High Resolution Radiometer
AVISO: Archiving, Validation and Interpretation of Satellite Oceanographic
E: Evaporation
CANIGO: Canary Islands Azores Gibraltar Observations
cm: centimeter
COADS: Comprehensive Ocean-Atmosphere Data Set
CTD: Conductivity Temperature Depth
DLR: Deutsches Zentrum für Luft- und Raumfahrt
ECCO: Estimating the Circulation and Climate of the Ocean
ECMWF: European Centre for Medium-Range Weather Forecasts
EMT: Eastern Mediterranean Transient
ENSO: El Niño - Southern Oscillation
ENVISAT: Environmental Satellite
EOF: Empirical Orthogonal Function
EPN: EUREF Permanent Network
ERS: European Remote Sensing
ESA: European Space Agency
EUREF: European Reference Frame
GCM: Global Circulation Model
GF: Gibraltar flux
GIA: Glacial Isostatic Adjustment
GPS: Global Positioning System
GRACE: Gravity Recovery And Climate Experiment

GS: Gibraltar Strait
GTS: Global Telecommunication System
IB: Inverse Barometer
IPCC: Intergovernmental Panel on Climate Change
ITRF: International Terrestrial Reference Frame
LEGOS: Laboratoire d'Études en Géophysique Et Océanographie Spatiales
m: meter
mm: millimeter
MSL: Mean Sea Level
MSLP: Mean Sea Level Pressure
NAO: North Atlantic Oscillation
NASA: National Aeronautic and Space Administration
NCEP: National Center for Environmental Prediction
NOAA: National Oceanic and Atmospheric Administration
OGCM: Ocean Global Circulation Model
OI: Optimally Interpolated
P: Precipitation
PC: Principal Components
PSMSL: Permanent Service for Mean Sea Level
R: River run-off
RLR: Revised Local Reference
S: Salinity
SELF: Sea Level Fluctuations
SL: Sea Level
SLA: Sea Level Anomaly
SLR: Satellite Laser Ranging
SLV: Sea Level Variations
SLV_{steric}: Sea level variations due to density changes in the water column.
SLV_{mass}: Sea level variations due to changes in the water budget of the ocean.
SSH: Sea Surface Height
SST: Sea Surface Temperature
T: Temperature
TG: Tide Gauge
T/P: Topex/Poseidon

Volver al índice/Tornar a l'índex

TVG: Time Variable Gravity
V: Gravity potencial of the Earth
VLBI: Very Long Baseline Interferometry
W: Watt
WOA: World Ocean Atlas
WTE: Water Thickness Equivalent
XBT: Expendable Bathythermograph